國立臺灣大學電機資訊學院電機工程學系
碩士論文
Department of Electrical Engineering
College of Electrical Engineering and Computer Science
National Taiwan University
Master Thesis

以飽和輸入控制之多代理人系統動態調控
Dynamic Maneuver Control of Multi-Agent System with
Input Saturation

陳昱文
Yu-Wen Chen

指導教授：傅立成 博士
Advisor: Li-Chen Fu, Ph.D.

中華民國 108 年 7 月
July, 2019

ii

誌謝

在研究所兩年的學習裡，碩士論文能如期完成，需要感激許多人，在此獻上最大的敬意。首先感謝指導教授傅立成老師。老師的非線性系統分析、適應性控制課程為我們打下紮實的控制理論基礎，亦感謝每周由博士後研究江明理學長、博士班劉安陞學長所帶領的英文書報討論，此不僅訓練了報告技巧、投影片設計，也精進了英文能力。感謝口試委員陳永耀、顏家鈺、練光祐和江明理教授對論文的指導。感謝江明理學長、劉安陞學長的頻繁討論以及投影片製作建議。感謝李懿萱助理在百忙之中協助安排口試事宜。感謝所有與我一起奮鬥、互相鼓勵和扶持的同學們，包括 AFM 組的劉逸霖；復健組的賈恩宇和簡雅慧；機器人組的朱啟維、蕭羽庭、張天時和詹少宏；影像組的劉宇閎。感謝所有其他尖端控制實驗室的同學，即使是短暫的對話或互動都是碩士生涯中的一陣甘霖。最後更要感謝父母親的養育之恩，有了家人的支持，讓我能安心完成學業，達成人生階段性的理想。

iv

摘要

本論文旨在研究多代理人系統 (MAS) 的編隊調控,近年來其因應用之普及,如:物體承載、海洋探勘及無人機偵查等而備受關注。以下我們枚舉本論文之部分目標。首先,我們的目標是設計各式調動控制以達成各種任務,包括軌跡追蹤、隊形旋轉,及更重要的線上調整。線上適應意味著可動態調整編隊,此為至關重要的問題,因其可防止於動態或未知之環境中產生碰撞。此外,我們還考慮了非完全運動約束、通信限制及輸入飽和,這一方面大幅提高了控制器設計之難度,卻也是對於將控制器付諸實踐不可或缺的。同時,我們採用本地參考座標 (local reference frame) 來取代一般研究所需之全域參考座標 (global refernce frame) 以提高通訊品質 (QoS)。其次,我們提出新穎設計使其能掌控 MAS 於軌跡循跡時之隊形方位,並提出了比現有結果更自然的軌跡循跡運動。再者,我們設計了"相位償罰流交換機制"以處理旋轉編隊中的順序問題而無需有所限制或假設;相對來說,現有研究結果通常需要各式條件以解決順序問題。最後,我們提供一些模擬場景與模擬結果以驗證理論推導。

關鍵字: 編隊控制、多代理人系統、動態編隊、飽和輸入、自然追蹤軌跡、有序性旋轉編隊

vi

Abstract

This thesis considers maneuver control of Multi-Agent System (MAS), which has drawn significant attention recently for its wide applications, such as object carrying, ocean exploring, and UAV scouting. The main objectives of this thesis are listed as follows. First of all, we aim to design general maneuver control law to support various tasks, including tracking, rotating, and especially, online adaptation. Online adaptation means that the formation can be dynamically adjusted, which is a crucial issue for preventing collisions in dynamic or unknown environments. Moreover, we take nonholonomic, communication, and input saturation constraints into account, which dramatically raise the difficulty of design but are crucial to put the design in practice. Meanwhile, we relax the requirement of global reference frame information for communication. Alternatively, local reference frame is adopted to enhance the quality of service. Furthermore, the orientation of MAS while tracking is designed in our novel method, and particularly, a more natural tracking movement than existing results is proposed. In addition, we devise a "phase penalty flow exchange mechanism" to deal with the issue of order in rotating formation without additional restrictions or assumptions, while existing results usually require various conditions to achieve it. Finally, several simulation scenarios are provided to validate our results.

Keywords: Maneuver control, Multi-Agent System (MAS), dynamic formation, input saturation, natural tracking, ordered rotating
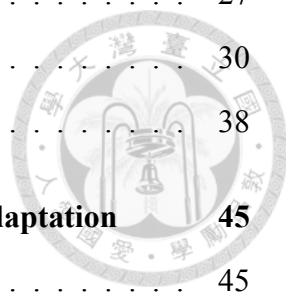
viii

Contents

List of Figures

List of Tables

Chapter 1

Introduction

In this chapter, we briefly introduce the motivations, importances, and objectives of this thesis. The organization in this chapter is as follows: Section 1.1 demonstrates some motivations for study of Multi-Agent System (MAS) formation control. Then, in Section 1.2, comprehensive literature survey are given to catch up with state of the art results. Based on the review of literature, in Section 1.3, we itemize some of the main contributions of this thesis compared with existing works. At last, in Section 1.4, we provide the organization of this thesis.

1.1 Motivation

The researches about control of Multi-Agent Systems (MAS) have attracted significant attention for its wide applications in the past two decades. One of the main reasons to this phenomenon is the rapid developments of robotics and unmanned aerial vehicles (UAVs) and their remarkable falling price. Thus, a large diversity of applications is carried out by the robots and UAVs emerge. Among these applications, Multi-Agent System (MAS) formation control is regarded as one of the most potential topic due to its value

1

of facilitating real-life tasks. The definition of *formation control* from [1] states that formation control aims to drive multiple agents to achieve prescribed constraints on their states. Generally speaking, the problem of formation control is to design the controller to steer a group of agents to form into a desired geometric pattern and complete various tasks cooperatively. The backgrounds of formation controller design cover not only control engineering but also consensus algorithm [2–7], algebraic graph theory [8–11], and matrix theory [8, 12–14], to name a few. As its rapid developments and wide coverage, we will provide a comprehensive literature review in next section.

"Maneuver control" is a related term to formation control. Though the term is somehow interchangeable with formation control in some existing works, it mainly emphasizes the functionalities of MAS instead of forming a static geometric pattern. According to the definition from [14], maneuver control refers that the centroid, orientation, scale, and other geometric parameters of the formation can be changed continuously. These maneuver actions supports various tasks and we will exemplify a few in the following. For example, in [3, 9, 15], the authors design maneuver control to steer the centroid of the formation to track a reference trajectory in addition to pattern formation. Such function supports the applications of surveillance or navigation. Besides, scaling the formation shape with predefined commands is considered in [9, 16, 17]. The scaling can help the MAS to prevent from colliding with obstacles. Still, authors in [18, 19] deal with rotating formation, that is, rotate around the centroid of MAS. This scenario is suitable for data collection or measurements due to bias reduction or denser scanned area.

In this thesis, we aim to design general dynamic maneuver control which enlarges and improves the aforementioned functionalities so that the MAS can compete for general real-life tasks. Such tasks cover surveillance, navigation, sensor measurement, resource dis-

2

pense, environment detection, data collection, source seeking, secure and rescue (SAR), etc, where some of the tasks are demonstrated in Figure 1.1. In the following, in order to provide more details of our objectives and validate our contributions compared with existing results, we first comprehensively review the literature about MAS formation (and maneuver) control in Section 1.2 and then summarize our contributions in Section 1.3.

(a) surveillance

(b) resource delivery

(c) source seeking

(d) secure and rescue
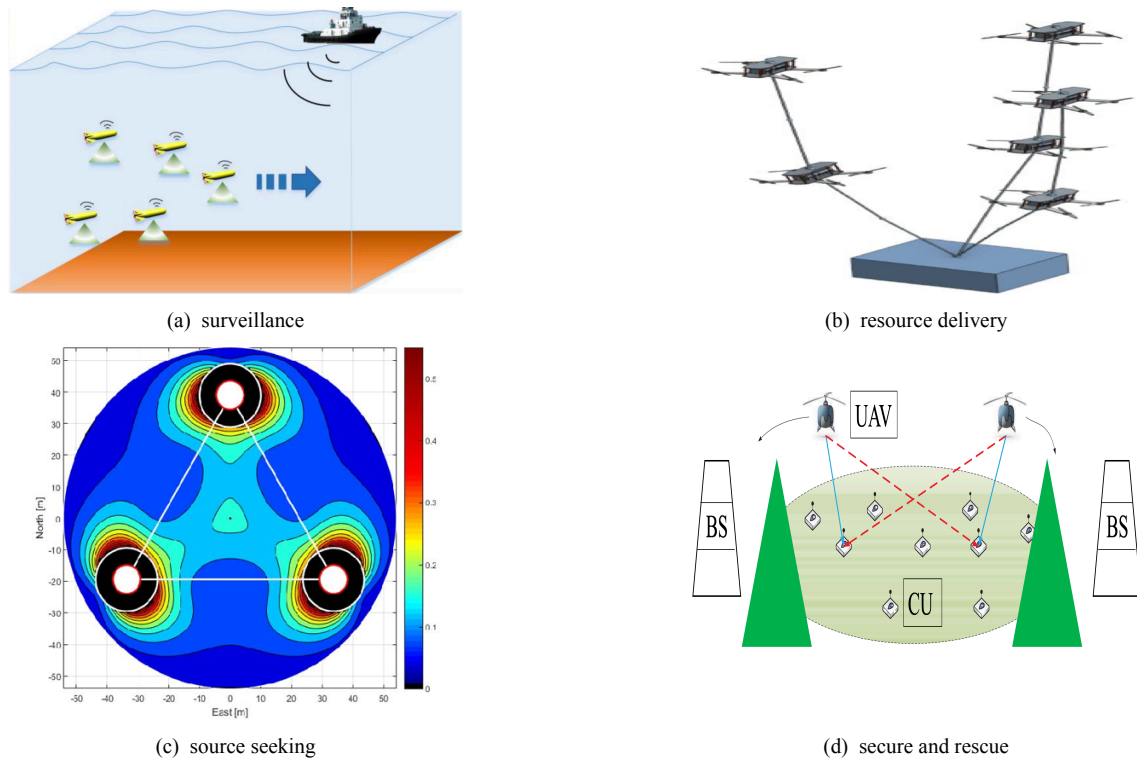
Figure 1.1: Some applications

1.2 Literature Review

Formation (Maneuver) control as one of the popular topics of MAS possesses great potential in practical applications. Its objective is to steer a group of agents to form into some predefined geometric pattern. The main components in formation control includes the agents' dynamic model, communication properties, and additional functionalities. These settings vary from paper to paper, and thus we will provide more details to some of the state of the art results in the following.

3

In practice, the dynamic models for robots, autonomous underwater vehicles (AUVs) or UAVs are all somehow complicated. As a result, simplified models are adopted for the controller design. The most common models are the integrator model, double-integrator model, and unicycle model. In [8, 15, 20], an integrator dynamic model is utilized due to its simplicity. However, the main shortcoming of such model is that it sometimes loses system characteristics such as the nonholonomic constraint. In other words, the heading information of the robots are lost. Therefore, unicycle model is adopted to address the issue, as in [21, 22], to name a few.

Communication links is another main factor of MAS, which is basically represented by a graph. In [8, 11, 14], the authors assume the bidirectional capability of exchanging information which is delineated by undirected graph. Nevertheless, this assumption is demanding in reality due to the sensing abilities, disturbances or delays. Thus, some authors relax the requirement and consider the directed graph, *e.g.*, in [13, 23]. No matter it is directed or not, the communication scenario can be separated into global (centralized) communication and local (distributed) communication. Centralized communication refers that the agents can have information of all the other agents, for example, [20, 24]. Since the global circulation of information generates huge computation burden, the global communication has become out of date. While global or centralized communications are assumed in earlier papers, local or distributed communication receives more attention recently. Distributed communication refers that each agent can only get information from their communicable agents and their local reference frame in the formation process, *e.g.*, [11, 13, 17, 25–28]. Instead of general distributed communication, some works consider special types of distributed communication topology due to the distance-based property or rigidity issue [8, 9].

Another classification of communication graph is static versus switching. Static graph

4

as in [14, 26, 29], which is usually distributed, states that each agent communicates with fixed neighbors. Though such scenario has improved computation burden compared to the centralized one, they do not consider the distance for communication. Since the distance affects the quality of service, the works [10, 23] extend the fixed communication to the switching case where agents communicate with each other based on the sensing range.

Still another issue is the global reference frame versus local reference frame. In [16, 17, 22, 23], the authors consider controllers that employ the absolute information of the MAS, which means the global reference frame is needed; in [3, 30], the desired relative position vectors are defined with respect to the global reference frame; in [31, 32], the information is measured in the aligned frame. In fact, to maintain a common reference frame in reality is challenging, and the obtained information is often noisy due to long range delivery. Thus, the control law based on each agent's local frame has drawn more attention and is discussed in some recent works [13, 15, 25, 28, 33, 34]. Such local frame scenario relaxes the requirements of advanced sensing capability; however, the controller design is more involved compared with the global reference frame case.

For additional functionalities of formation control, different tasks are considered in various works such as tracking the reference trajectory for surveillance or navigation [3, 9, 15], scaling the formation shape for obstacle avoidance or environment adaptation [9, 16, 17], rotating around a center for data collection or measurement [18, 19], etc. Early researches of formation control consider static formation at fixed desired positions without additional functionalities, as in [8, 13, 28]. Nevertheless, most of the applications require formation with movements. Thus, the controller is further designed such that the agents can track the trajectory in addition to static formation such as that in [3, 9, 15]. Some works further consider the case that the system has circular motion [12, 35] and the

5

formation shape can be further adjusted by affine transformation [9, 16, 17]. Moreover, the so-called rotating formation is studied in [16, 31, 35], where the MAS is designed to additionally rotate at a given angular velocity in addition to tracking. Overall speaking, the existing proposed functionalities include the objectives such as rotation [29], obstacle avoidance [21], constrained inputs [6, 21, 36], time-varying shape [17, 26], or connectivity preservation [27], to name a few.
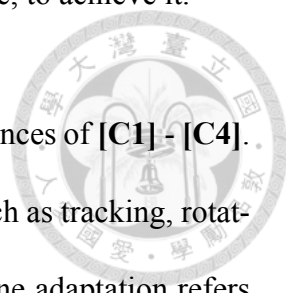
A brief review of existing results is given above, while more discussions about some closely related works will be provided with comparisons in Section 3.2 and Section 4.2, where the problems are described specifically.

1.3 Contribution

Based on the survey of the state of the art results, we enumerate some merits of the proposed design over existing works. The main contributions of this thesis is that we propose a general design of maneuver control which has the following 4 novelties:

[C1] The general maneuver control covers tracking, rotating, and transforming. Moreover, we endow the formation with ability of online adaptation.

[C2] We take three kinds of constraints into account, nonholonomic, communication, and input saturation, which dramatically raise the difficulty of controller design.

[C3] In our design, the MAS orientation can be generally designed while tracking, and a more natural tracking movement compared with existing works is proposed. Moreover, the existing tracking results can be regarded as special cases in our design.

[C4] We propose a "phase penalty flow exchange mechanism" to ensure the order relation in rotating formation, while existing papers require various conditions, such as

6

special initial conditions or requiring the global reference frame, to achieve it.

In this paragraph, we provide more discussions about the significances of **[C1]** - **[C4]**. For **[C1]**, we call it general since most existing maneuver actions, such as tracking, rotating, and transforming, are dealt with in this thesis. In addition, online adaptation refers to the dynamic adjustments to the formation, such as scaling and shearing. Adjusting formation is vital since the environments are varying where the formation should adapt to. Among the few results dealing with this crucial issue, most of them as [9, 17] assume that all agents have access to the adjustment command in advance which is fixed thereafter. While in our design, the assumption is relaxed, and thus the formation can be adjusted *online*. For **[C2]**, three main kinds of real-world constraints are considered to make the design more feasible. Especially for the input saturation, most existing papers of formation control, as in [13, 15, 17, 23, 26, 29, 30], to name a few, neglect the physical limitation of actuators and allow arbitrary magnitudes of inputs. Furthermore, some results such as [16, 17], overlooks the issue of singularity. As for the communication constraints, we consider distributed switching case, which in reality can maintain better quality of service than the fixed one as in [14, 26, 29]. Additionally, we relax the requirement of global reference frame so that agents can implement the control locally instead of communicating far way to global frame with noisy signals and spending lots of efforts maintaining shared information, as mentioned in [1]. Most existing results which consider distributed case and local reference frame at the same time have limited functionalities, while we can cover most existing maneuver actions. For **[C3]**, our approach can generally design the orientation motions of MAS while tracking. Particularly, "natural tracking movements" is proposed so that tasks like object tracking can be achieved more natural than existing tracking results, since the orientation of MAS is aligned with moving direction in our de-

7

sign. Besides, the existing tracking results can be regarded as special cases of our general design. For **[C4]**, the order refers to the relation among positions of agents, and such issue of order arises when the functionality is extended to rotation. To guarantee the agents form in pre-specified order, [25,28] impose restrictions on initial conditions, [23,31] require the global reference frame, and specific communication topology is assumed in [12,24,32]. In contrast to the existing results, we achieve pre-specified order via our proposed mechanism without imposing restrictions to initial conditions, requiring global frame information, or assuming specific communication scenario.

1.4   Thesis Organization

The remaining part of this thesis is organized as follows. In **Chapter 2**, some preliminaries are introduced which include algebraic graph theory for communication between agents and descriptions of desired geometric pattern. When in Chapter 3 and Chapter 4, these tools can facilitate to formulate the proposed problems. *In order to deal with general maneuver control of Multi-Agent System, we first focus on tracking formation* in Chapter 3 *and then extend to tracking with rotation* in Chapter 4. In **Chapter 3**, a concept called natural tracking is proposed to generalize the existing tracking results. Moreover, online adaptation of formation is realized by our design, which can avoid collisions with the environments. In **Chapter 4**, we consider the tracking with rotation case to further cover the existing applications. In the case of tracking with rotation, an issue of order between agents arises, which motivates us to propose the "phase penalty flow exchange mechanism" such that agents can rotate in a pre-specified order. Moreover, online adaptation is considered once again to achieve collision avoidance. In **Chapter 5**, we provide some simulation results for "Natural Tracking" designed in Chapter 3 and "Ordered Rotating"

designed in Chapter 4. At last, in **Chapter 6**, the conclusion of this thesis and some future

works are stated.

Chapter 2

Preliminaries

In this chapter, we provide some preliminaries and concepts which will be mentioned frequently. Section 2.1 is about *Algebraic Graph Theory* which relates to communications in MAS. Then, *affine transformation* is introduced in Section 2.2, which facilitates the dynamic adjustment of the desired formation. In Section 2.3, we propose a novel *description for desired formation* utilized throughout this thesis. In Section 2.4, the concept of switching communications is introduced with some notations.

2.1 Algebraic Graph Theory

Algebraic graph theory is commonly used to represent the communication links of MAS. A directed graph $\mathcal{G} = (V, E)$ consists of a set of nodes V and a set of directed edges E. Suppose there are N nodes indexed from 1 to N and denoted as V_i for $i = 1, \ldots, N$. A directed edge pointing from V_j to $V_i \in V$ is denoted as $(i, j) \in E$.

11

Definition 2.1 (Adjacency matrix)**.**

$$\textit{Adjacency matrix } \boldsymbol{A} \in \mathbb{R}^{N \times N} \textit{ with elements } a_{ij} := \begin{cases} 1, & \textit{if } (i,j) \in E \\ \\ 0, & \textit{otherwise} \end{cases}$$
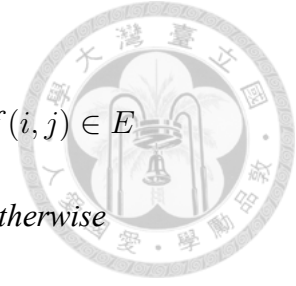
Definition 2.2 (in-Degree matrix)**.**

$$\textit{in-Degree matrix } \boldsymbol{D} \in \mathbb{R}^{N \times N} \textit{ with elements } d_{ij} := \begin{cases} \sum_{k=1}^{N} a_{ik}, & \textit{if } i = j \\ \\ 0, & \textit{otherwise} \end{cases}$$

Definition 2.3 (Laplacian matrix)**.** *Laplacian matrix* $\boldsymbol{L} \in \mathbb{R}^{N \times N} := \boldsymbol{D} - \boldsymbol{A}$.

Here we provide an graph instance, Figure 2.1, to explicitly define the matrices:

$$\boldsymbol{A} = \begin{bmatrix} 0 & 0 & 1 & 1 \\ 1 & 0 & 0 & 0 \\ 0 & 1 & 0 & 0 \\ 1 & 0 & 0 & 0 \end{bmatrix}, \boldsymbol{D} = \begin{bmatrix} 2 & 0 & 0 & 0 \\ 0 & 1 & 0 & 0 \\ 0 & 0 & 1 & 0 \\ 0 & 0 & 0 & 1 \end{bmatrix}, \boldsymbol{L} = \begin{bmatrix} 2 & 0 & -1 & -1 \\ -1 & 1 & 0 & 0 \\ 0 & -1 & 1 & 0 \\ -1 & 0 & 0 & 1 \end{bmatrix}.$$
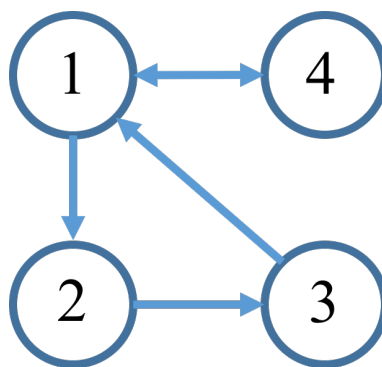
Figure 2.1: Directed graph

Definition 2.4 (Path)**.** *Given a directed graph* $\mathcal{G} = (V, E)$, *we say that there exists a path from* $V_i \in V$ *to* $V_j \in V$ *if there is a series of directed edges belong to* E *which connects from* V_i *to* V_j.

12

Definition 2.5 (Strongly Connected). *A directed graph $\mathcal{G} = (V, E)$ is strongly connected if given any two nodes $V_i, V_j \in V$, there exists a path from V_i to V_j and also a path from V_j to V_i.*
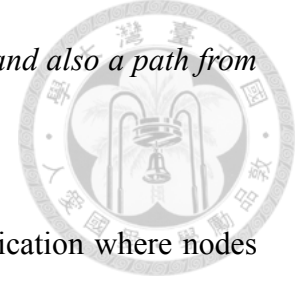
In this thesis, directed graph $\mathcal{G}$ represents the directed communication where nodes V and edges E represent the agents and the information passing directions, respectively. Define N_k as the set of nodes with edge pointing toward agent-k, *i.e.*, the neighbors that the agent-k can receive information from, and $|N_k|$ as the total number of neighbors of agent-k. For example, in Figure 2.1, $N_1 = \{\text{agent-}3, \text{ agent-}4\}$ and $|N_1| = 2$.

2.2 Affine Transformation

An affine transformation is a function with preservation of lines, points, and planes. Afterwards in our design, we will use it for implementation of formation with online adjustment. More rigorously, consider the Euclidean Space, and the mathematical definition is given as follows.

Definition 2.6 (Affine Transformation). *Consider two spaces $X \in \mathbb{R}^N$ and $Y \in \mathbb{R}^M$. An affine transformation $f : X \mapsto Y$ is defined as $x \mapsto Tx + b$, where $T \in \mathbb{R}^{M \times N}$ is a linear transformation and $b \in \mathbb{R}^M$ is a translation.*

In our applications, we focus on the cases that $N = M = 2$ and $N = M = 3$, where the former is called 2D case and the latter is a 3D one. Some common 2D linear transformations are listed in Table 2.1. Applying such transformations to a planar geometric shape results in another shape, for example, a unit circle by the scaling matrix in Table 2.1 becomes an ellipse, as shown in Figure 2.2. As for the 3D linear transformation, *e.g.*, in Table 2.2, they act on the spatial space.

13

Table 2.1: Examples for Linear Transformation $T \in \mathbb{R}^{2\times 2}$

scaling	reflection	rotation	shear
$\begin{bmatrix} 3 & 0 \\ 0 & 2 \end{bmatrix}$	$\begin{bmatrix} 1 & 0 \\ 0 & -1 \end{bmatrix}$	$\begin{bmatrix} \cos\phi & -\sin\phi \\ \sin\phi & \cos\phi \end{bmatrix}$	$\begin{bmatrix} 1 & 2 \\ 0 & 1 \end{bmatrix}$
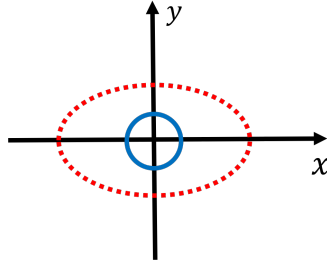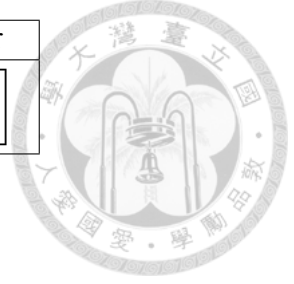
Figure 2.2: Applying scaling matrix to a circle (solid line) becomes an ellipse (dashed line).

2.3 Descriptions of the Desired Geometric Pattern

We propose a frame-invariant descriptions of the desired geometric pattern in this section, where the frame-invariant property facilitates the realization of the controller in each agent's local frame. The descriptions are constructed as follows: given any N-vertices desired geometric pattern, say Figure 2.3, draw the vectors from the centroid to each agent and denote as the center vectors $\boldsymbol{c}_k \in \mathbb{R}^2$ for $k = 1, \ldots, N$. Then, define d_k^* as the length of $\boldsymbol{c}_k$ and ϕ_{kj}^* as the desired relative *phase* (angle) between $\boldsymbol{c}_k$ and $\boldsymbol{c}_j$, where the term *phase* implies sign sensitivity, *i.e.*, $\phi_{kj}^* = -\phi_{jk}^*$. Note that ϕ_{kj}^* is defined within $(-\pi, \pi]$. By the constructions, $\{d_k^*, \phi_{kj}^* | \forall k, j = 1, \ldots, N\}$ can describe a desired geometric pattern without considering a specific reference frame. Moreover, when the MAS forms into desired geometric pattern and rotates around the centroid, although $\boldsymbol{c}_k$ keeps varying (rotating), the descriptions $\{d_k^*, \phi_{kj}^*\}$ still remain. As a result, instead of describing the formation

Table 2.2: Examples for Linear Transformation $T \in \mathbb{R}^{3\times 3}$

scaling	rotation w.r.t x-axis	rotation w.r.t y-axis	rotation w.r.t z-axis
$\begin{bmatrix} 3 & 0 & 0 \\ 0 & 2 & 0 \\ 0 & 0 & 1 \end{bmatrix}$	$\begin{bmatrix} 1 & 0 & 0 \\ 0 & \cos\phi & -\sin\phi \\ 0 & \sin\phi & \cos\phi \end{bmatrix}$	$\begin{bmatrix} \cos\phi & 0 & \sin\phi \\ 0 & 1 & 0 \\ -\sin\phi & 0 & \cos\phi \end{bmatrix}$	$\begin{bmatrix} \cos\phi & -\sin\phi & 0 \\ \sin\phi & \cos\phi & 0 \\ 0 & 0 & 1 \end{bmatrix}$

14

in terms of vectors c_k, we will consider the proposed descriptions of desired geometric pattern, $\{d_k^*, \phi_{kj}^* | \forall k, j = 1, \ldots, N\}$.
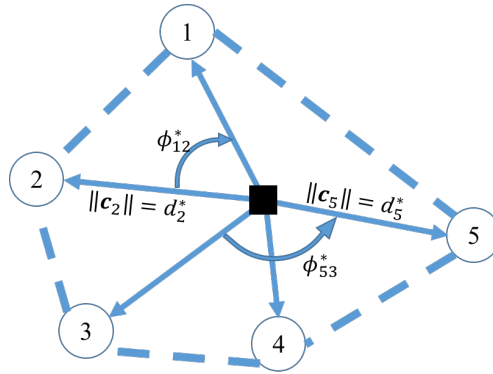
Figure 2.3: The desired formation shape is given in dash line with counter-clockwise order: 1-2-3-4-5. The square is the centroid. The arrowed vectors are center vectors, c_k, with lengths d_k^*, for $k = 1, \ldots, 5$. ϕ_{kj}^* is the signed relative angle between c_k and c_j, e.g., $\phi_{12}^* < 0$ and $\phi_{53}^* > 0$.

To systematically construct the descriptions tuple $\{d_k^*, \phi_{kj}^*\}$, we utilize the frame-invariant property and consider the polar coordinate system. Given any desired geometric pattern, translate the centroid to the origin, then we can get each agent's polar coordinate denoted as (d_k^*, ϕ_k^r) for $k = 1, \ldots, N$, as exemplified in Figure 2.4. Although the *constant* ϕ_k^r varies due to the rotations of same desired geometric pattern, as shown in Figure 2.4(a) and Figure 2.4(b), the relative phase $\phi_{kj}^r := \phi_k^r - \phi_j^r$ always equals to ϕ_{kj}^*. As a result, in real implementation, agent-k equips with d_k^* and ϕ_k^r, and when ϕ_{kj}^* is needed, the calculation of $\phi_k^r - \phi_j^r$ supports. In such implementation, agents carry their own θ_k^r instead of a table of ϕ_{kj}^*, which can save lots of memories.

2.4 Switching Communication

Switching communication means that the communication graphs may vary within a set of communication graphs. To describe when the communication graph is changed, a so-called switching signal is introduced. In the following, we provide the rigorous definition of related terms to switching communications.

15
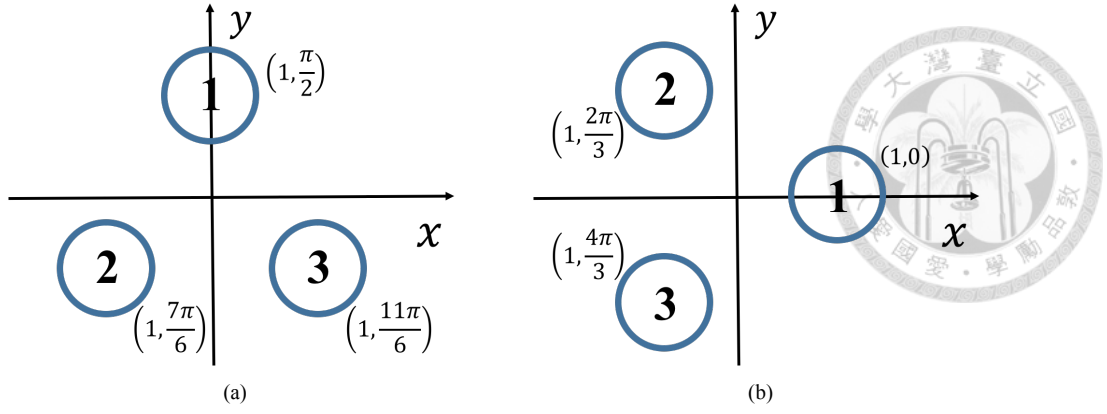
Figure 2.4: (a) $\phi_1^r = \frac{\pi}{2}$, $\phi_2^r = \frac{7\pi}{6}$, and $\phi_3^r = \frac{11\pi}{6}$. (b) $\phi_1^r = 0$, $\phi_2^r = \frac{2\pi}{3}$, and $\phi_3^r = \frac{4\pi}{3}$.

Consider s strongly connected graphs indexed from 1 to s and denote the set $S = \{1, \ldots, s\}$. Then, we can define the following notations.

Definition 2.7 (Switching signal $\sigma(t)$). *A switching signal $\sigma(t) : [0, +\infty) \to S$ indicates the corresponding indexed communication graph at time t.*

Definition 2.8 (Switching Sequence). *A switching sequence $\{t_n\}_{n \in \mathbb{N}}$ is a monotonically increasing sequence which collects the switching time instants $t_n, n \in \mathbb{N}$.*

Definition 2.9 (Dwell Time τ_0). *Given a switching sequence $\{t_n\}_{n \in \mathbb{N}}$, a dwell time τ_0 is the infimum of the switching period between two contiguous switching time instants, i.e.,*
$$\tau_0 \leq t_{n+1} - t_n, \forall n \in \mathbb{N}.$$

Note that τ_0 plays a crucial role when analyzing the stability of switching system.

Chapter 3

Natural Tracking Movements for MAS with Online adaptation

In this chapter, we propose a design such that the MAS can track a given reference trajectory with "natural" movements and be able to dynamically adjust the formation. The organization in this chapter is as follows: Section 3.1 explains the meaning of "natural" tracking movements. In Section 3.2, we describe the problem with discussion of its insights, and provide some state of the art related works. Then, the problem is formulated mathematically in Section 3.3. The next step is to design the controller, which is derived with stability analysis in Section 3.4. At last, in Section 3.5, our results are extended to switching communications.

3.1 Natural Tracking Movements

To seize the concept of "natural" tracking movements, one can first refer to Figure 3.1. In Figure 3.1(a), when the MAS tracks alone the reference centroid trajectory, each agent is at a fixed displacement with respect to the centroid in the global reference frame. In

17

other words, when tracking, the MAS is merely translating from a global viewpoint. Thus, the orientation of the geometric pattern keeps in the same direction without aligning to the tangent line of the trajectory. For example, the MAS orientation keeps heading North in Figure 3.1(a).
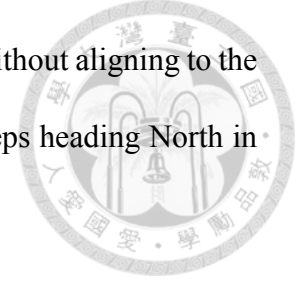
In contrast, the MAS orientation is aligned to tangent line of the trajectory in Figure 3.1(b), which we believe to be a more "natural" way when tracking. If from a global viewpoint, in addition to translation, the MAS is required to rotate with specific angular velocities at different positions. Such additional rotation remains a difficulty in existing results since the desired angular velocity is position-varying, while in our design, we utilize descriptions of geometric pattern proposed in Section 2.3 to help achieving "natural" tracking. Moreover, we can still achieve movements in Figure 3.1(a), since we propose a novel approach which can generally design the orientation while tracking.

(a) Fixed MAS orientation   (b) Aligned MAS orientation
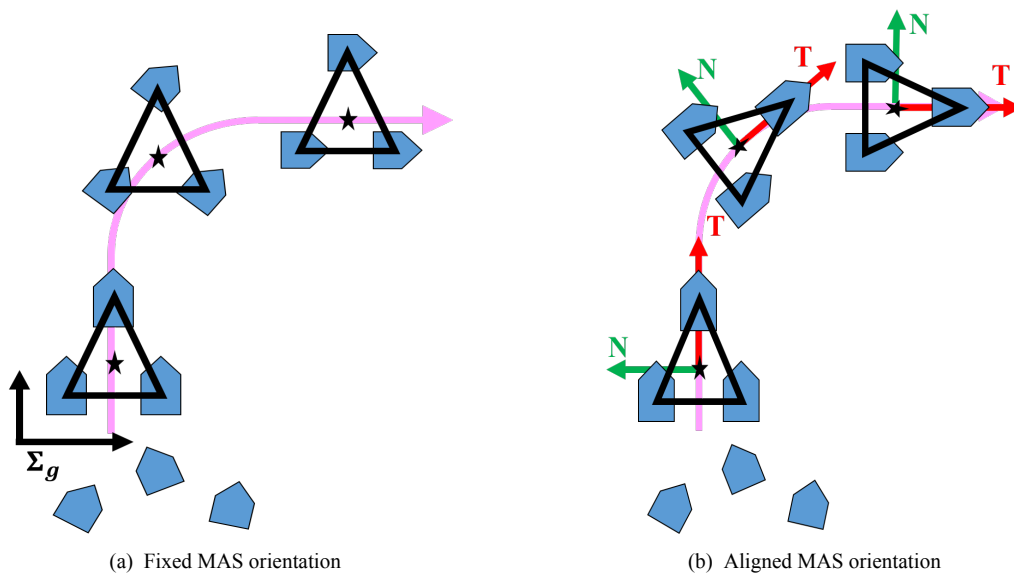
Figure 3.1: (a) The desired vectors from the centroid to agents are fixed with respect to the global frame, which results in fixed MAS orientation during tracking. (b) The desired vectors from the centroid to agents are fixed with respect to the Frenet-Serret frame, and this aligns the MAS orientation with centroid's velocity direction. In this case, a more "natural" tracking movement for MAS is achieved.

18

3.2 Problem Descriptions and Related Works

Before proceeding to the mathematical problem formulation and controller design, we first describe the goals in this chapter and provide some discussions about the related works. In this chapter, consider a MAS with numbered agents, the objective is to design a controller which is *constrained to a specified input range* to achieve the following tasks:

(i) *Desired numbered formation*: To form into a predefined geometric pattern represented by a polygon where each vertex is labeled with a number, and the numbered agents will converge to the positions of their corresponding vertices.

(ii) *Tracking*: To steer the centroid of the MAS to track a given reference trajectory.

(iii) *MAS orientation alignment*: To keep the desired position of each agent fixed to the Frenet-Serret (TNB) frame of reference centroid during tracking, as depicted in Figure 3.1(b). From viewpoint in global frame, the MAS will move along the reference centroid trajectory and meanwhile rotate around the reference centroid at the specific angular velocity which equals to the turning rate of the reference trajectory.

(iv) *Formation with online adaptation*: To avoid collisions with surroundings via dynamical adjustments of formation.

In addition, we will realize the controller in a distributed manner via the communication links and in each agent's local frame instead of the global reference frame, which implies that only relative measurements are used instead of absolute ones due to the lack of the global reference frame.

To highlight the appealing attribute of our design, which is "natural" tracking movements by task (iii) as depicted in Figure 3.1(b), we discuss more related works in the

following where most of the results move in the way as shown in Figure 3.1(a).

In [22, 37–39], they require a global reference frame to achieve desired numbered formation by assigning a constant displacement vector to each agent in advance. Thus, the desired formation cannot be online adjusted and the MAS orientation is fixed without aligning to centroid's velocity direction, which is the case in Figure 3.1(a). In [23, 26, 40], to achieve predefined time-varying formation, they require simultaneous clocks and a global reference frame to assign time-varying displacement vectors in advance. Since the time-varying displacement vectors are pre-given, the online adaptation is still not available. Note that suppose each displacement vector is designed properly based on the whole centroid trajectory in advance, then MAS orientation alignment may be achieved. Unfortunately, this cannot happen since the centroid trajectory is not known in advance nor globally accessible. In [13, 28], controller is designed in agents' local frames; however, the desired numbered formation is only static without considering tracking.

3.3   Problem Formulation

The problem described in Section 3.2 is formulated mathematically in this section. Consider a MAS composed of N numbered agents with unicycle model

$$\dot{\boldsymbol{r}}_k = v_k[\cos \psi_k, \sin \psi_k]^T$$

$$\dot{\psi}_k = \omega_k, \tag{3.1}$$

where $k = 1, 2, \ldots, N$, $\boldsymbol{r}_k \in \mathbb{R}^2$ and $\psi_k \in (-\pi, \pi]$ are agent-k's position and heading, v_k and ω_k are scalar inputs controlling linear velocity and angular velocity, respectively, as shown in Figure 3.2.

20
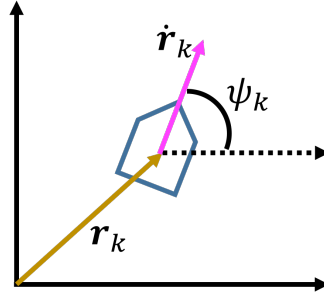
Figure 3.2: Unicycle model

Denote the index set $\mathcal{N} = \{1, \ldots, N\}$ and index-0 is reserved for representing exogenous reference signals afterwards. Given a directed communication graph $\mathcal{G}$ and the following predefined information for corresponding tasks:

(i) *Desired numbered formation*: descriptions of the desired numbered formation $\{d_k^*, \phi_{kj}^* | \forall k, j \in \mathcal{N}, k \neq j\}$ which is introduced in Section 2.3,

(ii) *Tracking*: a smooth reference centroid trajectory $\boldsymbol{r}_0 \in \mathbb{R}^2$ with scalar inputs v_0 and ω_0 which satisfies $\dot{\boldsymbol{r}}_0 = v_0[\cos\psi_0, \sin\psi_0]^T, \dot{\psi}_0 = \omega_0$,

(iii) *MAS orientation alignment*: desired *constant* relative phase ϕ_k^* required to maintain between $\dot{\boldsymbol{r}}_0$ and $\boldsymbol{c}_k$ (introduced in Section 2.3), for $k \in \mathcal{N}$, where ϕ_k^* and ϕ_j^* need to satisfy $\phi_k^* - \phi_j^* = \phi_{kj}^*, \forall k, j \in \mathcal{N}, k \neq j$, as shown in Figure 3.3, *i.e.*, we aim to align $\boldsymbol{c}_k$ to the direction of desired unit center vector $\boldsymbol{c}_k^* := [\cos(\psi_0 + \phi_k^*), \sin(\psi_0 + \phi_k^*)]^T$,

(iv) *Formation with online adaptation*: a reference affine transformation command $\boldsymbol{G}_0(t)$ $\in \mathbb{R}^{2 \times 2}$ which is a series products of transformation matrices, such as scaling, rotation, and shear matrix, as introduced in Section 2.2.

Then, we aim to design the constrained control inputs v_k and ω_k with locally and relatively measurable information through $\mathcal{G}$ such that

$$\boldsymbol{r}_k \to \boldsymbol{r}_0 + d_k^*\boldsymbol{G}_0[\cos(\psi_0 + \phi_k^*), \sin(\psi_0 + \phi_k^*)]^T \quad (= \boldsymbol{r}_0 + d_k^*\boldsymbol{G}_0\boldsymbol{c}_k^*) \qquad (3.2)$$

21
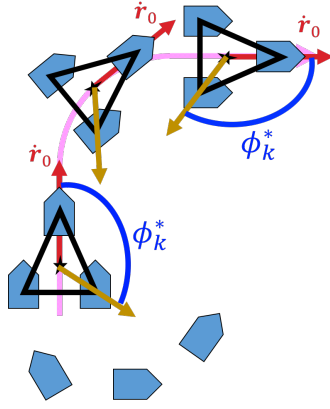
Figure 3.3: Definition of ϕ_k^* in natural tracking

asymptotically, for $k \in \mathcal{N}$. Moreover, the control inputs are constrained to specific input ranges, that is, for $k \in \mathcal{N}$, $v_k \in [v^-, v^+]$ and $\omega_k \in [\omega^-, \omega^+]$ with predefined constants $v^-, \omega^- < 0$ and $v^+, \omega^+ > 0$.

A key note is that the information given in (ii) - (iv) are 'not' accessible to all agents, since we consider the communication constraints. In general, only one agent will receive these exogenous information, while the rest of agents is required to estimate them. As a result, in the later design, lots of estimation laws will be proposed.

It is worth mentioning that three kinds of practical constraints are included in the considered problem. First, the dynamics of the agents are modeled by unicycle model, which takes nonholonomic constraints into account. Second, the controller inputs are constrained within a limited range due to the physical limitations, such as velocity saturation. Third, the communication constraints are considered, such as distributed links and local reference frames which ease the computation load and relax the requirements for advanced sensing capabilities of long-distance measurements, respectively.

Remark 3.1. *The right hand side of (3.2) is agent-k's desired trajectory which includes the four tasks. More precisely, d_k^* and ϕ_k^* relate to task (i), $\boldsymbol{r}_0$ relates to task (ii), $\psi_0 + \phi_k^*$ relates to task (iii), and $\boldsymbol{G}_0$ relates to task (iv).*

Remark 3.2. $\boldsymbol{c}_k^* = [\cos(\psi_0 + \phi_k^*), \sin(\psi_0 + \phi_k^*)]^T$ *relates to the MAS orientation alignment task. Most of the existing results can be transformed into our formulation with ψ_0 being a pre-given constant. Thus, in the existing results, the MASs move as in Figure 3.1(a), while in our design, we additionally consider tracking of ψ_0 from $\dot{\boldsymbol{r}}_0$, which leads to the more "natural" tracking movements as shown in Figure 3.1(b). In other words, most of the existing results can be regarded as the special cases of ours where ψ_0 is a constant or predefined signal.*

To solve the proposed problems, some reasonable assumptions, which will be discussed later in Remark 3.3, are made as follows:

Assumption 3.1. *The directed graph $\mathcal{G}$ is strongly connected. Moreover, at least one agent can receive the reference signals, $\boldsymbol{r}_0$, ψ_0, and the corresponding ϕ_k^*.*

Note that from Assumption 3.1, a diagonal matrix $\boldsymbol{B}$ is introduced where entries b_{kk} is 1 if agent-k can access to reference and 0 otherwise.

Assumption 3.2. *The reference linear velocity v_0 and angular velocity ω_0 are smooth and bounded: $v_0 \in [v_0^-, v_0^+]$ and $\omega_0 \in [\omega_0^-, \omega_0^+]$ with constants $v_0^-, \omega_0^- < 0$ and $v_0^+, \omega_0^+ > 0$. Moreover, $v_0^- > v^-, v_0^+ < v^+$ and $\omega_0^- > \omega^-, \omega_0^+ < \omega^+$, where $v^-, v^+, \omega^-, \omega^+$ are constants specified in Assumption 3.5.*

Assumption 3.3. *$\dot{v}_0, \dot{\omega}_0$ are bounded $\forall t \geq 0$.*

Assumption 3.4. *$\boldsymbol{G}_0, \dot{\boldsymbol{G}}_0, \ddot{\boldsymbol{G}}_0$ are bounded $\forall t \geq 0$.*

Assumption 3.5. *$||\frac{d}{dt}(\boldsymbol{r}_0 + d_k^* \boldsymbol{G}_0[\cos(\psi_0 + \phi_k^*), \sin(\psi_0 + \phi_k^*)]^T)|| \neq 0$ for $k \in \mathcal{N}, t \geq 0$. Moreover, assume that*

$$v^+ > \sup_{k \in \mathcal{N}, t \geq 0} [v_{max} + d_k^* \sigma(\dot{\boldsymbol{G}}_0) + d_k^* \omega_{max} \sigma(\boldsymbol{G}_0)] := \check{v}^+$$

23

$$\omega^+ > \sup_{k \in \mathcal{N}, t \geq 0} \mathscr{F}_k(t) := \breve{\omega}^+$$

$$v^- < -\sup_{k \in \mathcal{N}, t \geq 0} [v_{max} + d_k^* \sigma(\dot{\boldsymbol{G}}_0) + d_k^* \omega_{max} \sigma(\boldsymbol{G}_0)] := \breve{v}^-$$

$$\omega^- < \inf_{k \in \mathcal{N}, t \geq 0} \mathscr{F}_k(t) := \breve{\omega}^-,$$

where $v_{max} = \max(|v_0^-|, |v_0^+|)$, $\sigma(\boldsymbol{G}_0)$ is the largest singular value of $\boldsymbol{G}_0$, $\omega_{max} = \max($

$|\omega_0^-|, |\omega_0^+|)$, and $\mathscr{F}_k = \frac{\ddot{\boldsymbol{r}}_k^{*T} \boldsymbol{R}(\frac{\pi}{2}) \dot{\boldsymbol{r}}_k^*}{\dot{\boldsymbol{r}}_k^{*T} \dot{\boldsymbol{r}}_k^*}$, $\boldsymbol{R}(\frac{\pi}{2})$ is $90°$ counter clock wise rotation matrix and

$\dot{\boldsymbol{r}}_k^* = \frac{d}{dt}(\boldsymbol{r}_0 + d_k^* \boldsymbol{G}_0[\cos(\psi_0 + \phi_k^*), \sin(\psi_0 + \phi_k^*)]^T)$.

Note that $\dot{\boldsymbol{r}}_k^*$ and $\mathscr{F}_k$ are agent-k's desired velocity and angular velocity, respectively, where $\dot{\boldsymbol{r}}_k^*$ is from 3.2 and the derivation of $\mathscr{F}_k$ refers to [35].

Remark 3.3. *Assumption 3.1 ensures that the reference information can be passed on to each agent. Assumption 3.2-Assumption 3.4 provide feasibility condition for tracking. The first inequality in Assumption 3.5 states that the agents' desired velocities never vanish which prevents the occurrence of singularities along agents' desired trajectories. Moreover, the inequalities of $v^+, \omega^+, v^-, \omega^-$ in Assumption 3.5 are used to guarantee that the agents can track their desired trajectories based on larger input ranges.*

3.4 Controller Design and Stability Analysis

The considered problem will be solved with three steps in the following subsections, respectively. First, in Section 3.4.1, we propose a distributed adaptive estimation of the desired unit center vectors $\boldsymbol{c}_k^*$ for $k \in \mathcal{N}$. Recall that $\boldsymbol{c}_k^*$ is for MAS orientation alignment task, while it contains ψ_0 which is only accessible to few agents under Assumption 3.1. Thus, a distributed adaptive estimation is designed to estimate $\boldsymbol{c}_k^*$ from the given ϕ_{kj}^*. Second, in Section 3.4.2, we design distributed consensus algorithms and an observer for each

24

agent to estimate the reference centroid velocity $\dot{r}_0$, reference affine transformation command G_0, and the position errors with respect to desired position. At last, in Section 3.4.3, we derive a constrained controller based on coordinate transformation to achieve (3.2) based on the estimations in the first and second steps.

For consistence, we denote the reference information as agent-0 whose dynamics is $\dot{r}_0 = v_0[\cos\psi_0, \sin\psi_0]^T, \dot{\psi}_0 = \omega_0$. Then, define $\bar{N}_k$ as the extended set of N_k which additionally considers whether agent-k can receive information from agent-0 or not. Besides, let $R(\phi) \in \mathbb{R}^{2\times 2}$ be counterclockwise planar rotation matrix with given angle ϕ, I_2 be the 2-by-2 identity matrix, and $\otimes$ be the Kronecker product. Before proceeding to the three design steps, we first state the following lemma which is a byproduct of Assumption 3.1 and will be used in the stability proof of our design.

Lemma 3.1. *Given a directed communication graph $\mathcal{G}$ with its corresponding Laplacian matrix L and the diagonal matrix B where entries b_{kk} is 1 if agent-k can access to the reference signals and 0 otherwise. Then, under Assumption 3.1, all eigenvalues of $\bar{L} :=$ $L + B$ are positive.*

Proof. First, from the Gershgorin's Theorem, all of the eigenvalues of L and $L+B$ are at least nonnegative. As a result, it's sufficient to prove that no eigenvalue of $L + B$ equals 0. In the following, we prove it by contra-positive.

Suppose there exists an eigenvector $v \neq 0$ such that $(L + B)v = 0$. This implies that $v^T(L^T + B^T + L + B)v = 0$. Since $L^T + L$ is irreducible and $B^T + B(= 2B)$ has at least one positive diagonal entry, by Lemma 4 of [41], $L^T + B^T + L + B$ is positive definite which leads to the conclusion of $v = 0$. We have a contradiction. ∎

Now, we are ready to give the three design steps in the following subsections.

25

3.4.1 Adaptive Estimation of Desired Unit Center Vector c_k^*

Recall that $\boldsymbol{c}_k^* = [\cos(\psi_0 + \phi_k^*), \sin(\psi_0 + \phi_k^*)]^T$ stands for the MAS orientation alignment task, where $\boldsymbol{c}_k^*$ cannot be pre-given since it varies with ψ_0. With distributed links and Assumption 3.1, ψ_0 is not accessible to all agents, as a result, we need to estimate $\boldsymbol{c}_k^*$. Let $\hat{\boldsymbol{c}}_k \in \mathbb{R}^2$ be the estimation of $\boldsymbol{c}_k^*$ for $k \in \mathcal{N}$. Observe that $\boldsymbol{c}_k^*$ and $\boldsymbol{c}_j^*$ have desired relative phase ϕ_{kj}^* which is the known description of desired geometric pattern. As a result, one can feedback the estimation errors between $\hat{\boldsymbol{c}}_k$ and neighbors' estimations rotating with phases of ϕ_{kj}^*. In the following lemma, a distributed adaptive estimation of $\hat{\boldsymbol{c}}_k$ is proposed based on available measurements through $\mathcal{G}$ and ϕ_{kj}^*.

Lemma 3.2. *Given the communication graph $\mathcal{G}$, ψ_0, and constant ϕ_k^* for $k \in \mathcal{N}$. With Assumption 3.1-Assumption 3.3, and the distributed update law*

$$\dot{\hat{\boldsymbol{c}}}_k = \hat{\boldsymbol{z}}_k$$

$$\dot{\hat{\boldsymbol{z}}}_k = \frac{1}{|\bar{N}_k|} \sum_{j \in \bar{N}_k} \boldsymbol{R}(\phi_{kj}^*) \dot{\hat{\boldsymbol{z}}}_j + \frac{\alpha_1}{|\bar{N}_k|} \sum_{j \in \bar{N}_k} (\boldsymbol{R}(\phi_{kj}^*) \hat{\boldsymbol{z}}_j - \hat{\boldsymbol{z}}_k)$$

$$+ \frac{\alpha_2}{|\bar{N}_k|} \sum_{j \in \bar{N}_k} (\boldsymbol{R}(\phi_{kj}^*) \hat{\boldsymbol{c}}_j - \hat{\boldsymbol{c}}_k), \tag{3.3}$$

$\hat{\boldsymbol{c}}_k$ will converge to $[\cos(\psi_0 + \phi_k^*), \sin(\psi_0 + \phi_k^*)]^T (= \boldsymbol{c}_k^*)$ exponentially, for $k \in \mathcal{N}$, where $\alpha_i > 0, i = 1, 2$ are arbitrarily chosen constants. Moreover, $\phi_{k0}^* = \phi_k^*$, $\hat{\boldsymbol{z}}_0 = \dot{\hat{\boldsymbol{c}}}_0$, $\dot{\hat{\boldsymbol{z}}}_0 = \ddot{\hat{\boldsymbol{c}}}_0$, and $\hat{\boldsymbol{c}}_0 = [\cos\psi_0, \sin\psi_0]^T$, since agent-$0$ represents the reference information.

Proof. Let $\boldsymbol{p}_k = \boldsymbol{R}(-\phi_k^*)\hat{\boldsymbol{c}}_k$ and $\boldsymbol{q}_k = \boldsymbol{R}(-\phi_k^*)\dot{\hat{\boldsymbol{c}}}_k, \forall k \in \mathcal{N}$. Pre-multiply $\boldsymbol{R}(-\phi_k^*)$ to both sides of (3.3), then (3.3) is transformed into

$$\dot{\boldsymbol{p}}_k = \boldsymbol{q}_k$$

26

$$\dot{\boldsymbol{q}}_k = \frac{1}{|\bar{N}_k|} \sum_{j \in \bar{N}_k} \left[\dot{\boldsymbol{q}}_j + \alpha_1(\boldsymbol{q}_j - \boldsymbol{q}_k) + \alpha_2(\boldsymbol{p}_j - \boldsymbol{p}_k) \right]. \tag{3.4}$$

Slightly abuse the notation $\boldsymbol{p}_0 := \boldsymbol{R}(0)\hat{\boldsymbol{c}}_0 = [\cos\psi_0, \sin\psi_0]^T$, and define the transformed estimation error $\bar{\boldsymbol{p}}_k = \boldsymbol{p}_k - \boldsymbol{p}_0, \forall k \in \mathcal{N}$. Stack the errors into the error vector $\bar{\boldsymbol{p}} := [\bar{\boldsymbol{p}}_1^T, \ldots, \bar{\boldsymbol{p}}_N^T]^T \in \mathbb{R}^{2N}$. Then, we define the relative error vector, $\tilde{\boldsymbol{p}} = (\bar{\boldsymbol{L}} \otimes \boldsymbol{I}_2)\bar{\boldsymbol{p}} \in \mathbb{R}^{2N}$, which refers to the communications. With these definitions, (3.4) is expressed as $\ddot{\tilde{\boldsymbol{p}}} + \alpha_1 \dot{\tilde{\boldsymbol{p}}} + \alpha_2 \tilde{\boldsymbol{p}} = \boldsymbol{0}$. Due to Hurwitz property, $\tilde{\boldsymbol{p}}$ converges to $\boldsymbol{0}$ exponentially. Moreover, Lemma 3.1 states that $\bar{\boldsymbol{L}}$ is invertible which leads to the exponential convergence of $\bar{\boldsymbol{p}} \to \boldsymbol{0}$. As a result, $\hat{\boldsymbol{c}}_k \to [\cos(\psi_0 + \phi_k^*), \sin(\psi_0 + \phi_k^*)]^T$ exponentially. ∎

Remark 3.4. *In Lemma 3.2, we set $\hat{\boldsymbol{c}}_0$ to be $[\cos\psi_0, \sin\psi_0]^T$ which is the unit reference trajectory velocity, and this leads to the natural tracking movement scenario. More generally, in fact, the variable ψ_0 in $\hat{\boldsymbol{c}}_0$ can be arbitrarily assigned, such as a constant, a predefined signal, or a signal related to ψ_0, as long as it is common among agents. For example, the constant case cover the results in [22, 37–39], and the predefined signal case covers the results in [23, 26, 40]. In other words, our novel approach can determine the MAS movements in general while tracking.*

3.4.2 Consensus Algorithms and Distributed Observer

The desired center vector $\boldsymbol{c}_k^*$ is estimated by $\hat{\boldsymbol{c}}_k$ in previous section, which is used to determine the desired position error in this section. Recall the objective (3.2), then define desired position error

$$\boldsymbol{e}_k := \boldsymbol{r}_0 - \boldsymbol{r}_k + d_k^* \boldsymbol{G}_0 \boldsymbol{c}_k^*, \tag{3.5}$$

for $k \in \mathcal{N}$. Again consider the distributed links under Assumption 3.1, since the reference velocity v_0, ψ_0, and the reference affine transformation $\boldsymbol{G}_0$ are only accessible to a few

agents, as a result, $\hat{v}_k$, $\hat{\psi}_k$, and $\hat{\boldsymbol{G}}_k$ are introduced to estimate v_0, ψ_0, and $\boldsymbol{G}_0$, respectively. Note that with the above estimations, we can have the estimation of error dynamics $\dot{\boldsymbol{e}}_k$. Thus, the estimated desired position error $\hat{\boldsymbol{e}}_k$ is introduced with a distributed observer to estimate $\boldsymbol{e}_k$. The distributed consensus algorithms and the observer are derived in the following lemma.

Lemma 3.3. *Given the graph $\mathcal{G}$, the descriptions of desired geometric pattern $\{d_k^*, \phi_{kj}^*\}$, the smooth reference centroid trajectory $\boldsymbol{r}_0$, and the smooth reference affine transformation command $\boldsymbol{G}_0$. With Assumption 3.1-Assumption 3.3, the distributed control laws*

$$\dot{\hat{v}}_k = \frac{1}{|\bar{N}_k|} \sum_{j \in \bar{N}_k} \dot{\hat{v}}_j + \frac{\beta_1}{|\bar{N}_k|} \sum_{j \in \bar{N}_k} (\hat{v}_j - \hat{v}_k) \tag{3.6}$$

$$\dot{\hat{\psi}}_k = \frac{1}{|\bar{N}_k|} \sum_{j \in \bar{N}_k} \dot{\hat{\psi}}_j + \frac{\beta_2}{|\bar{N}_k|} \sum_{j \in \bar{N}_k} (\hat{\psi}_j - \hat{\psi}_k) \tag{3.7}$$

$$\ddot{\hat{\boldsymbol{G}}}_k = \frac{1}{|\bar{N}_k|} \sum_{j \in \bar{N}_k} \left[\ddot{\hat{\boldsymbol{G}}}_j + \beta_3(\dot{\hat{\boldsymbol{G}}}_j - \dot{\hat{\boldsymbol{G}}}_k) + \beta_4(\hat{\boldsymbol{G}}_j - \hat{\boldsymbol{G}}_k) \right] \tag{3.8}$$

$$\dot{\hat{\boldsymbol{e}}}_k = \beta_5 \sum_{j \in \bar{N}_k} \left[\hat{\boldsymbol{e}}_j - \hat{\boldsymbol{e}}_k + \boldsymbol{r}_j - \boldsymbol{r}_k + d_k^* \hat{\boldsymbol{G}}_k \hat{\boldsymbol{c}}_k - d_j^* \hat{\boldsymbol{G}}_j \hat{\boldsymbol{c}}_j \right]$$
$$+ \hat{v}_k \boldsymbol{u}(\hat{\psi}_k) - v_k \boldsymbol{u}(\psi_k) + d_k^* \hat{\boldsymbol{G}}_k \dot{\hat{\boldsymbol{c}}}_k + d_k^* \dot{\hat{\boldsymbol{G}}}_k \hat{\boldsymbol{c}}_k \tag{3.9}$$

drive $\hat{v}_k \to v_0$, $\hat{\psi}_k \to \psi_0$, $\dot{\hat{\psi}}_k \to \omega_0$, $\hat{\boldsymbol{G}}_k \to \boldsymbol{G}_0$, $\dot{\hat{\boldsymbol{G}}}_k \to \dot{\boldsymbol{G}}_0$, and $\hat{\boldsymbol{e}}_k \to \boldsymbol{e}_k$ exponentially, for $k \in \mathcal{N}$, where $\boldsymbol{u}(\psi) = [\cos\psi, \sin\psi]^T$, $\beta_i > 0, i = 1, \ldots, 5$. Moreover, $\dot{\hat{v}}_0$, $\hat{v}_0$, $\dot{\hat{\psi}}_0$, $\hat{\psi}_0$, $\ddot{\hat{\boldsymbol{G}}}_0$, $\dot{\hat{\boldsymbol{G}}}_0$, $\hat{\boldsymbol{G}}_0$, $\hat{\boldsymbol{e}}_0$, d_0^* equal to $\dot{v}_0, v_0, \dot{\psi}_0, \psi_0, \ddot{\boldsymbol{G}}_0, \dot{\boldsymbol{G}}_0, \boldsymbol{G}_0, [0, 0]^T, 0$, respectively, since agent-0 represents the reference information.

Proof. Define estimated linear velocity error $\bar{v}_k = \hat{v}_k - v_0, \forall k \in \mathcal{N}$, and stack the errors into the vector $\bar{\boldsymbol{v}} = [\bar{v}_1, \ldots, \bar{v}_N]^T \in \mathbb{R}^N$. Then, we define the relative linear velocity error vector $\tilde{\boldsymbol{v}} = \bar{\boldsymbol{L}}\bar{\boldsymbol{v}} \in \mathbb{R}^N$. With these definitions, (3.6) is expressed as $\dot{\tilde{\boldsymbol{v}}} + \beta_1\tilde{\boldsymbol{v}} = \boldsymbol{0}$, which implies $\tilde{\boldsymbol{v}} \to \boldsymbol{0}$ exponentially. Moreover, Lemma 3.1 states that $\bar{\boldsymbol{L}}$ is invertible which leads

28

to $\bar{v} \to \mathbf{0}$ exponentially. Similarly, (3.7) and (3.8) prove that $\hat{\psi}_k \to \psi_0$ and $\hat{G}_k \to G_0$ exponentially, respectively.

Base on above convergence analysis, Lemma 3.2, and eq. (3.9), now we are ready to prove that $\hat{e}_k \to e_k$ exponentially. Define $\boldsymbol{\epsilon} = [\boldsymbol{\epsilon}_1^T, \ldots, \boldsymbol{\epsilon}_N^T]^T \in \mathbb{R}^{2N}$ where $\boldsymbol{\epsilon}_k = \hat{e}_k - e_k - d_k^*(\hat{G}_k \hat{c}_k - G_0 c_k^*) \in \mathbb{R}^2$ and $\boldsymbol{\delta} = [\boldsymbol{\delta}_1^T, \ldots, \boldsymbol{\delta}_N^T]^T \in \mathbb{R}^{2N}$ where $\boldsymbol{\delta}_k = \hat{v}_k \boldsymbol{u}(\hat{\psi}_k) - v_0 \boldsymbol{u}(\psi_0) \in \mathbb{R}^2$ for $k \in \mathcal{N}$. Then, (3.9) can be expressed as

$$\dot{\boldsymbol{\epsilon}} = -\beta_5(\bar{L} \otimes I_2)\boldsymbol{\epsilon} + \boldsymbol{\delta}, \tag{3.10}$$

with the following property:

$$||\boldsymbol{\delta}_k|| = ||(\hat{v}_k - v_0)\boldsymbol{u}(\hat{\psi}_k) - v_0(\boldsymbol{u}(\psi_0) - \boldsymbol{u}(\hat{\psi}_k))|| \leq ||\hat{v}_k - v_0|| + |v_0|||\boldsymbol{u}(\psi_0) - \boldsymbol{u}(\hat{\psi}_k)||$$

$$\leq ||\hat{v}_k - v_0|| + \sqrt{2}v^+||\hat{\psi}_k - \psi_0||, \tag{3.11}$$

where the last inequality is by Assumption 3.2 and Lipschitz continuous of $\sin, \cos$. As a result, $\boldsymbol{\delta} \to \mathbf{0}$ exponentially due to exponential convergences of $\hat{v}_k$ and $\hat{\psi}_k$. Moreover, by Lemma 3.1, $-(\bar{L} \otimes I_2)$ is Hurwitz. These two facts ensure $\boldsymbol{\epsilon} \to \mathbf{0}$ exponentially by (3.10). Recall that $\hat{c}_k \to c_k^*$ exponentially by Lemma 3.2 and $\hat{G}_k \to G_0$. Thus, from the definition of $\boldsymbol{\epsilon}_k$, we prove that $\hat{e}_k \to e_k$ exponentially. ∎

Remark 3.5. *In fact, (3.3), (3.6), (3.7), (3.8), and (3.9) are given and analyzed in a global reference frame. Here, we demonstrate that the control laws can be equivalently realized in agents' local frames. Suppose agent-k's local frame has a "unknown" orientation $\mathcal{O}_k$ relative to the global frame, and denote superscript k as the obtainable measurements for agent-k in its local frame, which has the relation to measurement in global reference frame: $\hat{z}_k^k = \boldsymbol{R}(-\mathcal{O}_k)\hat{z}_k$. Then, we have the coordinate transform relations, e.g.,*

29

$\dot{\boldsymbol{z}}_j^k = \boldsymbol{R}(-\mathcal{O}_{kj})\dot{\boldsymbol{z}}_j^j$ and $\hat{\boldsymbol{G}}_j^k = \boldsymbol{R}(-\mathcal{O}_{kj})\hat{\boldsymbol{G}}_j^j\boldsymbol{R}(\mathcal{O}_{kj})$, where $\mathcal{O}_{kj} = \mathcal{O}_k - \mathcal{O}_j$ is the relative orientation accessible to agent-k. Thanks to these relations, agent-j's information measured in agent-k's local frame is obtainable through communications and $\mathcal{O}_{kj}$ without requiring $\mathcal{O}_k$. Pre-multiply $\boldsymbol{R}(-\mathcal{O}_k)$ or post-multiply $\boldsymbol{R}(\mathcal{O}_k)$ to both sides of the control laws (3.3), (3.6), (3.7), (3.8), and (3.9), then the control laws are equivalently realized in each agent's local frame as

$$\dot{\hat{\boldsymbol{c}}}_k^k = \hat{\boldsymbol{z}}_k^k$$

$$\dot{\hat{\boldsymbol{z}}}_k^k = \frac{1}{|\bar{N}_k|}\sum_{j\in\bar{N}_k}\boldsymbol{R}(\phi_{kj}^*)\dot{\hat{\boldsymbol{z}}}_j^k + \frac{\alpha_1}{|\bar{N}_k|}\sum_{j\in\bar{N}_k}(\boldsymbol{R}(\phi_{kj}^*)\hat{\boldsymbol{z}}_j^k - \hat{\boldsymbol{z}}_k^k)$$
$$+ \frac{\alpha_2}{|\bar{N}_k|}\sum_{j\in\bar{N}_k}(\boldsymbol{R}(\phi_{kj}^*)\hat{\boldsymbol{c}}_j^k - \hat{\boldsymbol{c}}_k^k) \tag{3.12}$$

$$\dot{\hat{v}}_k = \frac{1}{|\bar{N}_k|}\sum_{j\in\bar{N}_k}\dot{\hat{v}}_j + \frac{\beta_1}{|\bar{N}_k|}\sum_{j\in\bar{N}_k}(\hat{v}_j - \hat{v}_k) \tag{3.13}$$

$$\dot{\hat{\psi}}_k^k = \frac{1}{|\bar{N}_k|}\sum_{j\in\bar{N}_k}\dot{\hat{\psi}}_j^k + \frac{\beta_2}{|\bar{N}_k|}\sum_{j\in\bar{N}_k}(\hat{\psi}_j^k - \hat{\psi}_k^k) \tag{3.14}$$

$$\ddot{\hat{\boldsymbol{G}}}_k^k = \frac{1}{|\bar{N}_k|}\sum_{j\in\bar{N}_k}\left[\ddot{\hat{\boldsymbol{G}}}_j^k + \beta_3(\dot{\hat{\boldsymbol{G}}}_j^k - \dot{\hat{\boldsymbol{G}}}_k^k) + \beta_4(\hat{\boldsymbol{G}}_j^k - \hat{\boldsymbol{G}}_k^k)\right] \tag{3.15}$$

$$\dot{\hat{\boldsymbol{e}}}_k^k = \beta_5\sum_{j\in\bar{N}_k}\left[\hat{\boldsymbol{e}}_j^k - \hat{\boldsymbol{e}}_k^k + \boldsymbol{r}_{jk}^k + d_k^*\hat{\boldsymbol{G}}_k^k\hat{\boldsymbol{c}}_k^k - d_j^*\hat{\boldsymbol{G}}_j^k\hat{\boldsymbol{c}}_j^k\right]$$
$$+ \hat{v}_k\boldsymbol{u}(\hat{\psi}_k^k) - v_k\boldsymbol{u}(\psi_k^k) + d_k^*\hat{\boldsymbol{G}}_k^k\dot{\hat{\boldsymbol{c}}}_k^k + d_k^*\dot{\hat{\boldsymbol{G}}}_k^k\hat{\boldsymbol{c}}_k^k\ , \tag{3.16}$$

respectively, where all the signals are obtainable locally or through $\mathcal{G}$. Note that in (3.13), we omit the superscript since the velocity magnitude is irrelevant to frames.

3.4.3 Lyapunov-Based Constrained Controller

Our last step is to design the constrained control law which steers the estimated position error $\hat{\boldsymbol{e}}_k \to 0$ for $k \in \mathcal{N}$. Then, with the aid of $\hat{\boldsymbol{e}}_k \to \boldsymbol{e}_k$ in Lemma 3.3, $\boldsymbol{e}_k \to 0$ is

30

achieved. A design method is by second order dynamics equation, $\ddot{\hat{e}}_k + a_1 \dot{\hat{e}}_k + a_2 \hat{e}_k = \mathbf{0}$ with $a_1, a_2 > 0$, as in [17]. The feasibility is guaranteed because the equation can be rearranged into $\dot{v}_k \boldsymbol{u}(\psi_k) + \omega_k v_k \boldsymbol{R}(\frac{\pi}{2})\boldsymbol{u}(\psi_k) = \boldsymbol{f}(\cdot)$ where $\boldsymbol{f}(\cdot)$ is not a function of $\dot{v}_k$ and ω_k. Thus, $\dot{v}_k$ and ω_k are designed as $\boldsymbol{f}^T \boldsymbol{u}$ and $\frac{1}{v_k} \boldsymbol{f}^T(\boldsymbol{R}\boldsymbol{u})$, respectively. However, v_k may be close to 0 which makes ω_k large, namely, saturation is not addressed in such design. As a result, a coordination transformation is applied in our design where the saturation of v_k and ω_k can be directly dealt with, since the transformation decouples control inputs v_k and ω_k. To facilitate the design, we first recall agent-k's desired velocity $\dot{\boldsymbol{r}}_k^* = \frac{d}{dt}(\boldsymbol{r}_0 + d_k^* \boldsymbol{G}_0 \boldsymbol{c}_k^*)$ defined in Assumption 3.5 and transform it into unicycle model form.

Let $\check{v}_k^*[\cos \check{\psi}_k^*, \sin \check{\psi}_k^*]^T$ with $\dot{\check{\psi}}_k^* (= \check{\omega}_k^*)$ be the unicycle form of agent-k's desired velocity $v_0 \boldsymbol{u}(\psi_0) + d_k^* \boldsymbol{G}_0 \dot{\boldsymbol{c}}_k^* + d_k^* \dot{\boldsymbol{G}}_k \boldsymbol{c}_k^*$. Besides, let $\check{v}_k[\cos \check{\psi}_k, \sin \check{\psi}_k]^T$ with $\dot{\check{\psi}}_k (= \check{\omega}_k)$ be the unicycle form of $\hat{v}_k \boldsymbol{u}(\hat{\psi}_k) + d_k^* \hat{\boldsymbol{G}}_k \dot{\hat{\boldsymbol{c}}}_k + d_k^* \dot{\hat{\boldsymbol{G}}}_k \hat{\boldsymbol{c}}_k$. While desired $\check{v}_k^*$ and $\check{\omega}_k^*$ are not obtainable, $\check{v}_k$ and $\check{\omega}_k$ are the accessible estimated signals which will exponentially converge to $\check{v}_k^*$ and $\check{\omega}_k^*$, respectively, since $\hat{v}_k \boldsymbol{u}(\hat{\psi}_k) + d_k^* \hat{\boldsymbol{G}}_k \dot{\hat{\boldsymbol{c}}}_k + d_k^* \dot{\hat{\boldsymbol{G}}}_k \hat{\boldsymbol{c}}_k$ exponentially converges to $v_0 \boldsymbol{u}(\psi_0) + d_k^* \boldsymbol{G}_0 \dot{\boldsymbol{c}}_k^* + d_k^* \dot{\boldsymbol{G}}_k \boldsymbol{c}_k^*$ by Lemma 3.2 and Lemma 3.3.

Remark 3.6. *If $\hat{v}_k \boldsymbol{u}(\hat{\psi}_k) + d_k^* \hat{\boldsymbol{G}}_k \dot{\hat{\boldsymbol{c}}}_k + d_k^* \dot{\hat{\boldsymbol{G}}}_k \hat{\boldsymbol{c}}_k$ does not vanish, then $\check{\omega}_k$ exists. Due to its exponential convergence to agent-k's desired reference velocity $\boldsymbol{c}_k^*$, which satisfies Assumption 3.5, there exists a finite time T such that $||\hat{v}_k \boldsymbol{u}(\hat{\psi}_k) + d_k^* \hat{\boldsymbol{G}}_k \dot{\hat{\boldsymbol{c}}}_k + d_k^* \dot{\hat{\boldsymbol{G}}}_k \hat{\boldsymbol{c}}_k|| > 0$ for $t \geq T$. Moreover, a small compensate signal $\boldsymbol{\Delta}$ with bounded $\dot{\boldsymbol{\Delta}}$ can add to $\hat{v}_k \boldsymbol{u}(\hat{\psi}_k) + d_k^* \hat{\boldsymbol{G}}_k \dot{\hat{\boldsymbol{c}}}_k + d_k^* \dot{\hat{\boldsymbol{G}}}_k \hat{\boldsymbol{c}}_k$ to prevent it from vanishing for $t < T$ and guarantee the existence of $\check{\omega}_k$. As a result, an analysis of small perturbation in finite time period will be involved in Theorem 3.1.*

With the unicycle form of agents' desired velocities, we can derive the transformation as follows. Define $[\tilde{x}_k, \tilde{y}_k]^T := \boldsymbol{R}(-\psi_k)\hat{e}_k \in \mathbb{R}^2$ as the transformed desired position error

31

with respect to agent-k's moving direction modeled in (3.1), and $\tilde{\psi}_k := \check{\psi}_k - \psi_k \in \mathbb{R}$ as

agent-k's heading error. Then, the error dynamics of $[\tilde{x}_k, \tilde{y}_k, \tilde{\psi}_k]^T$ is derived with (3.9) as

$$
\begin{bmatrix} \dot{\tilde{x}}_k \\ \dot{\tilde{y}}_k \\ \dot{\tilde{\psi}}_k \end{bmatrix} = \begin{bmatrix} \omega_k \tilde{y}_k + \check{v}_k \cos \tilde{\psi}_k - v_k \\ -\omega_k \tilde{x}_k + \check{v}_k \sin \tilde{\psi}_k \\ \check{\omega}_k - \omega_k \end{bmatrix} + \begin{bmatrix} g_k^x \\ g_k^y \\ 0 \end{bmatrix}, \tag{3.17}
$$

where $[g_k^x, g_k^y]^T = \beta_5 \boldsymbol{R}(-\psi_k) \sum_{j \in \bar{N}_k} (\hat{\boldsymbol{e}}_j - \hat{\boldsymbol{e}}_k + \boldsymbol{r}_j - \boldsymbol{r}_k + d_k^* \hat{\boldsymbol{G}}_k \hat{\boldsymbol{c}}_k - d_j^* \hat{\boldsymbol{G}}_j \hat{\boldsymbol{c}}_j) \in \mathbb{R}^2$, for

$k \in \mathcal{N}$. Define the considered space χ for the error state $[\tilde{x}_k, \tilde{y}_k, \tilde{\psi}_k]^T$:

$$
\chi = \left\{ (\tilde{x}_k, \tilde{y}_k, \tilde{\psi}_k) | \tilde{x}_k \in \mathbb{R}, \tilde{y}_k \in \mathbb{R}, \tilde{\psi}_k \in (-\pi, \pi] \right\} \tag{3.18}
$$

As shorthands, the first and second part in the right hand side of (3.17) are denoted as

$\boldsymbol{F}_k(\cdot)$ and $\boldsymbol{g}_k(\cdot)$, respectively. In the following, we first consider $\boldsymbol{g}_k(\cdot)$ as a perturbation

and design v_k and ω_k in (3.17) with $\boldsymbol{g}_k(\cdot) \equiv \boldsymbol{0}$. Then, we prove that $\boldsymbol{g}_k(\cdot)$ asymptotically

converges. Note that the perturbation term contains state information, to rigorously prove

the convergence of (3.17), a supporting lemma is given as follows.

Lemma 3.4 ([42]). *Consider (3.17). Suppose (i) the unforced system, i.e., with $\boldsymbol{g}_k(\cdot) \equiv \boldsymbol{0}$,*

is GAS in χ, (ii) $\boldsymbol{g}_k(\cdot)$ globally asymptotically converges to $\boldsymbol{0}$ in χ, and (iii) the solution of

(3.17) is bounded. Then, the system (3.17) is globally asymptotically stable (GAS) in χ.

Proof. By Converging Input Bounded State (CIBS) property in [42]. ∎

Now, the main controller design is stated in the following theorem.

Theorem 3.1. *Given the communication graph $\mathcal{G}$, the descriptions of desired geometric*

pattern $\{d_k^*, \phi_{kj}^*\}$, the smooth reference centroid trajectory $\boldsymbol{r}_0$, the desired relative phase

ϕ_k^* between $\boldsymbol{c}_k$ and $\dot{\boldsymbol{r}}_0$, $\forall k \in \mathcal{N}$, and the smooth reference affine transformation command

32

$\boldsymbol{G}_0$. *If Assumption 3.1-Assumption 3.5 are hold, then by the control laws (3.12)-(3.16),*

and the constrained control input

$$\omega_k = \boldsymbol{sat}_{\mathcal{W}}(\breve{\omega}_k) + \frac{\boldsymbol{sat}_{\mathcal{V}}(\breve{v}_k)\tilde{y}_k(2 - \cos\tilde{\psi}_k)}{\gamma_1 + \frac{1}{2}\tilde{x}_k^2 + \frac{1}{2}\tilde{y}_k^2} + \boldsymbol{sat}_{\vartheta}(\gamma_2 \sin\tilde{\psi}_k)$$

$$v_k = \boldsymbol{sat}_{\mathcal{V}}(\breve{v}_k)\cos\tilde{\psi}_k + \boldsymbol{sat}_{\mathcal{X}}(\gamma_3\tilde{x}_k), \tag{3.19}$$

the control objective (3.2) is achieved via distributed measurements in each agent's local

frame, for $k \in \mathcal{N}$, where $\boldsymbol{sat}_{\mathcal{I}}(c)$ is a saturation function which projects scalar c into the

saturated interval $\mathcal{I} = [\mathcal{I}^-, \mathcal{I}^+]$, that is,

$$\boldsymbol{sat}_{\mathcal{I}}(c) = \begin{cases} \mathcal{I}^-, & \text{if } c < \mathcal{I}^- \\ c, & \text{if } \mathcal{I}^- \leq c \leq \mathcal{I}^+ \\ \mathcal{I}^+, & \text{if } c > \mathcal{I}^+ \end{cases} \cdot$$

The intervals in (3.19) are given as $\mathcal{W} = [\breve{\omega}^-, \breve{\omega}^+]$, $\mathcal{V} = [\breve{v}^-, \breve{v}^+]$, $\mathcal{X} = [-v_{gap}, v_{gap}]$

where $v_{gap} = \min\{\breve{v}^- - v^-, v^+ - \breve{v}^+\}$. Besides, γ_2, γ_3 are arbitrary positive constants,

while interval ϑ and positive constant γ_1 are design parameters to ensure $\omega_k \in [\omega^-, \omega^+]$.

Before proceeding to the proof, we provide two notes. The first is that the bound

of the term $\frac{\tilde{y}_k}{\gamma_1 + \frac{1}{2}\tilde{x}_k^2 + \frac{1}{2}\tilde{y}_k^2}$ in angular velocity input ω_k can be designed in advance based

on γ_1. The other is that the saturation function to $\breve{\omega}_k$ and $\breve{v}_k$ may be active, since they

are alternatives to $\breve{\omega}_k^*$ and $\breve{v}_k^r$, respectively, which are not the same initially and thus may

exceed the saturation intervals.

Proof. Rewrite (3.17) and add a small perturbation $\tilde{\boldsymbol{\Delta}}_k$ with bounded $\dot{\tilde{\boldsymbol{\Delta}}}_k$ in finite time

33

period as mentioned in Remark 3.6, then we have

$$
\begin{bmatrix} \dot{\tilde{x}}_k \\ \dot{\tilde{y}}_k \\ \dot{\tilde{\psi}}_k \end{bmatrix} = \begin{bmatrix} \omega_k \tilde{y}_k + \boldsymbol{sat}_{\mathcal{V}}(\breve{v}_k)\cos\tilde{\psi}_k - v_k \\ -\omega_k \tilde{x}_k + \boldsymbol{sat}_{\mathcal{V}}(\breve{v}_k)\sin\tilde{\psi}_k \\ \boldsymbol{sat}_{\mathcal{W}}(\breve{\omega}_k) - \omega_k \end{bmatrix} + \begin{bmatrix} g_k^x \\ g_k^y \\ 0 \end{bmatrix} + \begin{bmatrix} [\breve{v}_k - \boldsymbol{sat}_{\mathcal{V}}(\breve{v}_k)]\cos\tilde{\psi}_k \\ [\breve{v}_k - \boldsymbol{sat}_{\mathcal{V}}(\breve{v}_k)]\sin\tilde{\psi}_k \\ \breve{\omega}_k - \boldsymbol{sat}_{\mathcal{W}}(\breve{\omega}_k) \end{bmatrix} + \tilde{\boldsymbol{\Delta}}_k
$$

$$
:= \boldsymbol{f}_k(\cdot) + \boldsymbol{g}_k(\cdot) + \boldsymbol{s}_k(\cdot) + \tilde{\boldsymbol{\Delta}}_k(\cdot), \tag{3.20}
$$

where the first term $\boldsymbol{f}_k(\cdot)$ is viewed as the unforced system with the rest three being perturbed inputs, $\boldsymbol{g}_k(\cdot)$, $\boldsymbol{s}_k(\cdot)$, and $\tilde{\boldsymbol{\Delta}}_k(\cdot)$. Note that the perturbed error $\boldsymbol{g}_k$ comes from estimation error, the perturbed error $\boldsymbol{s}_k$ is due to saturation, and the perturbed error $\tilde{\boldsymbol{\Delta}}_k$ derives from singularity error. In the following, the proof is given in three steps. First, we prove that the unforced system is GAS by constrained control law (3.19) with $\boldsymbol{g}_k(\cdot) = \boldsymbol{s}_k(\cdot) = \tilde{\boldsymbol{\Delta}}_k(\cdot) \equiv \boldsymbol{0}$, that is, the three kinds of error are reduced to $\boldsymbol{0}$. Second, the asymptotically convergences of three perturbed inputs are proved. Third, we derive the boundedness of solutions to (3.20). Then, Lemma 3.4 is applied to prove the GAS of (3.20) in χ.

Consider the unforced system of (3.20), *i.e.*, with $\boldsymbol{g}_k(\cdot) = \boldsymbol{s}_k(\cdot) = \tilde{\boldsymbol{\Delta}}_k(\cdot) \equiv \boldsymbol{0}$, and propose a Lyapunov function candidate V_k:

$$
V_k = \frac{1}{2}(\tilde{x}_k^2 + \tilde{y}_k^2) + (\gamma_1 + \frac{1}{2}\tilde{x}_k^2 + \frac{1}{2}\tilde{y}_k^2)(1 - \cos\tilde{\psi}_k), \tag{3.21}
$$

to prove GAS of unforced system. Derive its derivatives

$$
\dot{V}_k = \left[\boldsymbol{sat}_{\mathcal{V}}(\breve{v}_k)\cos\tilde{\psi}_k - v_k\right]a_k\tilde{x}_k + b_k\sin\tilde{\psi}_k\left[\boldsymbol{sat}_{\mathcal{W}}(\breve{\omega}_k) - \omega_k + \frac{\boldsymbol{sat}_{\mathcal{V}}(\breve{v}_k)a_k\tilde{y}_k}{b_k}\right]
$$

$$
= -a_k\tilde{x}_k\boldsymbol{sat}_{\mathcal{X}}(\gamma_3\tilde{x}_k) - b_k\sin\tilde{\psi}_k\boldsymbol{sat}_{\vartheta}(\gamma_2\sin\tilde{\psi}_k), \tag{3.22}
$$

34

where $a_k = 2 - \cos\tilde{\psi}_k > 0, b_k = (\gamma_1 + \frac{1}{2}\tilde{x}_k^2 + \frac{1}{2}\tilde{y}_k^2) > 0$. Suppose the interval $\mathcal{I}$ lies from negative to positive, then $c\,\boldsymbol{sat}_\mathcal{I}(c) \geq 0$ and $c\,\boldsymbol{sat}_\mathcal{I}(c) = 0$ if and only if $c = 0$. Thus, V_k is lower bounded and $\dot{V}_k \leq 0$. Moreover, the function $f(x) := x\,\boldsymbol{sat}_\mathcal{I}(x)$ is proved to be uniformly continuous by the definition, which leads to uniform continuity of $\dot{V}_k$. As a result, by Lyapunov-like lemma, $\dot{V}_k \to 0$ is guaranteed which implies $\tilde{x}_k \to 0$ and $\tilde{\psi}_k \to 0$. Now, because $\tilde{x}_k \to 0$ states that the limit exists, once again consider the uniformly continuity of $\dot{\tilde{x}}_k$. Then, by Barbalat's lemma, $\dot{\tilde{x}}_k \to 0$ which results in $\tilde{y}_k \to 0$. Therefore, the unforced system is proved to be GAS in χ.

The next step is to prove the convergence to $\mathbf{0}$ of the perturbed inputs, $\boldsymbol{g}_k$, $\boldsymbol{s}_k$, and $\tilde{\boldsymbol{\Delta}}_k$, which come from estimation error, saturation error, and singularity error, respectively. For $\boldsymbol{g}_k(\cdot)$ term, consider its magnitude

$$||\boldsymbol{g}_k|| = \beta_5||\sum_{j \in \bar{N}_k}(\hat{\boldsymbol{e}}_j - \hat{\boldsymbol{e}}_k + \boldsymbol{r}_j - \boldsymbol{r}_k + d_k^*\hat{\boldsymbol{G}}_k\hat{\boldsymbol{c}}_k - d_j^*\hat{\boldsymbol{G}}_j\hat{\boldsymbol{c}}_j)|| = \beta_5||\sum_{j \in \bar{N}_k}(\boldsymbol{\epsilon}_j - \boldsymbol{\epsilon}_k)||,$$

where $\boldsymbol{\epsilon}_0$ is slightly abused notation defined as $\mathbf{0}$ and $\boldsymbol{\epsilon}_k$ has been proved to exponentially converge to $\mathbf{0}$ by (3.10). As a result, $||\boldsymbol{g}_k|| \to 0$ exponentially. For $\boldsymbol{s}_k(\cdot)$ term, consider its magnitude,

$$||\boldsymbol{s}_k|| = ||[\check{v}_k - \boldsymbol{sat}_\mathcal{V}(\check{v}_k), \check{\omega}_k - \boldsymbol{sat}_\mathcal{W}(\check{\omega}_k)]^T|| \leq ||[\check{v}_k - \check{v}_k^*, \check{\omega}_k - \check{\omega}_k^*]^T||.$$

The inequality holds because $\check{v}_k^* \in \mathcal{V}$ and $\check{\omega}_k^* \in \mathcal{W}$. By Lemma 3.2 and Lemma 3.3, $\hat{v}_k\boldsymbol{u}(\hat{\psi}_k) + d_k^*\hat{\boldsymbol{G}}_k\dot{\hat{\boldsymbol{c}}}_k + d_k^*\dot{\hat{\boldsymbol{G}}}_k\hat{\boldsymbol{c}}_k \to v_0\boldsymbol{u}(\psi_0) + d_k^*\boldsymbol{G}_0\dot{\boldsymbol{c}}_k^* + d_k^*\dot{\boldsymbol{G}}_k\boldsymbol{c}_k^*$ exponentially, $i.e.$, $\check{v}_k \to \check{v}_k^*$ and $\check{\omega}_k \to \check{\omega}_k^*$ exponentially. Thus, $||\boldsymbol{s}_k|| \to 0$ exponentially.

For $\tilde{\boldsymbol{\Delta}}_k(\cdot)$ term, it exists within finite time period, $i.e.$, $\tilde{\boldsymbol{\Delta}}_k \equiv \mathbf{0} \; \forall t \geq T$, as mentioned in Remark 3.6, where the relation between $\tilde{\boldsymbol{\Delta}}_k$ and $\boldsymbol{\Delta}_k$ is that $\tilde{\boldsymbol{\Delta}}_k = \left[[\boldsymbol{R}(-\psi_k)\boldsymbol{\Delta}_k]^T, 0\right]^T$.

35

The final step is to prove the boundedness of solutions to (3.20). Consider (3.21) again but differentiate it along the whole system (3.20), then we have

$$\dot{V}_k = -a_k \tilde{x}_k \boldsymbol{sat}_{\mathcal{X}}(\gamma_3 \tilde{x}_k) - b_k \sin \tilde{\psi}_k \boldsymbol{sat}_{\vartheta}(\gamma_2 \sin \tilde{\psi}_k) + \nabla V_k^T(\boldsymbol{g}_k + \boldsymbol{s}_k + \tilde{\boldsymbol{\Delta}}_k), \quad (3.23)$$

where $\nabla V_k = [a_k \tilde{x}_k, a_k \tilde{y}_k, b_k \sin \tilde{\psi}_k]^T$ with loose bound:

$$||\nabla V_k|| \leq \sqrt{9(\tilde{x}_k^2 + \tilde{y}_k^2) + \left(\gamma_1 + \frac{1}{2}\tilde{x}_k^2 + \frac{1}{2}\tilde{y}_k^2\right)^2} \leq \sqrt{\frac{9}{\tilde{x}_k^2 + \tilde{y}_k^2} + \left(\frac{\gamma_1}{\tilde{x}_k^2 + \tilde{y}_k^2} + \frac{1}{2}\right)^2} V_k.$$

Thus, $||\nabla V_k|| \leq c_1$ if $\tilde{x}_k^2 + \tilde{y}_k^2 \leq \mu$ and $||\nabla V_k|| \leq c_2 V_k$ if $\tilde{x}_k^2 + \tilde{y}_k^2 >= \mu$ from the first and second inequality, respectively, for some positive constants c_1, c_2, μ. Combine two results, then we have $||\nabla V_k|| \leq c_2 V_k + c_1$, and by (3.23), we have

$$\dot{V}_k \leq (c_2 V_k + c_1)||\boldsymbol{g}_k + \boldsymbol{s}_k + \tilde{\boldsymbol{\Delta}}_k||. \quad (3.24)$$

Rearrange and integrate both side from 0 to t as follows:

$$\int_0^t \frac{\dot{V}_k}{c_2 V_k + c_1} \, d\tau \leq \int_0^t ||\boldsymbol{g}_k + \boldsymbol{s}_k + \tilde{\boldsymbol{\Delta}}_k|| \, d\tau$$

$$\frac{1}{c_2}\left[\ln(c_2 V_k + c_1)\right]_0^t \leq \int_0^\infty ||\boldsymbol{g}_k + \boldsymbol{s}_k + \tilde{\boldsymbol{\Delta}}_k|| \, d\tau \quad (3.25)$$

Recall that $||\boldsymbol{g}_k|| \to 0$, $||\boldsymbol{s}_k|| \to 0$ exponentially and $||\tilde{\boldsymbol{\Delta}}_k|| \to 0$ in finite time with small $\tilde{\boldsymbol{\Delta}}_k$ and bounded derivative when $t < T$. Thus, all of them are absolute integrable, *i.e.*, $\int_0^\infty ||\boldsymbol{g}_k + \boldsymbol{s}_k + \tilde{\boldsymbol{\Delta}}_k|| \, d\tau = c_3 < \infty$. Then by (3.25),

$$V_k(t) \leq \frac{[c_2 V_k(0) + c_1]e^{c_2 c_3} - c_1}{c_2} \quad (3.26)$$

36

proves the boundedness of (3.20) in χ.

By the three steps and Lemma 3.4, the system (3.20) is GAS in χ which implies that $\hat{e}_k$ converges to $\mathbf{0}$. Moreover, by Lemma 3.2 and Lemma 3.3, $\hat{e}_k \to e_k$ is proved. As a result, e_k asymptotically converges to $\mathbf{0}$ for all k, which completes the proof. ∎

Remark 3.7. *Since the requirement of a global reference frame is relaxed in our settings, there is no common reference point among agents. To achieve localizations, the estimated $\hat{c}_k$ serves as the alternatives to the common global frame. More specifically, $\hat{c}_k \to c_k^*$ for $k \in \mathcal{N}$ by (3.12), and the designed control laws ensure the direction of $\hat{c}_k$ for $k \in \mathcal{N}$ to direct toward a point which will be the MAS centroid, and it becomes the common reference point among agents.*

To end this section, we elaborate some appealing attributes in our control laws. In [22, 37], the authors describe their desired geometric pattern via fixed desired displacement vectors in global reference frame. In addition to the shortcomings of requirement of global reference frame, fixed desired displacements between agents imply that the MAS merely translates while tracking, which results in the "unnatural" tracking movements as shown in Figure 3.1(a). Though authors in [23, 26, 40] consider time-varying desired displacements, the information is pre-given. Thus, the "natural" tracking movements still cannot be achieved, unless the reference centroid trajectory is available in advance and is known to all agents so that the varying displacements can be designed accordingly in advance. In fact, "natural" tracking movements require additional rotation other than translation. As a result, while using the displacement vectors to describe desired geometric pattern requires variation with rotation from perspective of global reference frame, by our design based on proposed descriptions of desired geometric pattern, the frame-invariant nature simplifies such issue. Moreover, $\boldsymbol{G}_0$ or $\boldsymbol{r}_0$ are not assumed globally accessible as

in [17], in our design, each agent track $\boldsymbol{G}_0$ by (3.15) through communications. As a result, $\boldsymbol{G}_0$ can be online adjusted which provides the ability of formation with online adaptation.

3.5 Extension to Switching Communications

In the previous sections, the discussions are based on fixed communication graph. However, in reality, communication range may be limited due to quality of service. Thus, deciding neighbors based on distance is more reasonable, which is a case of switching communications. As a result, we extend our results to the switching case in this section.

Consider s strongly connected graphs indexed from 1 to s and denote the set $S = \{1, \ldots, s\}$. Then, define a switching signal $\sigma(t) : [0, +\infty) \to S$ which indicates the corresponding communication graph at time t. With $\sigma(t)$ in mind, the neighbors of agent-k at time t is defined as $N_k^{\sigma(t)}$, and define the extended set $\bar{N}_k^{\sigma(t)}$ which additionally consider agent-0. Recall the switching sequence and dwell time τ_0 mentioned in Section 2.4, which serves as the lower bound of switching period, and it will play a crucial role in stability analysis.

Now, we extend (3.12)-(3.16) to the switching case as follows:

$$\dot{\hat{\boldsymbol{c}}}_k^k = \hat{\boldsymbol{z}}_k^k$$

$$\dot{\hat{\boldsymbol{z}}}_k^k = \frac{1}{|\bar{N}_k^{\sigma(t)}|} \sum_{j \in \bar{N}_k^{\sigma(t)}} \boldsymbol{R}(\phi_{kj}^*) \dot{\hat{\boldsymbol{z}}}_j^k + \frac{\alpha_1}{|\bar{N}_k^{\sigma(t)}|} \sum_{j \in \bar{N}_k^{\sigma(t)}} (\boldsymbol{R}(\phi_{kj}^*) \hat{\boldsymbol{z}}_j^k - \hat{\boldsymbol{z}}_k^k)$$

$$+ \frac{\alpha_2}{|\bar{N}_k^{\sigma(t)}|} \sum_{j \in \bar{N}_k^{\sigma(t)}} (\boldsymbol{R}(\phi_{kj}^*) \hat{\boldsymbol{c}}_j^k - \hat{\boldsymbol{c}}_k^k) \tag{3.27}$$

$$\dot{\hat{v}}_k = \frac{1}{|\bar{N}_k^{\sigma(t)}|} \sum_{j \in \bar{N}_k^{\sigma(t)}} \dot{\hat{v}}_j + \frac{\beta_1}{|\bar{N}_k^{\sigma(t)}|} \sum_{j \in \bar{N}_k^{\sigma(t)}} (\hat{v}_j - \hat{v}_k) \tag{3.28}$$

$$\dot{\hat{\psi}}_k^k = \frac{1}{|\bar{N}_k^{\sigma(t)}|} \sum_{j \in \bar{N}_k^{\sigma(t)}} \dot{\hat{\psi}}_j^k + \frac{\beta_2}{|\bar{N}_k^{\sigma(t)}|} \sum_{j \in \bar{N}_k^{\sigma(t)}} (\hat{\psi}_j^k - \hat{\psi}_k^k) \tag{3.29}$$

38

$$\ddot{\hat{\boldsymbol{G}}}_k^k = \frac{1}{|\bar{N}_k^{\sigma(t)}|} \sum_{j \in \bar{N}_k^{\sigma(t)}} [\ddot{\hat{\boldsymbol{G}}}_j^k + \beta_3(\dot{\hat{\boldsymbol{G}}}_j^k - \dot{\hat{\boldsymbol{G}}}_k^k) + \beta_4(\hat{\boldsymbol{G}}_j^k - \hat{\boldsymbol{G}}_k^k)] \tag{3.30}$$

$$\dot{\hat{\boldsymbol{e}}}_k^k = \beta_5 \sum_{j \in \bar{N}_k^{\sigma(t)}} \left[\hat{\boldsymbol{e}}_j^k - \hat{\boldsymbol{e}}_k^k + \boldsymbol{r}_{jk}^k + d_k^* \hat{\boldsymbol{G}}_k^k \hat{\boldsymbol{c}}_k^k - d_j^* \hat{\boldsymbol{G}}_j^k \hat{\boldsymbol{c}}_j^k\right]$$

$$+ \hat{v}_k \boldsymbol{u}(\hat{\psi}_k^k) - v_k \boldsymbol{u}(\psi_k^k) + d_k^* \hat{\boldsymbol{G}}_k^k \dot{\hat{\boldsymbol{c}}}_k^k + d_k^* \dot{\hat{\boldsymbol{G}}}_k^k \hat{\boldsymbol{c}}_k^k , \tag{3.31}$$

respectively. $\bar{N}_k$ is replaced with $\bar{N}_k^{\sigma(t)}$ which coincides with intuitions. Nevertheless, to achieve the objective (3.2), conditions on dwell time τ_0 are required. In the following, we provide the assumption of τ_0 and prove the convergence. Note that (3.27)-(3.31) are in agents' local frames, since they can be transformed to global reference frame as discussed in Remark 3.5, we will analyze the convergence in global reference frame with following global version of control laws:

$$\dot{\hat{\boldsymbol{c}}}_k = \hat{\boldsymbol{z}}_k$$

$$\dot{\hat{\boldsymbol{z}}}_k = \frac{1}{|\bar{N}_k^{\sigma(t)}|} \sum_{j \in \bar{N}_k^{\sigma(t)}} \boldsymbol{R}(\phi_{kj}^*)\dot{\hat{\boldsymbol{z}}}_j + \frac{\alpha_1}{|\bar{N}_k^{\sigma(t)}|} \sum_{j \in \bar{N}_k^{\sigma(t)}} (\boldsymbol{R}(\phi_{kj}^*)\hat{\boldsymbol{z}}_j - \hat{\boldsymbol{z}}_k)$$

$$+ \frac{\alpha_2}{|\bar{N}_k^{\sigma(t)}|} \sum_{j \in \bar{N}_k^{\sigma(t)}} (\boldsymbol{R}(\phi_{kj}^*)\hat{\boldsymbol{c}}_j - \hat{\boldsymbol{c}}_k) \tag{3.32}$$

$$\dot{\hat{v}}_k = \frac{1}{|\bar{N}_k^{\sigma(t)}|} \sum_{j \in \bar{N}_k^{\sigma(t)}} \dot{\hat{v}}_j + \frac{\beta_1}{|\bar{N}_k^{\sigma(t)}|} \sum_{j \in \bar{N}_k^{\sigma(t)}} (\hat{v}_j - \hat{v}_k) \tag{3.33}$$

$$\dot{\hat{\psi}}_k = \frac{1}{|\bar{N}_k^{\sigma(t)}|} \sum_{j \in \bar{N}_k^{\sigma(t)}} \dot{\hat{\psi}}_j + \frac{\beta_2}{|\bar{N}_k^{\sigma(t)}|} \sum_{j \in \bar{N}_k^{\sigma(t)}} (\hat{\psi}_j - \hat{\psi}_k) \tag{3.34}$$

$$\ddot{\hat{\boldsymbol{G}}}_k = \frac{1}{|\bar{N}_k^{\sigma(t)}|} \sum_{j \in \bar{N}_k^{\sigma(t)}} [\ddot{\hat{\boldsymbol{G}}}_j + \beta_3(\dot{\hat{\boldsymbol{G}}}_j - \dot{\hat{\boldsymbol{G}}}_k) + \beta_4(\hat{\boldsymbol{G}}_j - \hat{\boldsymbol{G}}_k)] \tag{3.35}$$

$$\dot{\hat{\boldsymbol{e}}}_k = \beta_5 \sum_{j \in \bar{N}_k^{\sigma(t)}} \left[\hat{\boldsymbol{e}}_j - \hat{\boldsymbol{e}}_k + \boldsymbol{r}_{jk} + d_k^* \hat{\boldsymbol{G}}_k \hat{\boldsymbol{c}}_k - d_j^* \hat{\boldsymbol{G}}_j \hat{\boldsymbol{c}}_j\right]$$

$$+ \hat{v}_k \boldsymbol{u}(\hat{\psi}_k) - v_k \boldsymbol{u}(\psi_k) + d_k^* \hat{\boldsymbol{G}}_k \dot{\hat{\boldsymbol{c}}}_k + d_k^* \dot{\hat{\boldsymbol{G}}}_k \hat{\boldsymbol{c}}_k . \tag{3.36}$$

39

In the following, two lemmas similar to Lemma 3.2 and Lemma 3.3 are proposed to prove the convergence. Denote $\sigma(\boldsymbol{M}), \sigma_{min}(\boldsymbol{M})$, and $\sigma_{max}(\boldsymbol{M})$ as the singular values, minimum of singular values, and maximum of singular values of matrix $\boldsymbol{M}$, respectively.

Lemma 3.5. *Given a switching signal $\sigma(t)$, ψ_0, and $\phi_k^*, \forall k \in \mathcal{N}$. With Assumption 3.1-Assumption 3.3, if the dwell-time*

$$\tau_0 > \frac{\ln C_{max}}{\tau_{\boldsymbol{c}}},$$

where $C_{max} = \frac{\sup_{i \in S} \sigma_{max}(\bar{\boldsymbol{L}}^i)}{\inf_{i \in S} \sigma_{min}(\bar{\boldsymbol{L}}^i)}$ and $\tau_{\boldsymbol{c}} = \frac{\sigma_{min}(\boldsymbol{Q})}{\sigma_{max}(\boldsymbol{P})}$, then the distributed update law (3.32) will drive $\hat{\boldsymbol{c}}_k \to \boldsymbol{c}_k^*$ exponentially, for $k \in \mathcal{N}$, where $\alpha_1, \alpha_2 > 0$. Moreover, $\phi_{k0}^* = \phi_k^*$, $\hat{\boldsymbol{c}}_0 = [\cos\psi_0, \sin\psi_0]^T$, $\hat{\boldsymbol{z}}_0 = \dot{\hat{\boldsymbol{c}}}_0$, $\dot{\hat{\boldsymbol{z}}}_0 = \ddot{\hat{\boldsymbol{c}}}_0$, since agent-0 represents the reference information.

Proof. Follow the definitions in Lemma 3.2, such as $\boldsymbol{p}_k$, $\boldsymbol{q}_k$, $\boldsymbol{p}_0$, $\bar{\boldsymbol{p}}_k$, and $\bar{\boldsymbol{p}}$, then define $\tilde{\boldsymbol{p}}^{\sigma(t)} = (\bar{\boldsymbol{L}}^{\sigma(t)} \otimes \boldsymbol{I}_2)\bar{\boldsymbol{p}} \in \mathbb{R}^{2N}$. With the variables, (3.4) is equivalent to

$$\begin{bmatrix} \dot{\tilde{\boldsymbol{p}}}^{\sigma(t)} \\ \ddot{\tilde{\boldsymbol{p}}}^{\sigma(t)} \end{bmatrix} = \left(\begin{bmatrix} 0 & 1 \\ -\alpha_2 & -\alpha_1 \end{bmatrix} \otimes \boldsymbol{I}_2 \right) \begin{bmatrix} \tilde{\boldsymbol{p}}^{\sigma(t)} \\ \dot{\tilde{\boldsymbol{p}}}^{\sigma(t)} \end{bmatrix} := \boldsymbol{A} \begin{bmatrix} \tilde{\boldsymbol{p}}^{\sigma(t)} \\ \dot{\tilde{\boldsymbol{p}}}^{\sigma(t)} \end{bmatrix}. \qquad (3.37)$$

Since $\boldsymbol{A}$ is Hurwitz, it ensures the existence of positive definite matrices $\boldsymbol{P}, \boldsymbol{Q} \in \mathbb{R}^{4 \times 4}$ such that $\boldsymbol{A}^T \boldsymbol{P} + \boldsymbol{P}\boldsymbol{A} = -\boldsymbol{Q}$. Denote $[\tilde{\boldsymbol{p}}^{\sigma(t)T}, \dot{\tilde{\boldsymbol{p}}}^{\sigma(t)T}]^T$ as $\boldsymbol{x} \in \mathbb{R}^4$ and consider Lyapunov function candidate $V = \boldsymbol{x}^T \boldsymbol{P}\boldsymbol{x}$. Since the digraph is fixed during $[t_k, t_{k+1}), \forall k \in \mathbb{N}$, we have $\dot{V} = -\boldsymbol{x}^T \boldsymbol{Q}\boldsymbol{x} \le -\tau_{\boldsymbol{c}}V$ for $t \in [t_k, t_{k+1})$. At t_{k+1}, $\boldsymbol{x}$ jumps due to the switching of $\bar{\boldsymbol{L}}^{\sigma(t)}$ which leads to jump of V. Such jump is utmost a factor of C_{max}, that is, $V(t_{k+1}) \le C_{max}V(t_{k+1}^-)$. Thus, we can derive the relations

$$V(t_{k+1}) < C_{max}e^{-\tau_{\boldsymbol{c}}(t_{k+1}-t_k)}V(t_k) < e^{lnC_{max}-\tau_{\boldsymbol{c}}\tau_0}V(t_k), \forall k \in \mathbb{N} \qquad (3.38)$$

40

$$V(t) < e^{-\tau_c(t-t_k)} \qquad\qquad\qquad , \forall t \in [t_k, t_{k+1}), \qquad (3.39)$$

that is, $\tilde{\boldsymbol{p}}^{\sigma(t)}$ exponentially converges to $\boldsymbol{0}$. Moreover, $\bar{\boldsymbol{L}}^{\sigma(t)}$ is invertible which states

$\bar{\boldsymbol{p}} \to \boldsymbol{0}$. As a result, we have $\hat{\boldsymbol{c}}_k \to \boldsymbol{c}_k^*$ exponentially. ∎

Lemma 3.6. *Given the switching signal $\sigma(t)$, the descriptions of desired geometric pattern*

$\{d_k^*, \phi_{kj}^*\}$, *the smooth reference centroid trajectory $\boldsymbol{r}_0$, and the smooth reference affine*

transformation $\boldsymbol{G}^*$. With Assumption 3.1-Assumption 3.3, if the dwell time

$$\tau_0 > max\left(\frac{\ln C_{max}}{\beta_1}, \frac{\ln C_{max}}{\beta_2}, \frac{\ln C_{max}}{\tau_{\boldsymbol{G}}}\right),$$

then the distributed control laws (3.32)-(3.36) will drive $\hat{v}_k \to v_0$, $\hat{\psi}_k \to \psi_0$, $\dot{\hat{\psi}}_k \to$

ω_0, $\hat{\boldsymbol{G}}_k \to \boldsymbol{G}_0$, $\dot{\hat{\boldsymbol{G}}}_k \to \dot{\boldsymbol{G}}_0$, *and $\hat{e}_k \to e_k$, exponentially, for $k \in \mathcal{N}$, where $\boldsymbol{u}(\psi) =$*

$[\cos\psi, \sin\psi]^T$, *$\beta_i > 0, i = 1, \ldots, 5$. Moreover, $\dot{\hat{v}}_0, \hat{v}_0, \dot{\hat{\psi}}_0, \hat{\psi}_0, \ddot{\hat{\boldsymbol{G}}}_0, \dot{\hat{\boldsymbol{G}}}_0, \hat{\boldsymbol{G}}_0, \hat{e}_0, d_0^*$ equal*

to $\dot{v}_0, v_0, \dot{\psi}_0, \psi_0, \ddot{\boldsymbol{G}}_0, \dot{\boldsymbol{G}}_0, \boldsymbol{G}_0, [0, 0]^T, 0$, respectively, since agent-0 is the reference.

Proof. Follow the definitions in Lemma 3.3, such as $\bar{v}_k$ and $\bar{\boldsymbol{v}}$, then define $\tilde{\boldsymbol{v}} = \bar{\boldsymbol{L}}^{\sigma(t)}\bar{\boldsymbol{v}} \in$

$\mathbb{R}^N$. With the variables, (3.33) is equivalent to $\dot{\tilde{\boldsymbol{v}}} = -\beta_1\tilde{\boldsymbol{v}}$ which has the similar form as

(3.37). As a result, $\bar{\boldsymbol{v}} \to \boldsymbol{0}$ exponentially can be derived. Similarly, (3.34) and (3.35) steer

$\hat{\psi}_k \to \psi_0$ and $\hat{\boldsymbol{G}}_k \to \boldsymbol{G}_0$ exponentially, respectively.

With same definitions of $\boldsymbol{\epsilon}$ and $\boldsymbol{\delta}$ as in Lemma 3.3, we obtain

$$\dot{\boldsymbol{\epsilon}} = -\beta_5(\bar{\boldsymbol{L}}^{\sigma(t)} \otimes \boldsymbol{I}_2)\boldsymbol{\epsilon} + \boldsymbol{\delta}, \qquad (3.40)$$

where $\boldsymbol{\delta} \to \boldsymbol{0}$ exponentially. Consider Lyapunov function candidate $V = \frac{1}{2}\boldsymbol{\epsilon}^T\boldsymbol{\epsilon}$ which has

no "jump" as in the case of Lemma 3.5 since ϵ does not vary with switching. Then,

$$\dot{V} = -\beta_5 \boldsymbol{\epsilon}^T (\bar{\boldsymbol{L}}^{\sigma(t)} \otimes \boldsymbol{I}_2) \boldsymbol{\epsilon} + \boldsymbol{\epsilon}^T \boldsymbol{\delta} \leq -k \boldsymbol{\epsilon}^T \boldsymbol{\epsilon} + \boldsymbol{\epsilon}^T \boldsymbol{\delta}, \qquad (3.41)$$

where $k = \beta_5 \inf_{i \in S} \sigma_{min}(\bar{\boldsymbol{L}}^i) > 0$, is obtained, which is input-to-state stable with respect to $\boldsymbol{\delta}$. Thus, $\boldsymbol{\epsilon}$ is bounded due to the boundedness of $\boldsymbol{\delta}$. Moreover, with the exponential convergence of $\boldsymbol{\delta}$, we have $|\boldsymbol{\epsilon}^T \boldsymbol{\delta}| \leq a e^{-bt}$ with positive constants a, b, that is,

$$\dot{V} \leq -2kV + a e^{-bt}. \qquad (3.42)$$

Rearrange into $\dot{V} + 2kV \leq a e^{-bt}$, multiply e^{2kt} to both sides and do the integration, then we have $V \to 0$ exponentially, *i.e.*, $\boldsymbol{\epsilon} \to \boldsymbol{0}$ exponentially. ∎

In this section, we successfully design the control laws (3.27)-(3.31) for switching case, and provide the stability analysis.

42

In Chapter 3, we consider a group of numbered agents subject to motion constraints, which are nonholonomic constraints, linear velocity constraints and angular velocity constraints. We design the adaptive estimation law, the distributed consensus algorithms, the distributed observer, and the constrained control inputs which are all realized in a distributed manner and in each agent's local frame with relative measurements. By our design, the MAS can achieve the desired geometric pattern, track a reference centroid trajectory, and align the MAS orientation to moving direction of the reference centroid as shown in Figure 3.1(b), a more "natural" way of tracking. Moreover, the formation can be dynamically adjusted to avoid collisions by affine transformation commands.

In reality, in addition to the tracking tasks as we focus on in Chapter 3, some applications additionally require the geometric pattern, which the MAS forms, to do self-rotating motion around its centroid. Especially when executing tasks about exploring or data collection, such self-rotating motion can increase the searching area and eliminate sensing bias. Therefore, the so-called rotating formation control is originated. As a result, to complete this thesis, we turn to study of rotating formation in the next chapter.

43

Chapter 4

Ordered Rotating Formation Control of MAS with Online Adaptation

In this chapter, we design controllers to make a MAS form into predefined ordered formation with rotation around the centroid and be able to dynamically adjust the formation. The organization in this chapter is as follows: Section 4.1 explains the term "ordered rotating formation". In Section 4.2, we describe the problem which is similar to that in Section 3.2 but focusing on the ordered rotating formation, and compare with some state of the art related works. Then, the problem is formulated mathematically in Section 4.3. The controller design based on our proposed "phase penalty flow exchange mechanism" is discussed in Section 4.4.

4.1   Ordered Rotating Formation

To seize the concept of ordered rotating formation, one can first refer to Figure 4.1, where the two subfigures are said to be with different order. In Figure 4.1(a), when the formed desired geometric pattern tracks with rotation around the centroid, the agents'

order relation is 1-2-3-4-5 in counter clock wise. While in Figure 4.1(b), although the MAS forms the same geometric pattern, the order relation is 1-4-2-5-3 in counter clock wise. In other words, ordered rotating formation determines not only the geometric pattern but also the order relation.
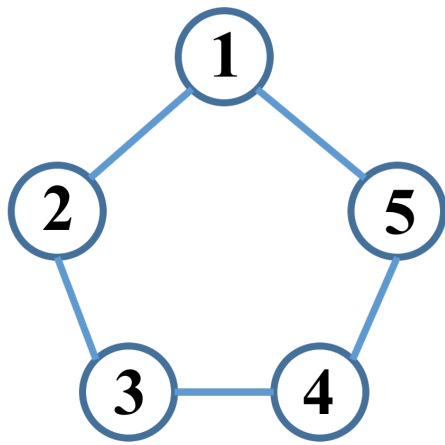

(a) order:1-2-3-4-5   (b) order:1-4-2-5-3
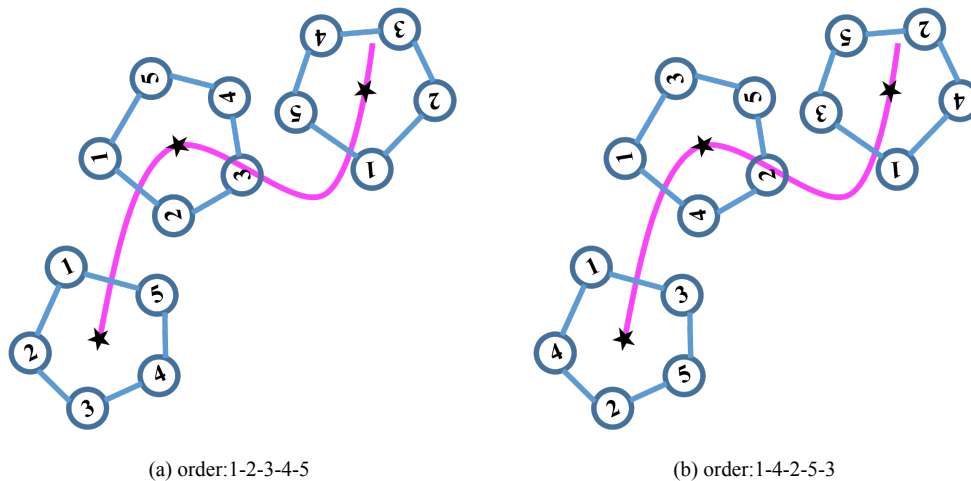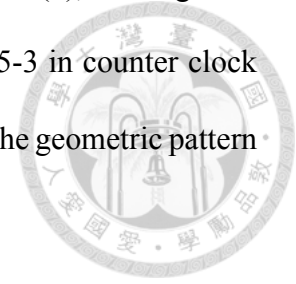
Figure 4.1: Ordered rotating formation determines the geometric pattern and is order-sensitive. That is, (a) and (b) though are with same geometric pattern, they are actually different ordered formation.

If a task only cares the formation with symmetric geometric pattern, *e.g.,* to form a evenly distributed circle, then the order relation is irrelevant. However, the order issue matters when forming into non-symmetric shapes, or more crucially, when merging groups of MASs into a larger synthesized structure. In Figure 4.2(a) and Figure 4.2(b), two formations are with the same geometric pattern but different order relation. While combining with other groups, *e.g.*, combining A to 3 and B to 4, such variation results in different synthesized pattern as shown in Figure 4.2(c) and Figure 4.2(d), respectively. Moreover, in data collection missions, when receiving local data indexed by agent numbers, we can reconstruct the global measurements by combining the indexed local data based on the order relation.
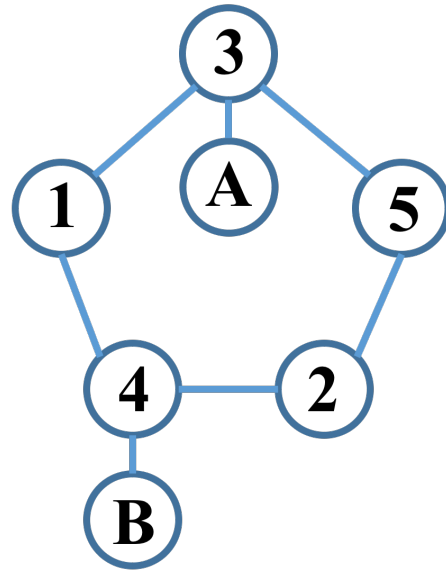
(a) Order relation: 1-2-3-4-5
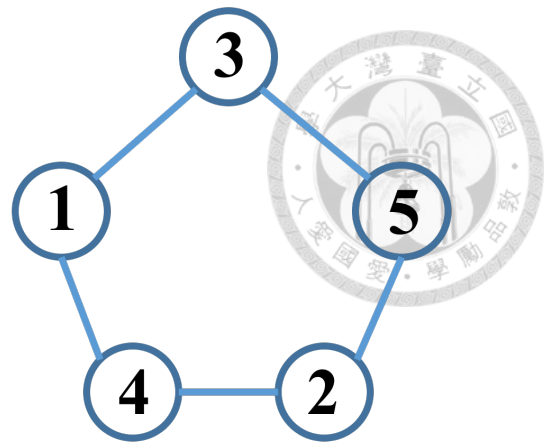
(b) Order relation: 1-4-2-5-3
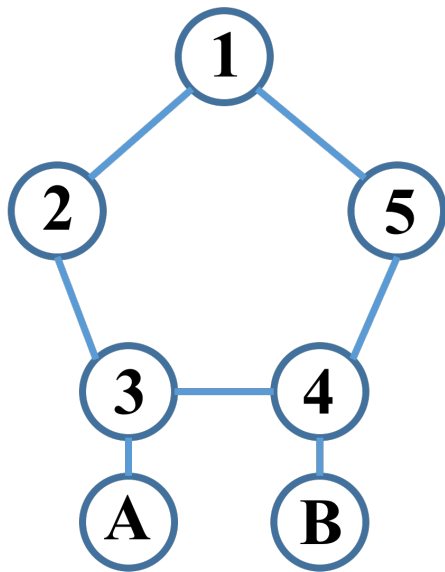
(c) Synthesis from (a)

(d) Synthesis from (b)

Figure 4.2: When combining A to 3 and B to 4, case (a) results in (c) while case (b) results in (d). As one can see, the order relation is crucial to achieve specified synthesis pattern.

4.2 Problem Descriptions and Related Works

Before proceeding to the mathematical problem formulation and controller design, we first describe the goals in this chapter and provide some discussions about the related works. In this chapter, consider a MAS with numbered agents, the objective is to design a controller which is constrained to a specified input to achieve the following tasks:

(i) *Desired numbered formation*: To form into a predefined geometric pattern.

47

(ii) *Tracking*: To steer the centroid of the MAS to track a given reference trajectory.

(iii) *Ordered Rotating*: To keep the formed geometric pattern rotating around its centroid with predefined order.

(iv) *Formation with online adaptation*: To avoid collisions with surroundings via dynamical adjustments of formation.

In addition, we will realize the controller in a distributed manner and in each agent's local frame instead of the global reference frame, which implies only relative measurements are used instead of absolute ones due to the lack of the global reference frame.

Recall that we aim to integrate non-rotating formation in Chapter 3 and rotating formation in Chapter 4, as a result, the concepts in Chapter 4 will refer that in Chapter 3. The proposed problem is basically the same as in Chapter 3 except for task (iii) there: orientation alignment task, since we focus on rotating formation in this chapter where the alignment issue no longer exists. As a derivative, the issue of ordered rotating, *i.e.*, task (iii) in this chapter, pops up. To deal with the issue, we propose "phase penalty exchange mechanism" to facilitate our design.

To highlight the hardness of issue of order, we discuss more related works in the following with their requirements and assumptions. In [12, 32], the authors propose a simple strategy where each agent pursues its front agent cyclically to form into ordered circular pattern. In such case, the formation is vulnerable due to merely single link for each agent. Note that though authors in [32] prove various ordered stable patterns, the order in formation may be affected by initial conditions, that is, pre-given order can not be achieved by their design. In [23, 31], the global reference frame is required to represent the displacement vector h which describes the vector from centroid to each agent and aids to achieve desired formation. In addition, [31] requires well-designed time-varying $h(t)$ in advance

48

to do rotating formation, which decreases flexibility. While [23] utilizes constant $\boldsymbol{h}$, some ordered patterns may fail for violating their assumptions. In [25, 28], their design allows formation to achieve specific order without global reference frame, but requires imposing restrictions on initial conditions. They assume close initial headings to prevent from forming with incorrect order.

As a comparison, in our design which benefits from proposed "penalty phase exchange mechanism", the issue of order can be solved in distributed manners and in agents' local reference frames without assumptions for initial conditions or pre-given $\boldsymbol{h}(t)$.

4.3   Problem Formulation

The problem described in Section 4.2 is formulated mathematically in this section. Consider a MAS composed of N numbered agents with unicycle model

$$\dot{\boldsymbol{r}}_k = v_k[\cos\psi_k, \sin\psi_k]^T$$

$$\dot{\psi}_k = \omega_k, \tag{4.1}$$

where $k = 1, 2, \ldots, N$, $\boldsymbol{r}_k \in \mathbb{R}^2$ and $\psi_k \in (-\pi, \pi]$ are agent-k's position and heading, v_k and ω_k are scalar inputs controlling linear and angular velocity, respectively.

Denote the index set $\mathcal{N} = \{1, \ldots, N\}$ and index-0 is reserved for representing exogenous reference signals afterwards. Given a directed communication graph $\mathcal{G}$ and the following predefined information for corresponding tasks:

(i) *Desired numbered formation*: descriptions of the desired numbered formation $\{d_k^*,$ $\phi_{kj}^*|\forall k, j \in \mathcal{N}, k \neq j\}$ which is introduced in Section 2.3,

(ii) *Tracking*: a smooth reference centroid trajectory $\boldsymbol{r}_0 \in \mathbb{R}^2$ with scalar inputs v_0 and

49

ω_0 which satisfies $\dot{\boldsymbol{r}}_0 = v_0[\cos\psi_0, \sin\psi_0]^T, \dot{\psi}_0 = \omega_0$,

(iii) *Ordered Rotating*: an constant angular velocity ϖ_0, and the relative phases $\phi_{kj}^*, \forall k, j$

$\in \mathcal{N}$ which are as in task (i),

(iv) *Formation with online adaptation*: a reference affine transformation command $\boldsymbol{G}_0(t)$

$\in \mathbb{R}^{2\times2}$ which is a series products of transformation matrices, such as scaling, rotation, and shear matrix, as introduced in Section 2.2.

Then, we want to design the constrained control inputs v_k and ω_k with locally and relatively measurable information through $\mathcal{G}$ such that

$$\boldsymbol{r}_k \to \boldsymbol{r}_0 + d_k^* \boldsymbol{G}_0[\cos\theta_k^*, \sin\theta_k^*]^T \quad \text{where} \quad \dot{\theta}_k^* = \varpi_0, \theta_k^* - \theta_j^* = \phi_{kj}^*, \qquad (4.2)$$

asymptotically, for $k, j \in \mathcal{N}$. Moreover, the control inputs are constrained to specific input ranges, that is, for $k \in \mathcal{N}$, $v_k \in [v_r^-, v_r^+]$ and $\omega_k \in [\omega_r^-, \omega_r^+]$ with predefined constants $v_r^-, \omega_r^- < 0$ and $v_r^+, \omega_r^+ > 0$. Note that θ_k^* can be arbitrarily rotating signal as long as it satisfies the differential and relative constraints.

As the considered problem in Chapter 3, the key note is that the information given in (ii) - (iv) are 'not' accessible to all agents, since we consider the communication constraints. In general, only one agent will receive these exogenous information, while the rest of agents is required to estimate them. As a result, in the later design, lots of estimation laws will be proposed.

Remark 4.1. *Once again, the right hand side of (4.2) is agent-k's desired trajectory which includes the four tasks. More precisely, d_k^* and ϕ_{kj}^* relate to task (i), $\boldsymbol{r}_0$ relates to task (ii), θ_k^* relates to task (iii), and $\boldsymbol{G}_0$ relates to task (iv).*

To clarify the reason we redesign in Chapter 4 compared to Chapter 3, we focus on the objectives 3.2 and 4.2. The intrinsic difference between problems in Chapter 3 and Chapter 4 is that having exogenous reference guidance signal or not. In 3.2, ψ_0 is an exogenous signal served as a guidance signal to MAS. In contrast, θ_k^* in 4.2 is an endogenous signal generated within agents, namely, there is no guidance in this case. As a result, such difference leads to the different design of controllers.

To solve the proposed problems, some reasonable assumptions, which are similar in Section 3.3, are made as follows:

Assumption 4.1. *The directed graph $\mathcal{G}$ is strongly connected. Moreover, at least one agent can receive the reference signals, $\boldsymbol{r}_0$, and ψ_0.*

Note that from Assumption 4.1, a diagonal matrix $\boldsymbol{B}$ is introduced where entries b_{kk} is 1 if agent-k can access to reference and 0 otherwise.

Assumption 4.2. *The reference linear velocity v_0 and angular velocity ω_0 are smooth and bounded: $v_0 \in [v_0^-, v_0^+]$ and $\omega_0 \in [\omega_0^-, \omega_0^+]$ with constants $v_0^-, \omega_0^- < 0$ and $v_0^+, \omega_0^+ > 0$. Moreover, $v_0^- > v_r^-, v_0^+ < v_r^+$ and $\omega_0^- > \omega_r^-, \omega_0^+ < \omega_r^+$, where $v_r^-, v_r^+, \omega_r^-, \omega_r^+$ are specified constants in Assumption 4.5.*

Assumption 4.3. *$\dot{v}_0, \dot{\omega}_0$ are bounded $\forall t \geq 0$.*

Assumption 4.4. *$\boldsymbol{G}_0, \dot{\boldsymbol{G}}_0, \ddot{\boldsymbol{G}}_0$ are bounded $\forall t \geq 0$.*

Assumption 4.5. *$||\frac{d}{dt}(\boldsymbol{r}_0 + d_k^* \boldsymbol{G}_0 [\cos\theta_k^*, \sin\theta_k^*]^T)|| \neq 0$ for $k \in \mathcal{N}, t \geq 0$. Moreover, assume that*

$$v_r^+ > \sup_{k \in \mathcal{N}, t \geq 0} [v_{max} + 2d_k^* \sigma(\dot{\boldsymbol{G}}_0) + 2d_k^* \varpi_0 \sigma(\boldsymbol{G}_0)] := \breve{v}_r^+$$

$$\omega_r^+ > \sup_{k \in \mathcal{N}, t \geq 0} \mathscr{F}_k(t) := \breve{\omega}_r^+$$

51

$$v_r^- < -\sup_{k\in\mathcal{N},t\geq 0}\left[v_{max} + 2d_k^*\sigma(\dot{\boldsymbol{G}}_0) + 2d_k^*\varpi_0\sigma(\boldsymbol{G}_0)\right] := \check{v}_r^-$$

$$\omega_r^- < \inf_{k\in\mathcal{N},t\geq 0}\mathscr{F}_k(t) := \check{\omega}_r^-,$$

where $v_{max} = \max(|v_0^-|, |v_0^+|)$, $\sigma(\boldsymbol{G}_0)$ is the largest singular value of $\boldsymbol{G}_0$, and $\mathscr{F}_k = \frac{\ddot{\boldsymbol{r}}_k^{*T}\boldsymbol{R}(\frac{\pi}{2})\dot{\boldsymbol{r}}_k^*}{\dot{\boldsymbol{r}}_k^{*T}\dot{\boldsymbol{r}}_k^*}$ with $\dot{\boldsymbol{r}}_k^* = \frac{d}{dt}(\boldsymbol{r}_0 + d_k^*\boldsymbol{G}_0[\cos\theta_k^*, \sin\theta_k^*]^T)$ and $\boldsymbol{R}(\frac{\pi}{2})$ is 90° counter clock wise rotation matrix.

Remark 4.2. *Assumption 4.1-Assumption 4.4 are similar to Assumption 3.1-Assumption 3.4, respectively, except for the subscripted r which stands for "rotating" case. Basically, Assumption 4.5 is also similar to Assumption 3.5, except that the desired velocity for agent-k, $\dot{\boldsymbol{r}}_k^*$, is the rotating case here.*

4.4 Controller Design and Stability Analysis

The considered problem is solved in this section, where we divide into three subsections. In Section 4.4.1, we demonstrate some present works with failure of ordered rotating. Then, the motivated concept of "phase penalty flow exchange mechanism" is illustrated. In Section 4.4.2, the estimated law is designed based on "phase penalty flow exchange mechanism" so that the estimations have ordered rotating property. Thank to the estimations, in Section 4.4.3, the controller is proposed based on such estimations with stability analysis, which is similar to the one in Section 3.4.3.

Before proceeding to the three subsections, we provide a further discussion. To solve the ordered rotating formation problem in this chapter, one may first try to extend the concepts of adaptive estimations in Section 3.4.1 with additional rotational motion, *e.g.*, things like $\dot{\hat{\boldsymbol{c}}}_k = \varpi\boldsymbol{R}(\frac{\pi}{2})\hat{\boldsymbol{c}}_k$. In fact, however, the intrinsic difference is the exogenous

signal, which involves in adaptive estimations in Section 3.4.1 but not in rotating case. More precisely, the exogenous reference signal, c_0, which serves as a guidance, participates the adaptive estimations in Lemma 3.2, while the rotating case has no such guidance since desired relative relations of $\theta_k^* - \theta_j^*$ in (4.2) are considered within agents and not with an exogenous signal. Without an exogenous reference, the agents may be stuck at some unwilling formation which will soon be exemplified in Section 4.4.1 and motivates the concept of "phase penalty flow exchange mechanism".

4.4.1 Phase Penalty Flow Exchange Mechanism

Recall that θ_k^* in objective (4.2) is actually unknown, as a result, we introduce $\hat{\theta}_k$ and aim to design control law such that $\hat{\theta}_{kj} := \hat{\theta}_k - \hat{\theta}_j$ converges to ϕ_{kj}^*, $\forall k, j \in \mathcal{N}$, and meanwhile, $\dot{\hat{\theta}}_k$ converges to ϖ_0, $\forall k \in \mathcal{N}$.

Consider a strongly connected communication graph $\mathcal{G}$ and let $\tilde{\theta}_{kj} = \hat{\theta}_{kj} - \phi_{kj}^*$ be the relative phase error between agent-k and j. A direct thought to achieve correct phase (or order) within agents, *i.e.*, $\tilde{\theta}_{kj} \to 0, \forall k, j \in \mathcal{N}$, is to feedback the phase error $\tilde{\theta}_{kj}, \forall k, \forall j \in N_k$, to the control. However, it is possible that the agents will stuck at positions which forms the right formation but does not have the right order relation. For example, given a 5-agent desired ordered geometric pattern as in Figure 4.3(a), a pentagon, and suppose that each agent's neighbors are the two adjacent numbered agents, that is, $N_1 = \{2, 5\}$, $N_2 = \{3, 1\}$, $N_3 = \{4, 2\}$, $N_4 = \{5, 3\}$, $N_5 = \{1, 4\}$. Now consider a special case with agents positions illustrated as in Figure 4.3(b), a pentagon with wrong order. Since agent-2 is one of the two neighbors of agent-1, the phase error between them is $\tilde{\theta}_{21} = \frac{4\pi}{5} - \frac{2\pi}{5}$ implies that agent-2 will attract agent-1 counter clock wise as in Figure 4.3(c). Likewise, the other neighbor, agent-5, will attract agent-1 clock wise as in Figure 4.3(d).

Unfortunately, these two attractions result in cancellation, since $\tilde{\theta}_{21} = -\tilde{\theta}_{51}$ leads addition to 0. As a result, agent-1 will stop moving due to the cancellation of two phase errors at the time instant. In fact, in Figure 4.3(d), all agents are stuck due to the cancellations, which makes the formation fixed in the wrong order relation. More rigorous derivation of this phenomenon will be provided mathematically in the proof of control design.
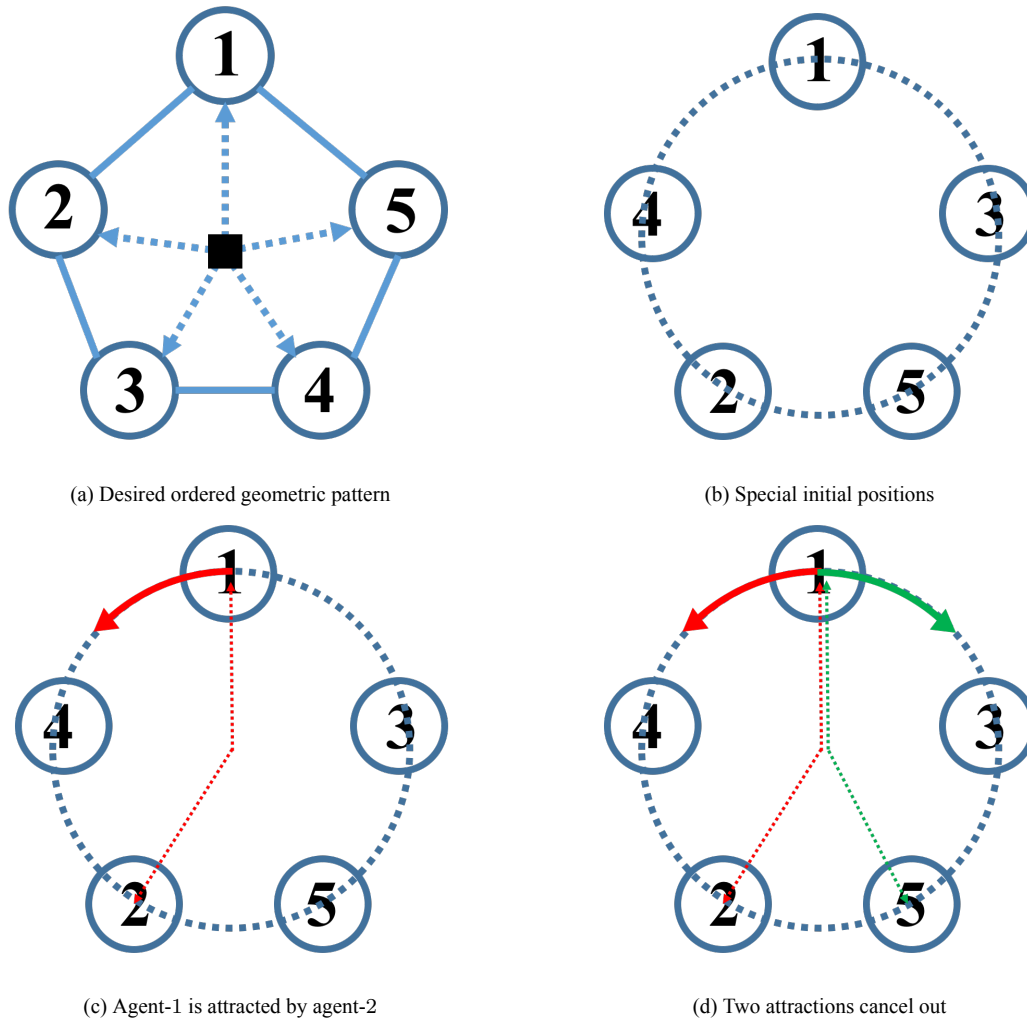

(a) Desired ordered geometric pattern

(b) Special initial positions

(c) Agent-1 is attracted by agent-2

(d) Two attractions cancel out

Figure 4.3: An example motivates the propose of phase penalty exchange mechanism to resolve cancellation.

To solve the above issue, we define the *phase weighting parameter* $w_k(t)$ of agent-k to avoid the agents from being trapped in an incorrect order due to error cancellations. The idea is to utilize the positive time varying parameter $w_k(t)$ as a weighting of the phase error, and thus the phase cancellation effect will not sustain since the value of $w_k(t)$ will change at the next time instant. To implement this idea, we first introduce some variables, and

54

then propose the *phase penalty exchange mechanism*. At last, the update law of weighting signal w_k is constructed accordingly. Suppose that $w_k(t) > 0$ is lower bounded by a positive constant $\underline{w}_k$, which will be examined after designing the update law $\dot{w}_k$.
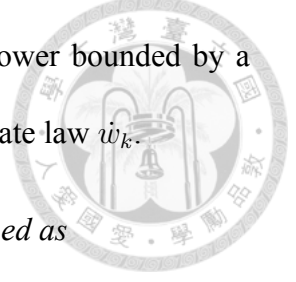
Definition 4.1 (Phase Penalty). *The phase penalty of agent-k is defined as*

$$\zeta_k = \sum_{j \in N_k} (1 - \cos \tilde{\theta}_{kj}) \geq 0$$

Note that phase penalty is an index about phase error. Once $\zeta_k = 0$, the agent-k forms correctly in order with its neighbors, *i.e.*, $\tilde{\theta}_{kj} = 0, \forall j \in N_k$.

Definition 4.2 (Phase Penalty Flow). *The phase penalty flow of agent-k is defined as*

$$\Phi_k = (w_k - \underline{w}_k)\zeta_k \geq 0$$

Note that the term *flow* implies the fluidity. More precisely, the constructed virtual phase penalty flow is able to be distributed through communication links.

The phase penalty flow exchange mechanism is to distribute the agent's phase penalty flow to its neighbors, that is, for agent-k, $\Phi_k = \sum_{j \in N_k} f_{kj}$, where $f_{kj} \geq 0$ is the value that agent-k distributes to its neighbor agent-j. The distributed rule here is via randomly partitioning the phase penalty flow Φ_k into $|N_k|$ parts and then distribute to its neighbors. By the above distribution process, the *net flow* of agent-k after an exchange iteration is $-\Phi_k + \sum_{j \in N_k} f_{jk}$, which includes distributing Φ_k out and receiving the penalty flow from its neighbors. During the formation process, if $\zeta_k = 0$, then agent-k is in a correct order with its neighbors and thus agent-k will be removed from the penalty flow exchange mechanism at the time instant. Note that f_{kj} and f_{jk} are not necessarily equal and in fact are usually different. Moreover, the distributed rule is not necessarily to be random.

55

Now, we design the update law of $w_k(t)$ according to the phase exchange mechanism. Consider the scenario that all agents are fixed at some positions and the flow exchanging mechanism is operating. Since the routed out flows are received by neighbors, the *total net flow* of the MAS is 0 for all time instant, *i.e.*,

$$\sum_{k=1}^{N} \left(-\Phi_k + \sum_{j \in N_k} f_{jk} \right) = 0, \ \forall t. \tag{4.3}$$

Moreover, since the formation shape remains unchanged, the time derivative of sum of phase penalty flow of all agents should be 0, that is, $\frac{d}{dt}(\sum_{k=1}^{N} \Phi_k) = 0$, which leads to constraints to $\dot{w}_k$. Particularly, $\dot{\zeta}_k = 0$ since the formation is fixed. As a result, we have $\frac{d}{dt}(\sum_{k=1}^{N} \Phi_k) = \sum_{k=1}^{N} \dot{w}_k \zeta_k = 0$. To satisfy the equality, we design an update law of w_k based on (4.3):

$$\dot{w}_k = \begin{cases} \frac{\delta}{\zeta_k} \left\{ -\Phi_k + \sum_{j \in N_k} f_{jk} \right\} & , \text{if } \zeta_k \neq 0, \\ 0 & , \text{if } \zeta_k = 0, \end{cases} \tag{4.4}$$

for $k \in \mathcal{N}$, where δ is a positive constant that can be arbitrarily chosen. Here, to complete the mechanism, we verify the assumption that $w_k(t)$ is lower bounded by $\underline{w}_k$. It can be seen by the fact that once w_k decreases to $\underline{w}_k$, then $\Phi_k = (w_k - \underline{w}_k)\zeta_k$ becomes 0 and this leads to $\dot{w}_k \geq 0$ by (4.4).

The concepts of the time-varying w_k and its update law from phase penalty flow exchange mechanism are clearly illustrated in this subsection to prevent from being stuck due to the error cancellations. Moreover, it serves as the foundation of the design of update law for $\hat{\theta}_k$ in the next subsection.

4.4.2 Design for Order Estimator

In this subsection, the update law of $\hat{\theta}_k$ is designed so that $\dot{\hat{\theta}}_k \to \varpi_0$ and $\hat{\theta}_{kj} \to \phi^*_{kj}$, for all $k, j \in \mathcal{N}$, are achieved.

Lemma 4.1. *Consider a strongly connected graph $\mathcal{G}$. With the control law*

$$\dot{\hat{\theta}}_k = \hat{\varpi}_k$$

$$\dot{\hat{\varpi}}_k = -c_1(\hat{\varpi}_k - \varpi_0) - c_2 \sum_{j \in N_k} (w_k + w_j) \sin \tilde{\theta}_{kj}, \tag{4.5}$$

where $c_1, c_2 > 0$ and w_k is the phase weighting parameter with (4.4), for all $k \in \mathcal{N}$, that $\dot{\hat{\theta}}_k \to \varpi_0$ and $\hat{\theta}_{kj} \to \phi^*_{kj}$, for all $k, j \in \mathcal{N}$ are achieved.

Proof. Consider Lyapunov function candidate

$$V = \frac{1}{2} \sum_{k \in \mathcal{N}} (\hat{\varpi}_k - \varpi_0)^2 + c_2 \sum_{k \in \mathcal{N}} \sum_{j \in N_k} w_k(1 - \cos \tilde{\theta}_{kj}), \tag{4.6}$$

then we have the time derivative

$$\dot{V} = \sum_{k \in \mathcal{N}} \dot{\hat{\varpi}}_k(\hat{\varpi}_k - \varpi_0) + c_2 \sum_{k \in \mathcal{N}} \sum_{j \in N_k} \dot{w}_k(1 - \cos \tilde{\theta}_{kj}) + c_2 \sum_{k \in \mathcal{N}} \sum_{j \in N_k} w_k \dot{\tilde{\theta}}_{kj} \sin \tilde{\theta}_{kj}$$

$$= \sum_{k \in \mathcal{N}} \dot{\hat{\varpi}}_k(\hat{\varpi}_k - \varpi_0) + c_2 \sum_{k \in \mathcal{N}} \dot{w}_k \zeta_k$$

$$\quad + c_2 \sum_{k \in \mathcal{N}} \sum_{j \in N_k} \left[w_k(\dot{\hat{\theta}}_k - \varpi_0) \sin \tilde{\theta}_{kj} + w_k(\dot{\hat{\theta}}_j - \varpi_0) \sin \tilde{\theta}_{jk} \right]$$

$$= \sum_{k \in \mathcal{N}} \dot{\hat{\varpi}}_k(\hat{\varpi}_k - \varpi_0) + 0 + c_2 \sum_{k \in \mathcal{N}} (\hat{\varpi}_k - \varpi_0) \sum_{j \in N_k} (w_k + w_j) \sin \tilde{\theta}_{kj}$$

$$= -c_1 \sum_{k \in \mathcal{N}} (\hat{\varpi}_k - \varpi_0)^2 \le 0 \tag{4.7}$$

57

By Invariance Principle, we have $\dot{\hat{\theta}}_k \to \varpi_0$, which further leads to

$$\sum_{j \in N_k} (w_k + w_j) \sin \tilde{\theta}_{kj} \to 0 \qquad (4.8)$$

by (4.5), for all $k \in \mathcal{N}$, and all relative phases $\tilde{\theta}_{kj}, \forall k, j \in \mathcal{N}$, converge to some constants. Moreover, the weightings $w_k, \forall k$, keep updating. Overall speaking, we have constants $\tilde{\theta}_{kj}$ with time-varying coefficients summing to 0. As a result, the only constant solution to that is $\tilde{\theta}_{kj} \to 0, \forall k, \forall j \in N_k$. ∎

In fact, though the phase weighting parameter w_k updates via design law (4.4), we can further make the weighting be upper bounded by some predefined constant $\bar{w}_k$. This is realized by resetting the weighting parameter w_k to a number within range $[\underline{w}_k, \overline{w}_k)$ whenever w_k reaches the upper bound $\overline{w}_k$. One can switch the weighting parameter lower without disturbing the convergence of $\tilde{\theta}_{kj}$ since such switching lowers down the value of Lyapunov function proposed in (4.6).

Remark 4.3. *Suppose without our proposed exchange mechanism, that is, the weightings $w_k, \forall k \in \mathcal{N}$ are constants, then we can still follow the proof of Lemma 4.1 and obtain the same equation (4.8) but with constant coefficients. In such case, whether $\tilde{\theta}_{kj} \to 0$ or not remains inconclusive. For example, in the motivation example Figure 4.3 where w_k are the same constants. We will have $\sin \tilde{\theta}_{12} + \sin \tilde{\theta}_{15} = 0$ as shown in Figure 4.3(d), which satisfies (4.8) but without $\tilde{\theta}_{kj}$ converging to 0. As a result, the introduced time-varying weighting parameter w_k with the update law (4.4) is the key to resolve order issue.*

Essentially, Lemma 4.1 plays the same role as in Lemma 3.2. More precisely, the vector $[\cos \hat{\theta}_k, \sin \hat{\theta}_k]^T$ indicates the estimated direction of centroid in the rotating case as $\hat{c}_k$ of Lemma 3.2 in tracking case. Once the estimated direction is obtained, the remaining

design follows the process in Section 3.4. Therefore, in the next section, the consensus algorithms and distributed observer are first proposed, then the formation controller is designed in subsequence.

4.4.3 Lyapunov-Based Constrained Controller

To design the control inputs v_k and ω_k, we first recall the objective (4.2) and define position error accordingly, $\boldsymbol{e}_k := \boldsymbol{r}_0 - \boldsymbol{r}_k + d_k^* \boldsymbol{G}_0 [\cos \theta_k^*, \sin \theta_k^*]^T$. Note that by Assumption 4.1, v_0, ψ_0 for reference velocity, and $\boldsymbol{G}_0$ for reference affine transformation are only accessible to a few agents, as a result, $\hat{v}_k, \hat{\psi}_k$, and $\hat{\boldsymbol{G}}_k$ are introduced to estimate v_0, ψ_0, and $\boldsymbol{G}_0$, respectively. Further with the above estimations, we have the estimation of error dynamics $\dot{\boldsymbol{e}}_k$. Thus, the estimated desired position error $\hat{\boldsymbol{e}}_k$ is introduced with a distributed observer to estimate $\boldsymbol{e}_k$. As one can examine, these design concepts follow exactly as in Section 3.4.2, which motivates the following lemma.

Lemma 4.2. *Given the graph $\mathcal{G}$, the descriptions of desired geometric pattern $\{d_k^*, \phi_{kj}^*\}$, the smooth reference centroid trajectory $\boldsymbol{r}_0$, and the smooth reference affine transformation command $\boldsymbol{G}_0$. With Assumption 4.1-Assumption 4.3, the distributed control laws*

$$\dot{\hat{v}}_k = \frac{1}{|\bar{N}_k|} \sum_{j \in \bar{N}_k} \dot{\hat{v}}_j + \frac{\beta_1}{|\bar{N}_k|} \sum_{j \in \bar{N}_k} (\hat{v}_j - \hat{v}_k) \tag{4.9}$$

$$\dot{\hat{\psi}}_k = \frac{1}{|\bar{N}_k|} \sum_{j \in \bar{N}_k} \dot{\hat{\psi}}_j + \frac{\beta_2}{|\bar{N}_k|} \sum_{j \in \bar{N}_k} (\hat{\psi}_j - \hat{\psi}_k) \tag{4.10}$$

$$\ddot{\hat{\boldsymbol{G}}}_k = \frac{1}{|\bar{N}_k|} \sum_{j \in \bar{N}_k} \left[\ddot{\hat{\boldsymbol{G}}}_j + \beta_3 (\dot{\hat{\boldsymbol{G}}}_j - \dot{\hat{\boldsymbol{G}}}_k) + \beta_4 (\hat{\boldsymbol{G}}_j - \hat{\boldsymbol{G}}_k) \right] \tag{4.11}$$

$$\dot{\hat{\boldsymbol{e}}}_k = \beta_5 \sum_{j \in \bar{N}_k} \left[\hat{\boldsymbol{e}}_j - \hat{\boldsymbol{e}}_k + \boldsymbol{r}_j - \boldsymbol{r}_k + d_k^* \hat{\boldsymbol{G}}_k \boldsymbol{u}(\hat{\theta}_k) - d_j^* \hat{\boldsymbol{G}}_j \boldsymbol{u}(\hat{\theta}_j) \right]$$

$$+ \hat{v}_k \boldsymbol{u}(\hat{\psi}_k) - v_k \boldsymbol{u}(\psi_k) + \hat{\varpi}_k d_k^* \hat{\boldsymbol{G}}_k \boldsymbol{R}(\frac{\pi}{2}) \boldsymbol{u}(\hat{\theta}_k) + d_k^* \dot{\hat{\boldsymbol{G}}}_k \boldsymbol{u}(\hat{\theta}_k) \tag{4.12}$$

59

drive $\hat{v}_k \to v_0$, $\hat{\psi}_k \to \psi_0$, $\dot{\hat{\psi}}_k \to \omega_0$, $\hat{\boldsymbol{G}}_k \to \boldsymbol{G}_0$, $\dot{\hat{\boldsymbol{G}}}_k \to \dot{\boldsymbol{G}}_0$, *and* $\hat{\boldsymbol{e}}_k \to \boldsymbol{e}_k$ *exponentially,*

for $k \in \mathcal{N}$, *where* $\boldsymbol{u}(\psi) = [\cos\psi, \sin\psi]^T$, $\hat{\theta}_k$ *and* $\hat{\varpi}_k$ *follow (4.5), and* $\beta_i > 0, i =$

$1, \ldots, 5$. *Moreover,* $\dot{\hat{v}}_0$, $\hat{v}_0$, $\dot{\hat{\psi}}_0$, $\hat{\psi}_0$, $\ddot{\hat{\boldsymbol{G}}}_0$, $\dot{\hat{\boldsymbol{G}}}_0$, $\hat{\boldsymbol{G}}_0$, $\hat{\boldsymbol{e}}_0$, d_0^* *equal to* $\dot{v}_0, v_0, \dot{\psi}_0, \psi_0, \ddot{\boldsymbol{G}}_0, \dot{\boldsymbol{G}}_0, \boldsymbol{G}_0$,

$[0,0]^T, 0$, *respectively, since agent-0 represents the reference information.*

Proof. Refer to the proof of Lemma 3.3. ∎

In fact, if one denotes $\boldsymbol{u}(\hat{\theta}_k)$ as $\hat{\boldsymbol{c}}_k$, then Lemma 4.2 becomes exactly the same as Lemma 3.3. This implies that the remaining designs can directly utilize the ones proposed in Section 3.4.3, such as coordinate transformation and constrained controller design. As a result, we let

$$\hat{\boldsymbol{c}}_k = \boldsymbol{u}(\hat{\theta}_k) \tag{4.13}$$

so that the proposed control law (3.19) remains valid. In the following, the main theorem for ordered rotating is proposed which states exactly the same as in Theorem 3.1 by virtue of the re-definition of $\hat{\boldsymbol{c}}_k$ in (4.13).

Theorem 4.1. *Given the communication graph* $\mathcal{G}$, *the descriptions of desired geometric pattern* $\{d_k^*, \phi_{kj}^*\}$, *the smooth reference centroid trajectory* $\boldsymbol{r}_0$, *the desired constant angular velocity* ϖ_0, *and the smooth reference affine transformation command* $\boldsymbol{G}_0$. *If Assumption 4.1-Assumption 4.5 are hold, then by the designed laws (4.4), (4.5), (4.9)-(4.12), and the re-definition (4.13) for deriving the constrained control input*

$$\omega_k = \boldsymbol{sat}_{\mathcal{W}}(\check{\omega}_k) + \frac{\boldsymbol{sat}_{\mathcal{V}}(\check{v}_k)\tilde{y}_k(2 - \cos\tilde{\psi}_k)}{\gamma_1 + \frac{1}{2}\tilde{x}_k^2 + \frac{1}{2}\tilde{y}_k^2} + \boldsymbol{sat}_{\vartheta}(\gamma_2 \sin\tilde{\psi}_k)$$

$$v_k = \boldsymbol{sat}_{\mathcal{V}}(\check{v}_k)\cos\tilde{\psi}_k + \boldsymbol{sat}_{\mathcal{X}}(\gamma_3 \tilde{x}_k), \tag{4.14}$$

the control objective (4.2) is achieved via distributed measurements, for $k \in \mathcal{N}$, *where*

$sat_{\mathcal{I}}(c)$ *is a saturation function which projects scalar* c *into the saturated interval* $\mathcal{I} =$ $[\mathcal{I}^-, \mathcal{I}^+]$, *that is,*

$$sat_{\mathcal{I}}(c) = \begin{cases} \mathcal{I}^-, & if\, c < \mathcal{I}^- \\ c, & if\, \mathcal{I}^- \leq c \leq \mathcal{I}^+ \\ \mathcal{I}^+, & if\, c > \mathcal{I}^+ \end{cases} .$$

The intervals in (4.14) are given as $\mathcal{W} = [\check{\omega}^-, \check{\omega}^+]$, $\mathcal{V} = [\check{v}^-, \check{v}^+]$, $\mathcal{X} = [-v_{gap}, v_{gap}]$ *where* $v_{gap} = \min\{\check{v}^- - v^-, v^+ - \check{v}^+\}$. *Besides,* γ_2, γ_3 *are arbitrary positive constants, while interval* ϑ *and positive constant* γ_1 *are design parameters to ensure* $\omega_k \in [\omega^-, \omega^+]$.

Proof. Refer to the proof of Theorem 3.1. ∎

In addition, as mentioned in Remark 3.5, the designed control laws, (4.9)-(4.12), can be realized in agent's local frames. As a result, we state a corollary of Theorem 4.1 which realizes the control laws in agents' local frames in the following.

Corollary 4.1.1. *Given the communication graph* $\mathcal{G}$, *the descriptions of desired geometric pattern* $\{d_k^*, \phi_{kj}^*\}$, *the smooth reference centroid trajectory* $\boldsymbol{r}_0$, *the desired constant angular velocity* ϖ_0, *and the smooth reference affine transformation command* $\boldsymbol{G}_0$. *If Assumption 4.1-Assumption 4.5 are hold, then by the control laws (4.5),*

$$\dot{\hat{v}}_k = \frac{1}{|\bar{N}_k|} \sum_{j \in \bar{N}_k} \dot{\hat{v}}_j + \frac{\beta_1}{|\bar{N}_k|} \sum_{j \in \bar{N}_k} (\hat{v}_j - \hat{v}_k) \tag{4.15}$$

$$\dot{\hat{\psi}}_k^k = \frac{1}{|\bar{N}_k|} \sum_{j \in \bar{N}_k} \dot{\hat{\psi}}_j^k + \frac{\beta_2}{|\bar{N}_k|} \sum_{j \in \bar{N}_k} (\hat{\psi}_j^k - \hat{\psi}_k^k) \tag{4.16}$$

$$\ddot{\hat{G}}_k^k = \frac{1}{|\bar{N}_k|} \sum_{j \in \bar{N}_k} \left[\ddot{\hat{G}}_j^k + \beta_3(\dot{\hat{G}}_j^k - \dot{\hat{G}}_k^k) + \beta_4(\hat{G}_j^k - \hat{G}_k^k) \right] \tag{4.17}$$

61

$$\dot{\boldsymbol{e}}_k^k = \beta_5 \sum_{j \in \bar{N}_k} \left[\hat{\boldsymbol{e}}_j^k - \hat{\boldsymbol{e}}_k^k + \boldsymbol{r}_{jk}^k + d_k^* \hat{\boldsymbol{G}}_k^k \boldsymbol{u}(\hat{\theta}_k) - d_j^* \hat{\boldsymbol{G}}_j^k \boldsymbol{u}(\hat{\theta}_j) \right]$$

$$+ \hat{v}_k \boldsymbol{u}(\hat{\psi}_k^k) - v_k \boldsymbol{u}(\psi_k^k) + \hat{\varpi}_k d_k^* \hat{\boldsymbol{G}}_k^k \boldsymbol{R}(\frac{\pi}{2}) \boldsymbol{u}(\hat{\theta}_k) + d_k^* \dot{\hat{\boldsymbol{G}}}_k^k \boldsymbol{u}(\hat{\theta}_k), \qquad (4.18)$$

and the re-definition (4.13) for deriving the constrained control input (4.14), for $k \in \mathcal{N}$,

the control objective (4.2) is achieved via distributed measurements in each agent's local

frame.

Remark 4.4. *The high similarity of Corollary 4.1.1 and Theorem 3.1 is due to consistent*

design concepts. As a byproduct, tasks can be easily altered between two major classes

of literature about Multi-Agent System formation control, tracking and tracking with ro-

tation. While most of the existing results focus on merely one of the two major classes and

even have inconsistent dynamic models or design concepts, we readily integrate the major

classes due to the consistent design process, as a side-benefit.

62

Chapter 5

Simulation Results

In this chapter, we provide some simulation scenarios to validate our design results which include Natural Tracking designed in Chapter 3 and Ordered Rotating designed in Chapter 4. The organization in this chapter is as follows: in Section 5.1, we focus on results for natural tracking. Moreover, we show that existing works serve as special cases of ours. In Section 5.2, the results of ordered rotating is demonstrated and compared with existing works which are most disordered cases.

5.1 Results for Natural Tracking

Recall the considered problem in Chapter 3: we aim to design control law such that the objective (3.2), which includes four tasks, *desired numbered formation*, *tracking*, *MAS orientation alignment*, and *formation with online adaptation*, can be achieved. In the following, we will provide several simulation results to validate the novelty and generality of our design for natural tracking movements.

- *Simulation I: results of Theorem 3.1*

  In this simulation, we provide the overall results for considered problem in Chapter 3.

Then, in the following simulation scenarios, we will demonstrate the novelty and generality of our design over existing works.

Consider a MAS with 5 numbered agents with the desired numbered geometric pattern as shown in Figure 5.1, where $d_1^* = 5.6$, $d_2^* = 4.1$, $d_3^* = 6$, $d_4^* = 6$, $d_5^* = 4.1$, and $\phi_1^r = 1.6$, $\phi_2^r = 2.6$, $\phi_3^r = -2.2$, $\phi_4^r = -1$, $\phi_5^r = 0.5$, as defined in Section 2.3. Besides, the switching signal is depicted in Figure 5.2, where the 4 strongly connected communication graphs are shown in Figure 5.3. Given initial conditions of tracking trajectory: $\boldsymbol{r}_0(0) = [7.1, 3.4]^T$ and $\psi_0(0) = 0.15$ with inputs $v_0 = 0.4 + 0.2\cos(0.2t)$ and $\omega_0 = 0.015 - 0.01\sin(0.2t)$, where $t \in [0, 200]$ is the simulation time, the relative phase for orientation alignment: $\phi_1^* = 0$, $\phi_2^* = 1$, $\phi_3^* = 2.5$, $\phi_4^* = -2.5$, $\phi_5^* = -1$, and the reference affine transformation command $\boldsymbol{G}_0 = (1 + 0.4\sin(0.02t))\boldsymbol{I}_2$, where $\boldsymbol{I}_2$ is 2-by-2 identity matrix. Note that these information are 'not' globally accessible.
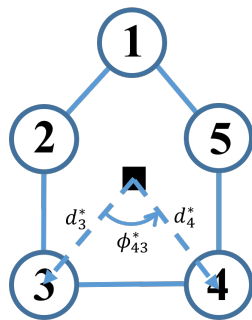
Figure 5.1: Desired numbered geometric pattern
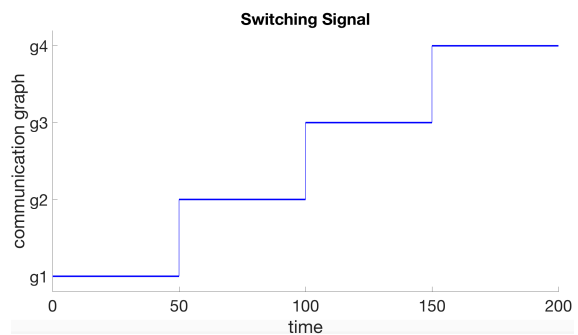
Figure 5.2: Switching signal

(a) $\mathcal{G}_1$ (b) $\mathcal{G}_2$ (c) $\mathcal{G}_3$ (d) $\mathcal{G}_4$
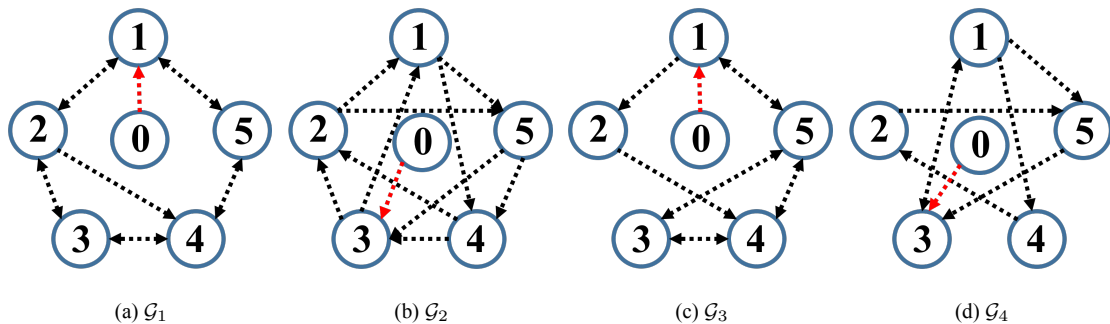
Figure 5.3: Four strongly connected communication graphs (agent-0 denotes exogenous reference)

The parameters in control laws are selected as $\alpha_1 = 2$, $\alpha_2 = 1$, $\beta_1 = 3$, $\beta_2 = 3$,

64

$\beta_3 = 2$, $\beta_4 = 1$, $\beta_5 = 5$, $\gamma_1 = 2$, $\gamma_2 = 0.8$, $\gamma_3 = 1$. Then, with the proposed distributed control laws (3.27) - (3.31) and the constrained control inputs (3.19), the simulation result is demonstrated in Figure 5.4. As one can see, the MAS forms into the desired numbered geometric pattern, keeps its centroid tracking $\boldsymbol{r}_0$, aligns the orientation to thee direction of $\dot{\boldsymbol{r}}_0$ during tracking which results in natural tracking, and dynamically scales smaller to safely pass through the valley by $\boldsymbol{G}_0$. We emphasize that our designed control laws, (3.27) - (3.31) and (3.19), are distributed and realized in each agent's local reference frame.

In the following, we demonstrate the adaptive estimation process of $\boldsymbol{c}_k^*$, which is proposed in Lemma 3.5, in Figure 5.5, where the straight lines are the directions of estimated $\hat{\boldsymbol{c}}_k, \forall k = 1, \ldots, 5$. By our adaptive estimation law (3.32), the estimated directions will intersect to a point, the centroid, at the fourth sampling time in Figure 5.5.
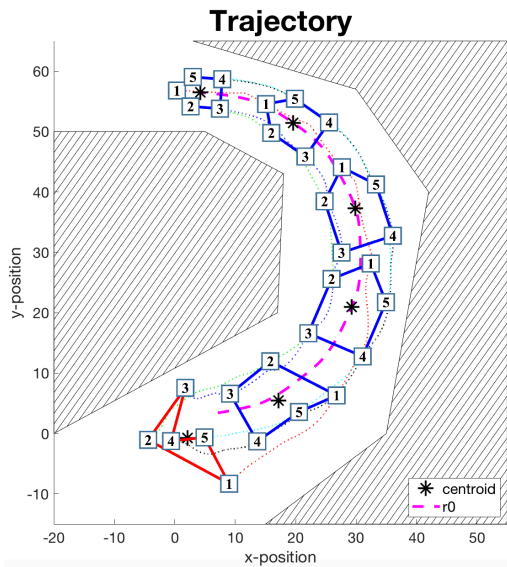
Figure 5.4: Overall results of natural tracking   Figure 5.5: Adaptive estimation process
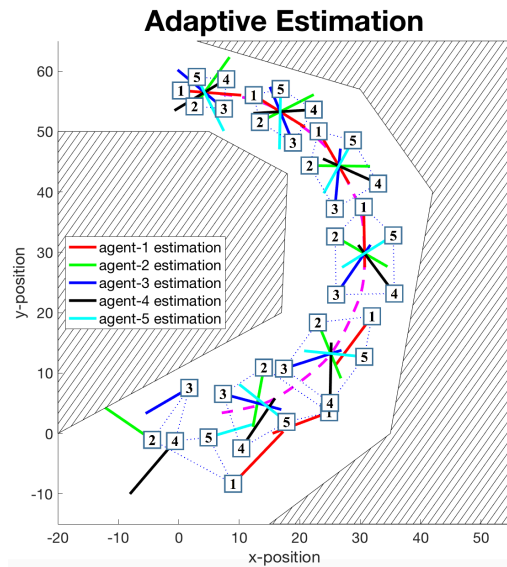
In addition, since we consider saturation constraints of control inputs v_k and ω_k, the saturated linear velocity command and saturated angular velocity command are shown in Figure 5.6(a) and Figure 5.6(b), respectively, to validate our design. The simulation results display that the control inputs are more likely to be constrained in early stage due to the random initial estimations which lead to larger errors.

65

(a) linear velocity input, v_k (b) angular velocity input, ω_k
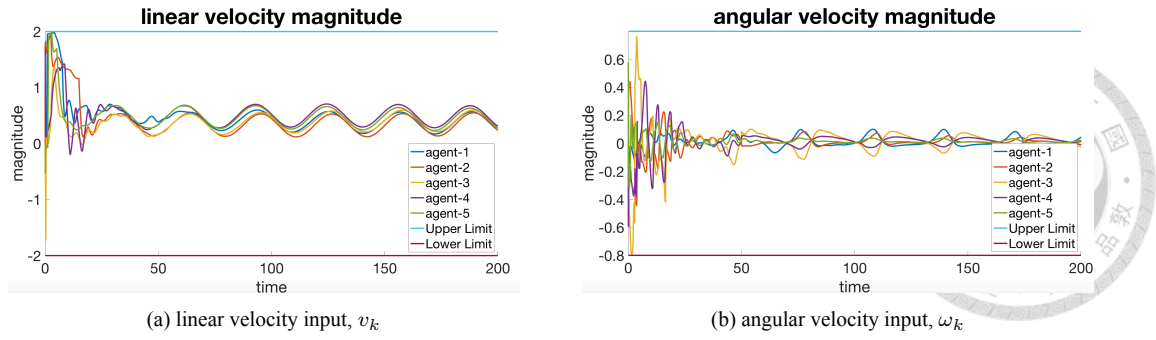
Figure 5.6: Inputs are within saturation ranges

To sum up, the proposed control laws, which are distributed and realized in each agent's local reference frame, are validated by simulation that the considered problem in Chapter 3 is solved. To further demonstrate that our control laws support various desired geometric patterns and reference trajectories, we provide another example with different geometric pattern from Figure 5.1 and different r_0. Then, the following simulation scenarios II - IV that compares with existing works will base on this example.

Consider a MAS with 5 numbered agents with the desired numbered geometric pattern as shown in Figure 5.7, where $d_1^* = 8.4$, $d_2^* = 4$, $d_3^* = 4.7$, $d_4^* = 4$, $d_5^* = 8.4$, and $\phi_1^r = 0$, $\phi_2^r = 0.6$, $\phi_3^r = 2$, $\phi_4^r = 3.3$, $\phi_5^r = 3.9$. Given initial conditions of tracking trajectory: $r_0(0) = [1.8, 5]^T$ and $\psi_0(0) = 0.8$ with inputs $v_0 = 0.4 + 0.2\cos(0.2t)$ and $\omega_0 = 0.015 - 0.01\sin(0.2t) - t/4000$, where $t \in [0, 200]$ is the simulation time, the relative phase for orientation alignment: $\phi_1^* = -2$, $\phi_2^* = -1.4$, $\phi_3^* = 0$, $\phi_4^* = 1.4$, $\phi_5^* = 2$, and the reference affine transformation command $G_0 = (1 + 0.4\sin(0.02t))I_2$. Then, with proposed design, the results are demonstrated in Figure 5.8, where the MAS forms into desired numbered geometric pattern, keeps the centroid tracking r_0, achieves natural tracking, and adapts to the environments by G_0.

In the following, we will demonstrate via simulation II - IV based on this example that some of the existing works are special cases of ours.

- *Simulation II: achieving fixed orientation as existing woks*

66
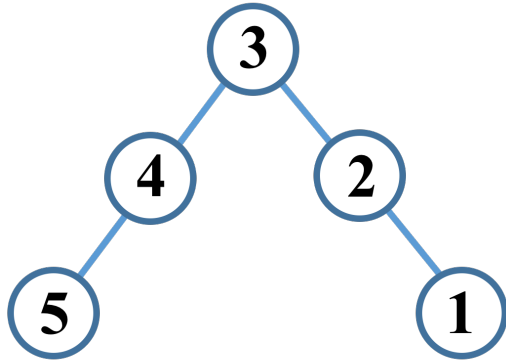
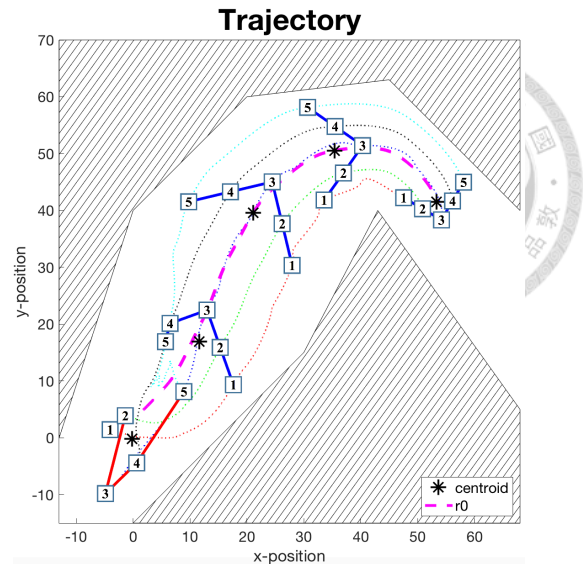Figure 5.7: Desired numbered geometric pattern

Figure 5.8: Overall natural tracking results

In this simulation, we will demonstrate that the existing works [22, 37–39], which consider tracking with fixed orientation, are special cases in our design. In contrast, their design cannot achieve natural tracking movements as ours.

The results of their design are depicted in Figure 5.9, where the formation is merely translated with fixed orientation but not interacting with trajectory while tracking. More specifically, no matter where the formation is and how the reference trajectory changes, the MAS orientation remains directing toward northwest. To achieve the case of tracking with fixed orientation, we can simply replace ψ_0 in the desired center vector $\boldsymbol{c}_k^*$ by a constant, as claimed in Remark 3.2. In this example, $\boldsymbol{c}_k^*$ is changed to $[\cos\left(\frac{3\pi}{4} + \phi_k^*\right), \sin\left(\frac{3\pi}{4} + \phi_k^*\right)]^T$, for $k = 1, \ldots, 5$, such that the MAS orientation points to northwest invariantly. The result of our method is demonstrated in Figure 5.10, where tracking with fixed orientation is successfully achieved. Moreover, the rest of features, such as saturated inputs, online adaptation, still remain. As a result, their results as in Figure 5.9 may collide with the environments, while ours in Figure 5.10 do not. Note that compare Figure 5.8 with Figure 5.10, we believe the former is with more natural movements while tracking.

- *Simulation III: achieving pre-defined orientation as existing works*

67
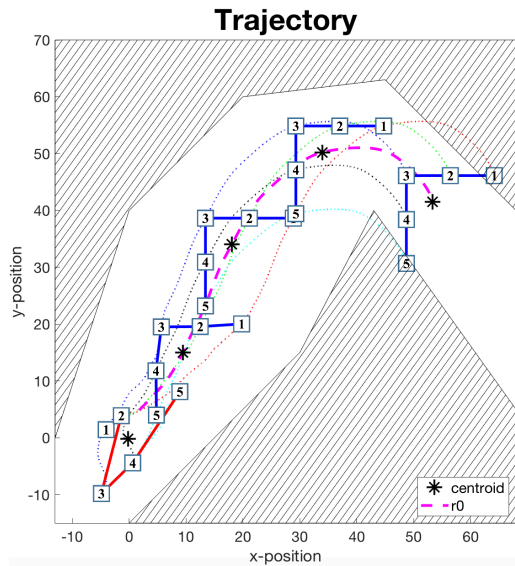
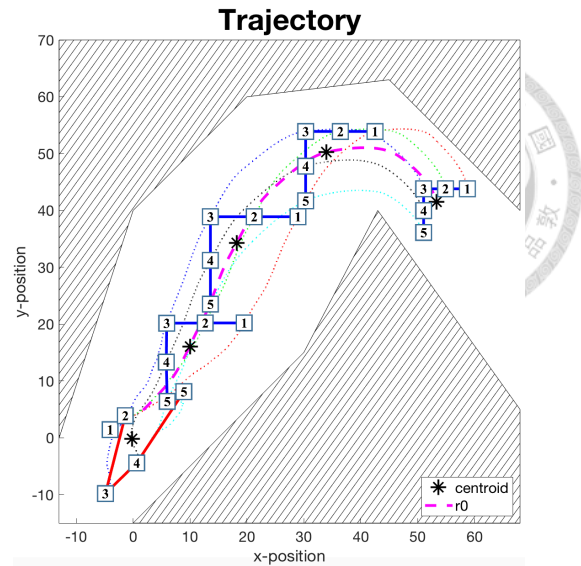Figure 5.9: Tracking with fixed orientation by existing works

Figure 5.10: Tracking with fixed orientation by our design

In this simulation, we will illustrate that the existing works [23,26,40], which consider tracking with pre-defined orientation, are still special cases in our design. Likewise, their design still cannot achieve natural tracking movements as ours.

Similar to simulation II, to achieve the case of tracking with pre-defined orientation, we can simply replace ψ_0 in the desired center vector $\boldsymbol{c}_k^*$ by the pre-defined signal, as claimed in Remark 3.2. For example, we change ψ_0 to be pre-defined signal $\frac{3\pi}{4}\cos(0.05t)$, that is, $\boldsymbol{c}_k^* = [\cos\left(\frac{3\pi}{4}\cos(0.05t) + \phi_k^*\right), \sin\left(\frac{3\pi}{4}\cos(0.05t) + \phi_k^*\right)]$. Then, the simulation result is provided in Figure 5.11, where the MAS orientation is varying according to the pre-defined signal while tracking. Once again, the rest of features, such as distributed communications, realizing in local reference frames, still remain. In contrast, the existing works require a global reference frame and simultaneous clock to achieve the result as in Figure 5.11, since they directly design the desired position of each agent with respect to the global reference frame at each time instant without or with scarce cooperation.

Moreover, it seems that natural tracking can be achieved by designing the pre-defined signal manually according to the reference trajectory. However, in fact, their design can-

68

not achieve natural tracking neither, since the trajectory is neither globally accessible nor known in advance, or say, may dynamically changes. As a result, the pre-defined signal cannot incorporate information of the reference trajectory in advance. In other words, the natural tracking cannot be achieved by manually designing the pre-defined signal.
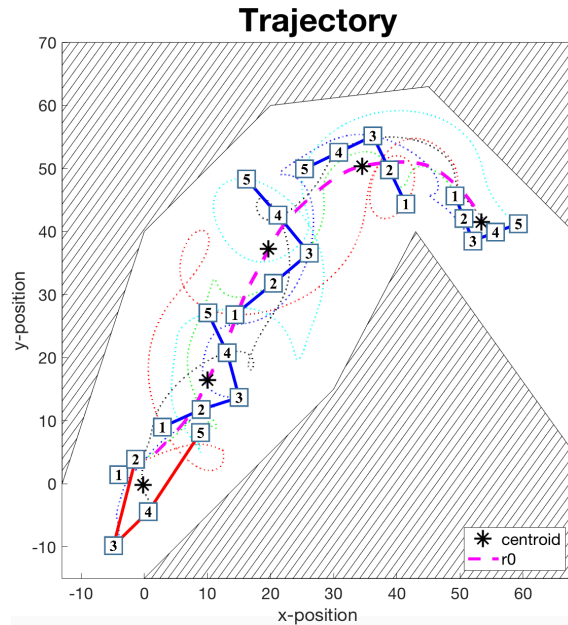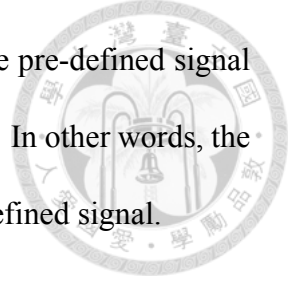

Figure 5.11: Tracking with pre-defined orientation by our design

- *Simulation IV: affine transformation of desired geometric pattern*

In this simulation, we will show that our design also has the capability of supporting affine transformation for desired geometric pattern as in [14]. Moreover, we relax the requirements of special assumptions on communications they impose.

Given the reference affine transformation $\boldsymbol{G}_0 \in \mathbb{R}^{2 \times 2}$ defined as

$$\boldsymbol{G}_0 = b(t)\boldsymbol{I}_2 + (a(t) - b(t))[\cos\psi_0, \sin\psi_0]^T[\cos\psi_0, \sin\psi_0],$$

where $a(t) = 1 + 0.25\sin(0.08t - 4.4)$ and $b(t) = 0.6 + 0.4\cos(0.08t - 4.4)$. Note that $\boldsymbol{G}_0$ requires information of ψ_0, and since both of them are accessible to the agent communicates with 'agent-0', it is feasible in our settings. The reason of including ψ_0 is to

69

make the affine transformation act on the moving direction, which coordinates with natural tracking movements. The result carried out by our design is demonstrated in Figure 5.12, where the desired geometric pattern is scaling and transforming such that the spreading angle of the pattern is altering.
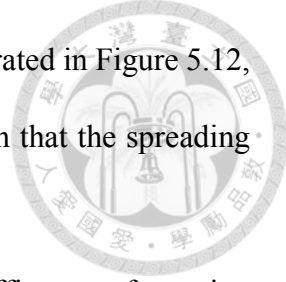
As mentioned in the first paragraph, [14, 43] can achieve such affine transformation as depicted in Figure 5.12. However, they require the communication graph to be rigid, be undirected, and have at least three agents to receive reference information. Even more, they assume the communication graph is known *in advance*, and cannot be altered after the controller is designed. More specifically, since their design requires the knowledge of communication graph, once the controller is designed, it can merely support *the only* communication. While in our design, the controller can support all directed and undirected communications as long as satisfying Assumption 3.1. In addition, case of switching communication is considered in our design, while the result in [14] sticks to fixed communication since the controller is only valid to *the* communication graph.
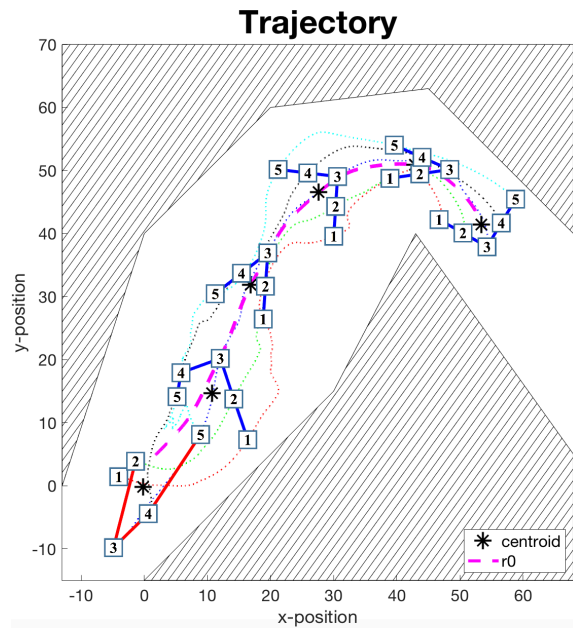
Figure 5.12: Affine transformation coordinating with natural tracking by our design

• *Simulation V: inputs with saturation versus inputs without saturation*

70

In this simulation, we will focus on the issue of input saturation which is crucial but most existing works ignore. The comparison between inputs with saturation and inputs without saturation by our method is demonstrated in Figure 5.13, where Figure 5.13(a) is the same as Figure 5.8. Note that the inputs without saturation by our method means that the saturation function constrained on (3.19) is removed.
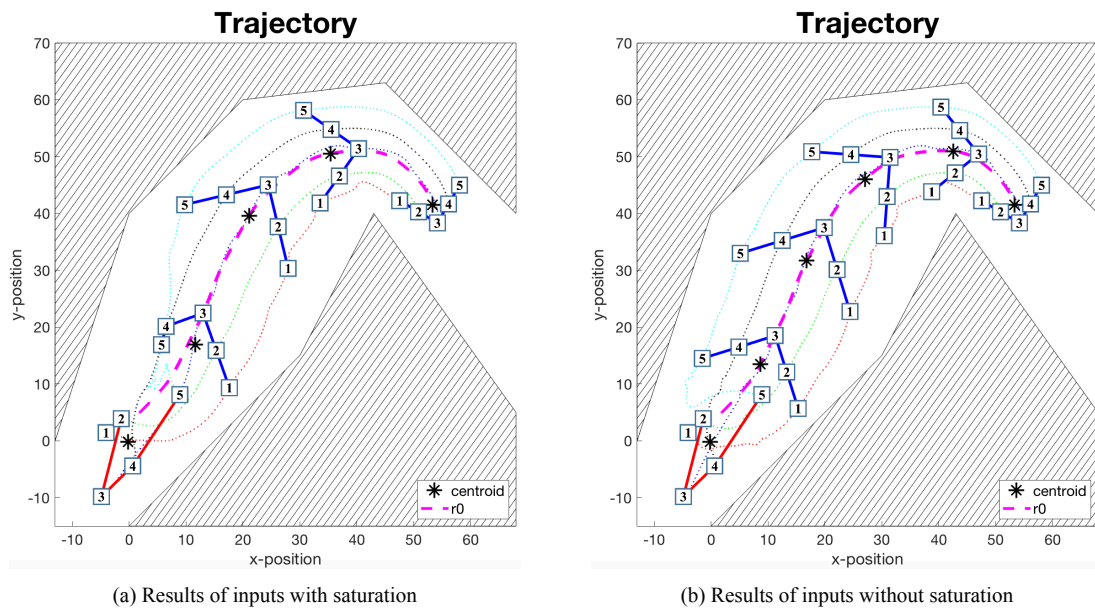

(a) Results of inputs with saturation (b) Results of inputs without saturation

Figure 5.13: The results of inputs with and without saturation are provided in (a) and (b), respectively, where the case of inputs without saturation has faster convergence.

As one can see from the results in Figure 5.13, the case of inputs without saturation has faster convergence. Such acceleration of convergence is expected due to the larger gain, larger inputs range. As a result, the control inputs of both cases are provided in Figure 5.14 to validate the speculation. Despite that larger inputs lead to the faster convergence, saturation constraints are crucial in reality due to the physical limitations. As a result, clinging the inputs to constrained ranges is the more feasible design.
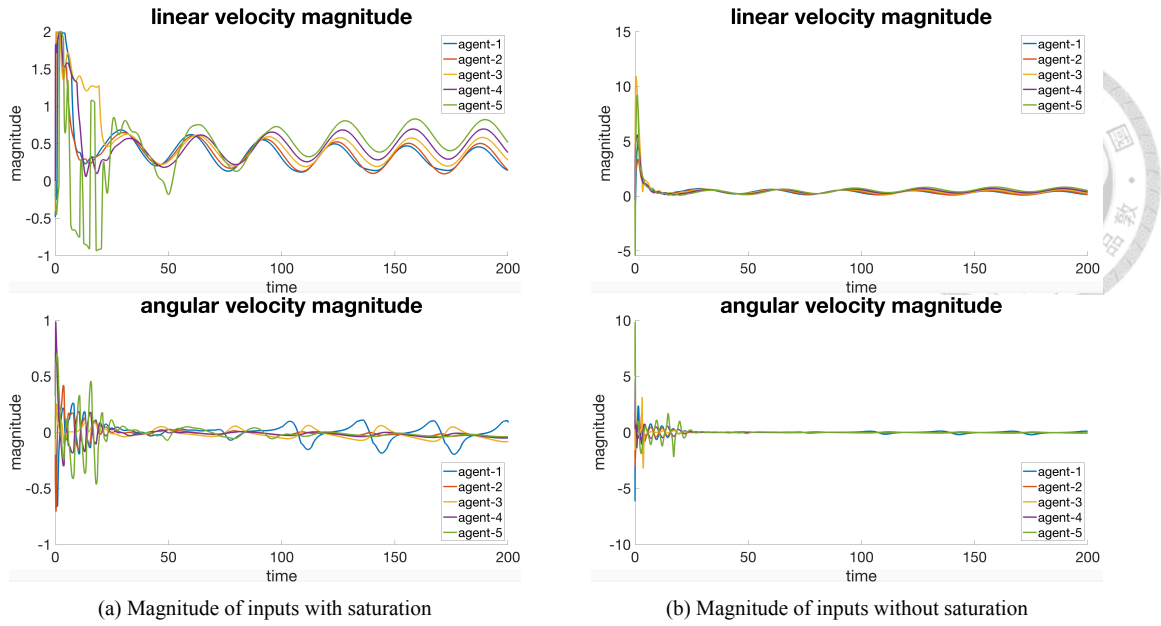
71

(a) Magnitude of inputs with saturation   (b) Magnitude of inputs without saturation

Figure 5.14: The magnitudes of inputs are much larger in the case of without saturation, which results in the faster convergence.

5.2 Results for Ordered Rotating

In this section, we will provide simulation for the design in Chapter 4, where the MAS is extended to the case of tracking with incessant rotation. Since most of the features of our design have been demonstrated in Section 5.1, we will focus on the property of ordered rotating formation in the following.

● *Simulation VI: results of Theorem 4.1*

In this simulation, we provide the overall results for considered problem in Chapter 4. Then, in the following simulation scenarios, we will demonstrate the novelty of *ordered rotating formation* over existing works.

Consider a MAS with 5 numbered agents with the desired numbered geometric pattern as shown in Figure 5.1, where $d_k^* = 5$ for $k = 1, \ldots, 5$, and $\phi_1^r = 0$, $\phi_2^r = \frac{2\pi}{5}$, $\phi_3^r = \frac{4\pi}{5}$, $\phi_4^r = \frac{6\pi}{5}$, $\phi_5^r = \frac{8\pi}{5}$, as defined in Section 2.3. Besides, the switching signal is depicted in Figure 5.16, where the 4 strongly connected communication graphs are shown in Figure 5.17. Given initial conditions of tracking trajectory: $\boldsymbol{r}_0(0) = [1.8, 4.9]^T$ and $\psi_0(0) =$

72

0.77 with inputs $v_0 = 0.4 + 0.2\cos(0.2t)$ and $\omega_0 = 0.015 - 0.01\sin(0.2t) - t/4000$, where $t \in [0, 200]$ is the simulation time, the desired angular velocity $\varpi_0 = 0.1$, and the reference affine transformation command $\boldsymbol{G}_0 = (1 + 0.4\sin(0.02t))\boldsymbol{I}_2$, where $\boldsymbol{I}_2$ is 2-by-2 identity matrix. Note that these information are 'not' globally accessible.
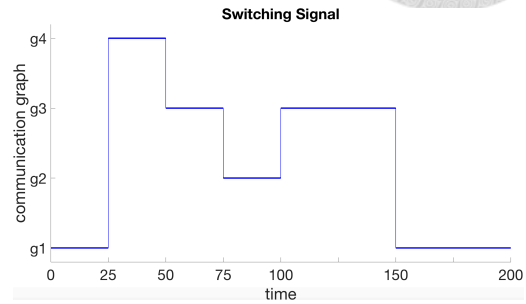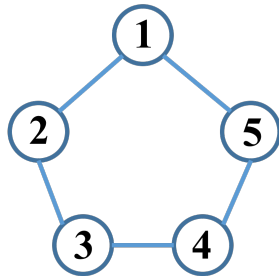
Figure 5.15: Desired numbered geometric pattern for ordered rotating

Figure 5.16: Switching signal for ordered rotating

(a) $\mathcal{G}_1$ (b) $\mathcal{G}_2$ (c) $\mathcal{G}_3$ (d) $\mathcal{G}_4$
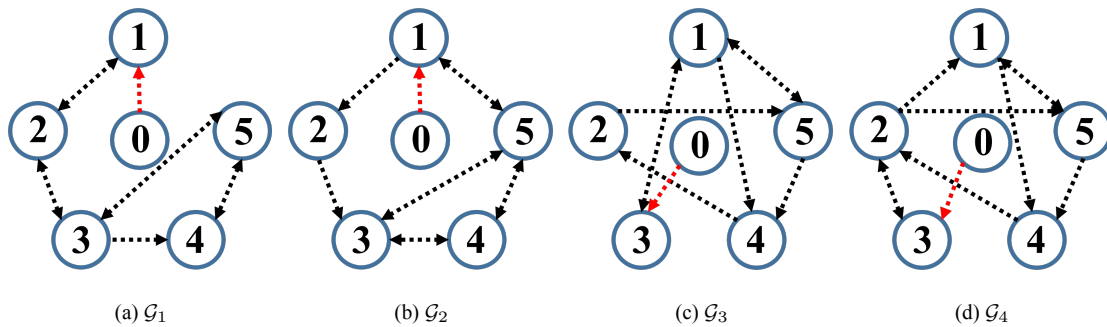
Figure 5.17: Four strongly connected communication graphs (agent-0 denotes exogenous reference)

The parameters in control laws are selected as $c_1 = 2$, $c_2 = 1$, $\beta_1 = 3$, $\beta_2 = 3$, $\delta = 0.3$, $\beta_3 = 2$, $\beta_4 = 1$, $\beta_5 = 5$, $\gamma_1 = 2$, $\gamma_2 = 0.8$, $\gamma_3 = 1$. Then, with the update law (4.4), the proposed distributed control laws (4.5), (4.15) - (4.18) and the constrained control inputs (4.14), the simulation result is demonstrated in Figure 5.18. As one can see, the MAS forms into the desired numbered geometric pattern, keeps its centroid tracking $\boldsymbol{r}_0$, rotates around the centroid, and dynamically scales smaller to safely pass through the valley by $\boldsymbol{G}_0$. We emphasize that our designed control laws, (4.5), (4.15) - (4.18) and (4.14), are distributed and realized in each agent's local reference frame.

Once again, since we consider saturation constraints of control inputs v_k and ω_k, the
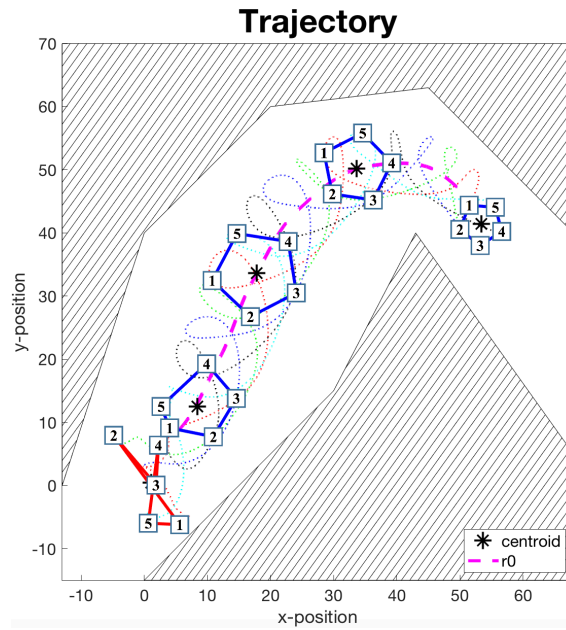
73

Figure 5.18: Overall results of ordered rotating

saturated linear velocity command and saturated angular velocity command are shown in

Figure 5.19(a) and Figure 5.19(b), respectively, to validate our design.

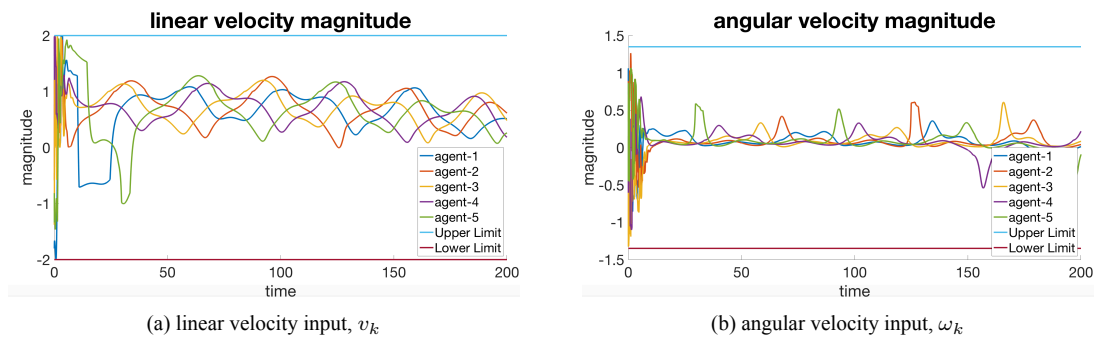(a) linear velocity input, v_k (b) angular velocity input, ω_k

Figure 5.19: Inputs are within saturation ranges

- *Simulation VII: ordered rotating by our design vs. non-ordered cases in existing works*

In this simulation, we will compare our design for ordered rotating with existing works, such as [25, 28, 32], which mostly do not consider the issue of order. In the following, we will provide two scenarios with different initial agents' positions but the same of rest settings, and then show that existing works will lead to different order cases, while by or design, the same pre-defined order can be guaranteed.

Consider two cases of initial conditions: (1) $\boldsymbol{r}_1(0) = [5.6, -6.2]^T$, $\boldsymbol{r}_2(0) = [-4.8, 8]^T$,

74

$\boldsymbol{r}_3(0) = [1.9, 0.1]^T$, $\boldsymbol{r}_4(0) = [2.3, 6.4]^T$, $\boldsymbol{r}_5(0) = [0.6, -6]^T$, and (2) $\boldsymbol{r}_1(0) = [-8.6, 4.1]^T$,

$\boldsymbol{r}_2(0) = [8.6, -3.8]^T$, $\boldsymbol{r}_3(0) = [3, -7]^T$, $\boldsymbol{r}_4(0) = [3.9, 2.5]^T$, $\boldsymbol{r}_5(0) = [-9.1, 6]^T$. With the

rest of signals and parameters as given in Simulation VI, the results are demonstrated in

Figure 5.20 and Figure 5.21, which are by our design and existing works, respectively. By

our design, the formation is guaranteed to achieve ordered pentagon in both cases. While

by existing works, though the patterns are correctly formed, the orders are *not* guaranteed

as depicted in Figure 5.21(a) and Figure 5.21(b). In other words, the order of formation

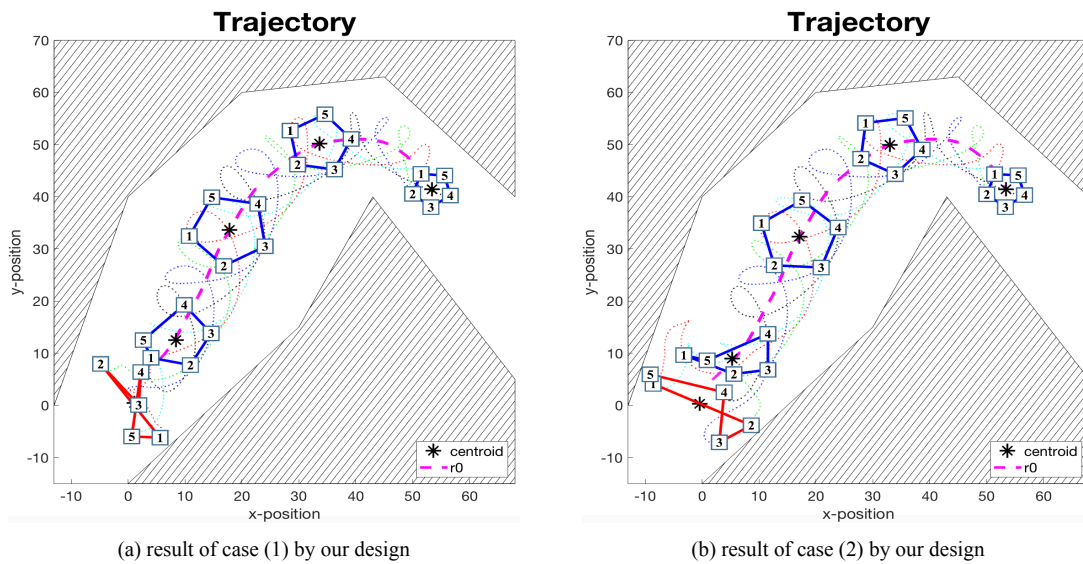by their designs is affected by initial conditions, and thus cannot be predicted.

(a) result of case (1) by our design   (b) result of case (2) by our design

Figure 5.20: Results of two initial positions by our design, where the order is guaranteed

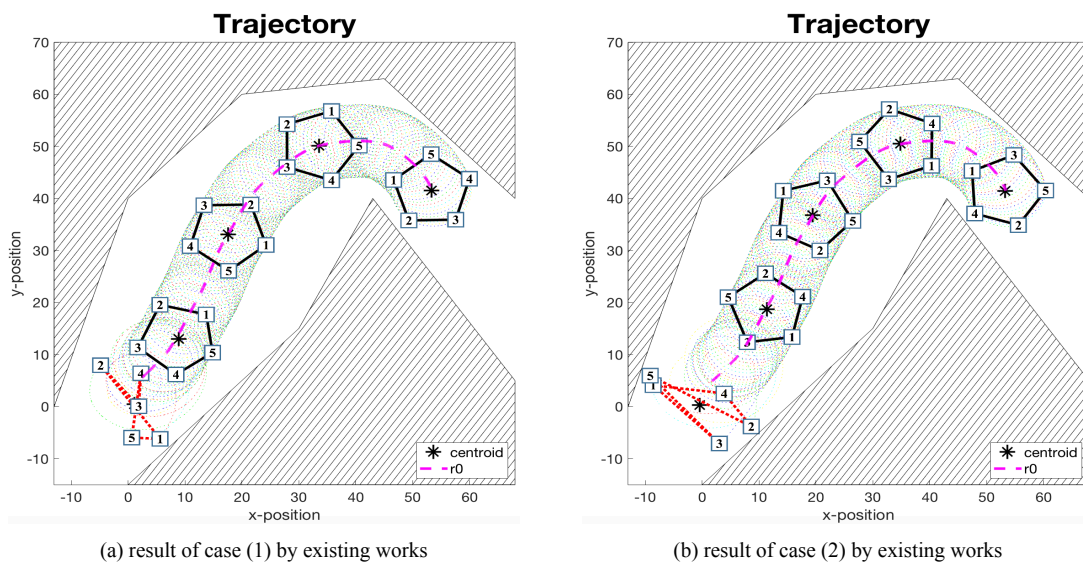(a) result of case (1) by existing works   (b) result of case (2) by existing works

Figure 5.21: Results of two initial positions by existing works, where the order alters

75

- *Simulation VIII: issue of online adaptation and constrained inputs*

In this simulation, since few existing works, such as [16, 17], consider transformation of desired geometric pattern, we will provide some discussions and comparisons in the following. The results by our design and by their controllers are shown in Figure 5.22(a) and Figure 5.22(b), respectively.
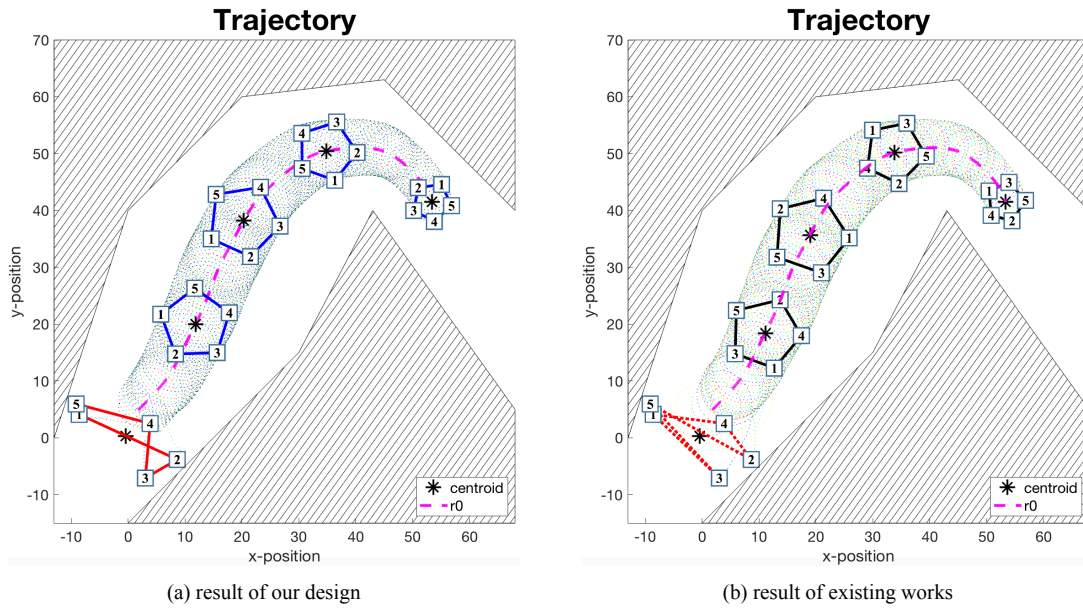

(a) result of our design   (b) result of existing works

Figure 5.22: Results of our design and existing works in ordered rotating with transformation

It seems that the results in Figure 5.22 have no much difference. In fact, from one aspect, the results of existing works cannot achieve ordered rotating as depicted in Figure 5.22(b). From another aspect, the control inputs have remarkable differences, as shown in Figure 5.23. The reason is that the authors in [16, 17] apply model transformation from integrator model to unicycle model, where the singularity may happen. As a result, the control inputs of their design may lead to large magnitudes as drawn in Figure 5.23(b).
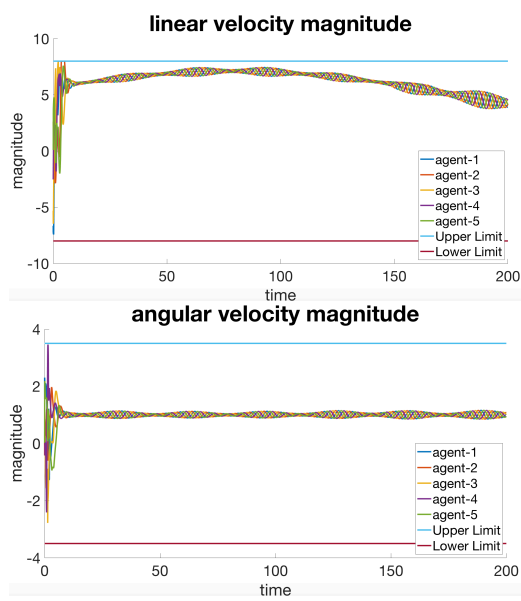
(a) Magnitude of inputs by our design
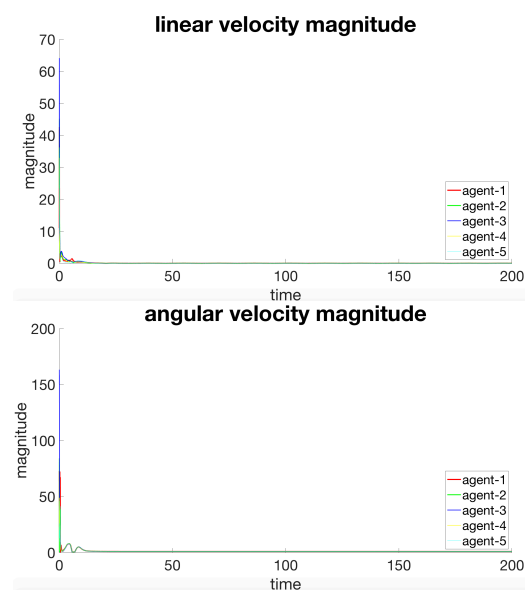
(b) Magnitude of inputs by existing works

Figure 5.23: The magnitudes of inputs are much larger in the case of existing works.

78

Chapter 6

Conclusion

In this thesis, we consider general dynamic maneuver control of Multi-Agent System, which includes tracking, rotating, and transforming. Moreover, the designed approach endows the formation with ability of online adaptation. In contrast to most existing works which neglect physical limitations, we consider nonholonomic constraints, communication constraints, and input saturation, which makes our design more feasible in reality. In other words, our proposed control laws are in distributed manners and realized in agents' local reference frames; in addition, the linear and angular velocity inputs are constrained within specified ranges which reflect physical restrictions.

The main results are given in Chapter 3 and Chapter 4. In Chapter 3, the constrained controls are designed such that the MAS can track a reference trajectory with online adaptation via affine transformation of desired geometric pattern. An appealing attribute of our design is that the MAS orientation while tracking is generally designed, and particularly, the concept of natural tracking movements is proposed which is a more natural motion compared with existing works. In Chapter 4, to cover more maneuver actions which then supports more real applications, we extend the tracking results to the case of tracking with

rotation around centroid of MAS. The controls such that the MAS can track a reference trajectory with online adaptation and meanwhile rotate around the centroid are designed. Moreover, the issue of ordered rotating is solved by our proposed 'phase penalty flow exchange mechanism'.

In the future work, we may consider communication delays which is a realistic issue when considering communication constraints.
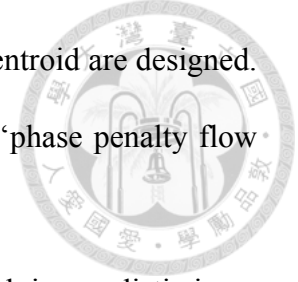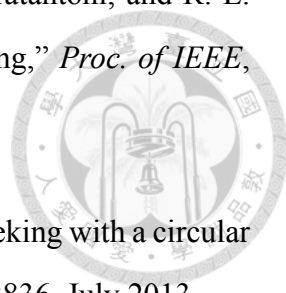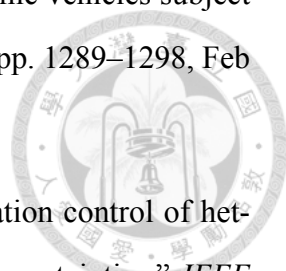
Bibliography

[1] K.-K. Oh, M.-C. Park, and H.-S. Ahn, "A survey of multi-agent formation control," *Automatica*, vol. 53, pp. 424 – 440, 2015.

[2] W. Ren, "Consensus seeking in multi-vehicle systems with a time-varying reference state," in *Proc. of Amer. Control Conf.*, pp. 717–722, July 2007.

[3] W. Ren, "Second-order consensus algorithm with extensions to switching topologies and reference models," in *Proc. of Amer. Control Conf.*, pp. 1431–1436, July 2007.

[4] J. Qin, W. X. Zheng, and H. Gao, "Consensus of multiple second-order vehicles with a time-varying reference signal under directed topology," *Automatica*, vol. 47, no. 9, pp. 1983 – 1991, 2011.

[5] W. Ni and D. Cheng, "Leader-following consensus of multi-agent systems under fixed and switching topologies," *Syst. Control Lett.*, vol. 59, no. 3, pp. 209 – 217, 2010.

[6] Z. Meng, Z. Zhao, and Z. Lin, "On global leader-following consensus of identical linear dynamic systems subject to actuator saturation," *Syst. Control Lett.*, vol. 62, no. 2, pp. 132 – 142, 2013.

[7] X. You, C.-C. Hua, H.-N. Yu, and X.-P. Guan, "Leader-following consensus for high-order stochastic multi-agent systems via dynamic output feedback control," *Automatica*, vol. 107, pp. 418 – 424, 2019.

[8] Z. Lin, L. Wang, Z. Han, and M. Fu, "Distributed formation control of multi-agent systems using complex laplacian," *IEEE Trans. on Autom. Control*, vol. 59, pp. 1765–1777, July 2014.

[9] S. Zhao, "Affine formation maneuver control of multiagent systems," *IEEE Trans. on Autom. Control*, vol. 63, pp. 4140–4155, Dec 2018.

[10] D. V. Dimarogonas and K. H. Johansson, "Stability analysis for multi-agent systems using the incidence matrix: Quantized communication and formation control," *Automatica*, vol. 46, no. 4, pp. 695 – 700, 2010.

[11] K. Sakurama, "Distributed control of networked multi-agent systems for formation with freedom of special euclidean group," in *Proc. of 55th IEEE Conf. Decision Control*, pp. 928–932, Dec 2016.

[12] H. Rezaee and F. Abdollahi, "Pursuit formation control scheme for double-integrator multi-agent systems," in *Proc. of 19th IFAC World Congress*, pp. 10054 – 10059, 2014.

[13] B.-H. Lee and H.-S. Ahn, "Distributed formation control via global orientation estimation," *Automatica*, vol. 73, pp. 125 – 129, 2016.

[14] S. Zhao, "Affine formation maneuver control of multiagent systems," *IEEE Trans. on Autom. Control*, vol. 63, pp. 4140–4155, Dec 2018.

[15] S.-M. Kang and H.-S. Ahn, "Shape and orientation control of moving formation in multi-agent systems without global reference frame," *Automatica*, vol. 92, pp. 210 – 216, 2018.

[16] L. B. Arranz, A. Seuret, and C. C. de Wit, "Elastic formation control based on affine transformations," in *Proc. of Amer. Control Conf.*, pp. 3984–3989, June 2011.

[17] L. Briñón-Arranz, A. Seuret, and C. C. de Wit, "Cooperative control design for time-varying formations of multi-agent systems," *IEEE Trans. on Autom. Control*, vol. 59, pp. 2283–2288, Aug 2014.

[18] N. E. Leonard, D. A. Paley, F. Lekien, R. Sepulchre, D. M. Fratantoni, and R. E. Davis, "Collective motion, sensor networks, and ocean sampling," *Proc. of IEEE*, vol. 95, pp. 48–74, Jan 2007.

[19] L. Briñón-Arranz and L. Schenato, "Consensus-based source-seeking with a circular formation of agents," in *Proc. of Eur. Control Conf.*, pp. 2831–2836, July 2013.

[20] N. E. Leonard and E. Fiorelli, "Virtual leaders, artificial potentials and coordinated control of groups," in *Proc. of 40th IEEE Conf. Decision Control*, vol. 3, pp. 2968–2973 vol.3, Dec 2001.

[21] S. Zhao, D. V. Dimarogonas, Z. Sun, and D. Bauso, "A general approach to coordination control of mobile agents with motion constraints," *IEEE Trans. on Autom. Control*, vol. 63, pp. 1509–1516, May 2018.

[22] A. Loria, J. Dasdemir, and N. Jarquín-Alvarez, "Decentralized formation-tracking control of autonomous vehicles on straight paths," in *Proc. of 40th IEEE Conf. Decision Control*, pp. 5399–5404, Dec 2014.

[23] X. Dong and G. Hu, "Time-varying formation control for general linear multi-agent systems with switching directed topologies," *Automatica*, vol. 73, pp. 47 – 55, 2016.

[24] R. Sepulchre, D. A. Paley, and N. E. Leonard, "Stabilization of planar collective motion: All-to-all communication," *IEEE Trans. on Autom. Control*, vol. 52, pp. 811–824, May 2007.

[25] E. Montijano, D. Zhou, M. Schwager, and C. Sagues, "Distributed formation control without a global reference frame," in *Proc. of Amer. Control Conf.*, pp. 3862–3867, June 2014.

[26] D. Tran and T. Yucelen, "On control of multiagent formations through local interactions," in *Proc. of 55th IEEE Conf. Decision Control*, pp. 5177–5182, Dec 2016.

[27] C. K. Verginis, A. Nikou, and D. V. Dimarogonas, "Position and orientation based formation control of multiple rigid bodies with collision avoidance and connectivity maintenance," in *Proc. of 56th IEEE Conf. Decision Control*, pp. 411–416, Dec 2017.

[28] K. Oh and H. Ahn, "Formation control and network localization via orientation alignment," *IEEE Trans. on Autom. Control*, vol. 59, pp. 540–545, Feb 2014.

[29] Y. Li, Y. Huang, P. Lin, and W. Ren, "Distributed rotating consensus of second-order multi-agent systems with nonuniform delays," *Syst. Control Lett.*, vol. 117, pp. 18 – 22, 2018.

[30] C. Sun, G. Hu, L. Xie, and M. Egerstedt, "Robust finite-time connectivity preserving consensus tracking and formation control for multi-agent systems," in *Proc. of Amer. Control Conf.*, pp. 1990–1995, May 2017.

[31] P. Lin and Y. Jia, "Distributed rotating formation control of multi-agent systems," *Syst. Control Lett.*, vol. 59, no. 10, pp. 587 – 595, 2010.

[32] J. A. Marshall, M. E. Broucke, and B. A. Francis, "Formations of vehicles in cyclic pursuit," *IEEE Trans. on Autom. Control*, vol. 49, pp. 1963–1974, 2004.

[33] G. Jing and L. Wang, "Multi-agent flocking with angle-based formation shape control," *IEEE Trans. on Autom. Control*, 2019.

[34] S. Zhao, Z. Li, and Z. Ding, "Bearing-only formation tracking control of multi-agent systems," *IEEE Trans. on Autom. Control*, 2019.

[35] L. B. Arranz, A. Seuret, and C. C. de Wit, "Translation control of a fleet circular formation of auvs under finite communication range," in *Proc. of 48h IEEE Conf. Decision Control and 28th Chinese Control Conf.*, pp. 8345–8350, Dec 2009.

[36] T. Yang, Z. Meng, D. V. Dimarogonas, and K. H. Johansson, "Global consensus for discrete-time multi-agent systems with input saturation constraints," *Automatica*, vol. 50, no. 2, pp. 499 – 506, 2014.

[37] X. Yu and L. Liu, "Distributed formation control of nonholonomic vehicles subject to velocity constraints," *IEEE Trans. on Ind. Electron.*, vol. 63, pp. 1289–1298, Feb 2016.

[38] S. Li, J. Zhang, X. Li, F. Wang, X. Luo, and X. Guan, "Formation control of heterogeneous discrete-time nonlinear multi-agent systems with uncertainties," *IEEE Trans. on Ind. Electron.*, vol. 64, pp. 4730–4740, June 2017.

[39] X. Ge and Q. Han, "Distributed formation control of networked multi-agent systems using a dynamic event-triggered communication mechanism," *IEEE Trans. on Ind. Electron.*, vol. 64, pp. 8118–8127, Oct 2017.

[40] Y. Hua, X. Dong, Q. Li, and Z. Ren, "Distributed time-varying formation robust tracking for general linear multiagent systems with parameter uncertainties and external disturbances," *IEEE Trans. on Cybern.*, vol. 47, pp. 1959–1969, Aug 2017.

[41] G. Wen, C. L. P. Chen, and Y. Liu, "Formation control with obstacle avoidance for a class of stochastic multiagent systems," *IEEE Trans. on Ind. Electron.*, vol. 65, pp. 5847–5855, July 2018.

[42] E. D. Sontag, "Remarks on stabilization and input-to-state stability," in *Proc. of 28th IEEE Conf. Decision Control*, pp. 1376–1378 vol.2, Dec 1989.

[43] Q. Yang, Z. Sun, M. Cao, H. Fang, and J. Chen, "Stress-matrix-based formation scaling control," *Automatica*, vol. 101, pp. 120 – 127, 2019.